Table of Content

THE STRUCTURAL OPTIMIZING OF METALLURGICAL INSTALLATIONS AND MECHANISMS

Viorel MUNTEANU[1], Simona SAVA[2]

[1]University "Dunarea de Jos" of Galați,
[2]S.C. Uzinsider Engineering S.A. Galați,
e-mail: viorel.munteanu@ugal.ro

ABSTRACT

The structural optimizing of used mechanisms in the machines construction and metallurgy through the further liberty degrees creation is essential projection problem, as it enters the closing mechanisms case with sliding case for steel teeming ladles.

KEYWORDS: sliding gate nozzle, casting steel, spatial mechanism.

1. The mechanisms structure optimizing through the further liberty degrees creation

In the fashionable machines construction and metallurgy, a distinguished attention must attached realization to some installations and machines fiabile, because the excited stops failures and bugs sundries, as well as the interventions for repairs tend important production loss, to extra costs and the labour productivity reduction. Therefore, the mechanisms structure optimizing through the further liberty degrees creation (in meaning Reşetov) it is an essential projection problem, as it will reason in the closing mechanisms case with case for steel teeming ladles [1].

Use experience to those in working metallurgical behaviour, it manages to the solution necessity to the next problems:

> ➤ The mechanisms tun in thermic valir behaviour, introducing needed his realization with big games;
> ➤ The practice failure of a parallelism faultless of joints journals;
> ➤ The fitting mistakes of mechanism in the difficult conditions, making failures production possibility;
> ➤ The mechanism jams owing to deformability in time.

These problems can solve themselves through the further liberty degrees creation, replacing the cylindric joints from the points c and d (figure 1), such as it was realized mechanism structure in the first stage, with round joints. In this case, it appears and a further mobility (the turnover tiller 4 around own journal).

Fig. 1. *Skeleton diagram of spatial mechanism.*

At the beginning it is presented, the mechanism configurations fixing in this considered situation like a spatial mechanism. Further, it entails kinematic and kinetostatic mechanism, considering same respect.

The further tiller mobility to treat as in (1), observing as in any other position of tiller 4, must tested, generally, the equation:

$$\overline{CD} \times \overline{F}_{54} + \overline{CS}_4 \times \overline{F}_4 + \overline{M}_4 = \overline{0} \qquad (1)$$

which, projected on the $\overline{CD}$ direction, becomes:

$$\left(\overline{CS}_4 \times \overline{F}_4 + \overline{M}_4\right)\overline{CD} = \overline{0} \qquad (2)$$

in which:

S_4 is the centre of tiller mass 4, non-collinear with the CD direction. In the physical collinearity case, S_4 is an arbitrarypoint in which decreases the forces torsor applied to the tiller 4.

$\overline{F_4}, \overline{M_4}$ - the torsor elements of the forces system (active and of inertia) applied to the tiller. In the effected computations considered only the own weight of tiller $\overline{G}_4$ and, therefore, the relation (1) becomes:

$$\left(\overline{CS_4} \times \overline{G_4}\right) \cdot \overline{CD} = \overline{0} \qquad (3)$$

The torsor inertia rates negligible related the active forces through relative creeping mouvements.

2. The spatial mechanism configuration fixing

The mechanism reports to a determinate system journals of co-ordinate Oxyz, as in figure 1 (axis Oy is vertical).

Structural, the mechanism is constituted from a plan linkage and a spatial linkage, the point position D being defined of the unit vector components $\overline{u}_5$.

Case guide journal runs through the point E, considered stiff with layer and has the evinced direction through unit vector $\overline{u}_5$.

The centre of tiller mass 4, S$_4$, has excentricity d toward journal $\overline{CD}$ of tiller (from the processing mistakes and the dilatation owing to thermic field). For the space arrangement of tiller 4 is necessary to knowledge the point position S$_4$. Therefore, the input dates for the positions fixing are the following::

$\ell_{AB}, \ell_{CB}, \ell_{CC}, \ell_{BC}, A(x_A, y_A, z_A), \ell_{CD}$, $E(x_E, y_E, z_E), \quad \overline{u}_5, \quad d = \ell_{PS_4}$ (it con-sidered $\overline{PS_4} \perp \overline{CD}$, P being the middle of segment $\overline{CD}$).

The B point coordinates results from the equations:

$$\left(x_B - x_A\right)^2 + \left(y_B - y_A\right)^2 = L_{AB}^2$$
$$x_B^2 + y_B^2 = \ell_{OB}^2 \qquad (4)$$
$$z_A = 0; z_B = 0$$

The C point coordinates calculates from the equations:

$$\left(x_C - x_B\right)^2 + \left(y_C - y_B\right)^2 = \ell_{BC}^2$$
$$\left(x_C - x_O\right)^2 + \left(y_C - y_O\right)^2 = \ell_{OC}^2 \qquad (5)$$
$$z_C = 0$$

The D point coordinates entails from the equation:

$$\left(x_C - x_D\right)^2 + \left(y_C - y_D\right)^2 + z_D^2 = \ell_{CD}^2 \quad (6)$$

whereupon it adds the relation:

$$\overline{ED} = \overline{u}_5 \cdot L_{ED} \qquad (7)$$

which, written scalar, results:

$$x_D - x_E = u_{5x} \cdot L_{ED}$$
$$y_D - y_E = u_{5y} \cdot L_{ED} \qquad (7')$$
$$z_D - z_E = u_{5z} \cdot L_{ED}$$

The P point coordinates results as subtotal to the co-ordinated points C și D, so that:

$$x_P = \frac{x_C + x_D}{2}$$
$$y_P = \frac{y_C + y_D}{2} \qquad (8)$$
$$z_P = \frac{z_C + z_D}{2}$$

The point position S$_4$ results from the equations:

$$\overline{CP} \cdot \overline{PS_4} = 0 \qquad (9)$$
$$\left|\overline{PS_4}\right| = d \qquad (10)$$

whereupon it adds the relation (3).

In this case, the excentricity d appears effective through dilatation owing to thermic valid field and of processing, considering the execution necessity from more catches (also, you see the chamfering for key).

The relations (9) and (3), written scalar, become:

$$\left(x_P - x_C\right)\left(x_{S_4} - x_P\right) +$$
$$+ \left(y_P - y_C\right)\left(y_{S_4} - y_P\right) + \qquad (9')$$
$$+ z_P\left(z_{S_4} - z_P\right) = 0$$

$$\left(x_P - x_{S_4}\right)^2 + \left(y_P - y_{S_4}\right)^2 +$$
$$+ \left(z_P - z_{S_4}\right)^2 = d^2 \qquad (10')$$

$$z_D\left(x_{S_4} - x_C\right) = \left(x_D - x_C\right)z_{S_4} \qquad (3')$$

(G$_4$ has component obly after journal y).

3. The fixing spatial mechanism kinematics

In accelerations and speeds computation were considered the kinematic detached parameters, relative speed v_{21} and relative acceleration a_{21}.

3.1 Speeds fixing

For the points B and C they act themselves in classic mode:

$$B \in 3,2$$
$$\overline{v}_B = \overline{v}_{B1} + \overline{v}_{BB1}, \text{or}$$
$$\overline{\omega}_3 \times \overline{OB} = \overline{\omega}_1 \times \overline{AB} + v_{21}\frac{\overline{AB}}{L_{AB}} \qquad (11)$$

which, expressed numeric, put down themselves:

$$-y_B \cdot \omega_3 = (y_A - y_B)\omega_1 +$$

$$+ \frac{v_{21}}{L_{AB}}(x_B - x_A)$$

$$x_B \cdot \omega_3 = (x_B - x_A)\omega_1 +$$

$$+ \frac{v_{21}}{L_{AB}}(x_B - y_A) \qquad (11')$$

whence it results ω_1 and ω_3.

$$\overline{v}_C = \omega_3 \times \overline{OC} \qquad (12)$$

or written numeric

$$v_{Cx} = -y_C \cdot \omega_3$$

$$v_{Cy} = x_C \cdot \omega_3 \qquad (12')$$

For fixing v_D and v_{CD}, put down themselves the equations:

$$\overline{v}_D \cdot \overline{u}_5 = \overline{\omega}_3 \times \overline{OC} + v_{DC} \qquad (13)$$

$$\overline{v}_{DC} \cdot \overline{DC} = 0 \qquad (14)$$

which, for numeric computation, put down themselves so:

$$v_D \cdot u_{5x} = -y_C \cdot \omega_3 + v_{DCx}$$

$$v_D \cdot u_{5y} = x_C \cdot \omega_3 + v_{DCy} \qquad (13')$$

$$v_D \cdot u_{5z} = 0 + v_{DCz}$$

(in considered case $u_{5z} = 0$)

$$v_{DCx}(x_C - x_D) + v_{DCy}(x_C - x_D) -$$

$$- v_{DCz} \cdot z_D = 0 \qquad (14')$$

For vector computation $\overline{\omega}_4$, puts down:

$$\overline{v}_{\underline{D}} = \overline{\overline{v}}_{\underline{DC}} + \overline{v}_{\underline{DC}}$$

$$\overline{v}_D = \overline{v}_C + \overline{\omega}_4 \times \overline{CD} \qquad (15)$$

from which take either two written numeric equations so:

$$v_{Dx} = v_{Cx} + z_D \cdot \omega_{4y} -$$

$$- \omega_{4z}(y_D - y_C)$$

$$v_{Dy} = v_{Cy} + \omega_{4z}(x_D - x_C) - \qquad (15')$$

$$- \omega_{4x} \cdot z_D$$

whereupon it combines differential equation (3)

$$\left[\overline{\omega}_4 \times (\overline{CD} \times \overline{CS}_4)\right] \cdot \overline{G}_4 = 0, \text{sau}$$

$$\left[\overline{CD} \cdot (\overline{\omega}_4 \cdot \overline{CS}_4) - \overline{CS}_4(\overline{\omega}_4 \cdot \overline{CD})\right] \cdot \qquad (16)$$

$$\cdot \overline{G}_4 = 0$$

which written numeric, becomes:

$$(\omega_{4x}CS_{4x} + \omega_{4y}CS_{4y} + \omega_{4z}CS_{4z}) \cdot$$

$$\cdot (-CD_y G_4) -$$

$$- (\omega_{4x}CD_x + \omega_{4y}CD_y + \omega_{4z}CD_z) \cdot \qquad (16')$$

$$\cdot CS_{4y} \cdot G_4 = 0$$

3.2 Accelerations fixing

For fixing ε_1 and ε_3 puts down the equation:

$$\overline{a}_B^n + \overline{a}_B^t = \overline{a}_{B_1}^n + \overline{a}_{B_1}^t + \overline{a}_{BB} + \overline{a}_{BB_1}^c \qquad (17)$$

in which:

$$\overline{a}_B^n = -\omega_3^2 \|OB\|$$

$$\overline{a}_B^t = \overline{\varepsilon}_3 \times \overline{OB}$$

$$\overline{a}_{B_1}^n = -\omega_1^2 \cdot AB$$

$$\overline{a}_{B_1}^t = \overline{\varepsilon}_1 \times \|\overline{AB}\|$$

$$\overline{a}_{BB_1} = 0 \text{ (deoarece } v_{BB_1} = ct)$$

$$a_{BB_1}^c = 2 \cdot \omega_1 \times \overline{v}_{BB_1}$$

Numeric, the equation (17) it expresses so:

$$-\omega_3^2 \cdot x_B - \varepsilon_3 \cdot y_B = -\omega_1^2(x_B - x_A) -$$

$$- \varepsilon_1(y_B - y_A) - (y_B - y_A)\frac{2\omega_1 \cdot v_{21}}{L_{AB}}$$

$$-\omega_3^2 \cdot y_B - \varepsilon_3 \cdot x_B = -\omega_1^2(y_B - y_A) - \qquad (17')$$

$$- \varepsilon_1(x_B - x_A) - (x_B - x_A)\frac{2\omega_1 \cdot v_{21}}{L_{AB}}$$

For the point acceleration computation C puts down the equation:

$$\overline{a}_C = \overline{a}_C^n + \overline{a}_C^t, \text{ or} \qquad (18)$$

$$a_{Cx} = -\omega_3^2 x_C - \varepsilon_3 \cdot y_C$$

$$a_{Cy} = -\omega_3^2 y_C - \varepsilon_3 \cdot x_C \qquad (18')$$

For the angular acceleration computation ε_4 puts down the equations:

$$\overline{a}_D = \overline{a}_C + \overline{\varepsilon}_4 \times \overline{CD} + \overline{\omega}_4 \times \overline{v}_{DC} \qquad (19)$$

or

$$a_{Dx} = a_{Cx} + z_D \cdot \varepsilon_{4y} -$$

$$- \varepsilon_{4z}(y_D - y_C) + \omega_{4y} \cdot v_{DCz} -$$

$$- \omega_{4z} \cdot v_{DCy}$$

$$a_{Dy} = a_{Cy} + \varepsilon_{4z}(x_D - x_C) -$$

$$-\varepsilon_{4x} \cdot z_D + \omega_{4z} \cdot v_{DCx} - \qquad (19')$$

$$-\omega_{4x} \cdot v_{DCz}$$

$$a_{Dz} = a_{Cz} + \varepsilon_{4x} \cdot z_D -$$

$$-\varepsilon_{4z}(x_D - x_C)$$

$$+\omega_{4x} \cdot v_{DCy} -$$

$$-\omega_{4z} \cdot v_{DCx}$$

whereupon it adds the relations:

$$a_{Dx} = a_D \cdot u_{5x}$$

$$a_{Dy} = a_D \cdot u_{5y} \qquad (19'')$$

$$a_{Dz} = a_D \cdot u_{5z}$$

and the auxiliary equation obtained through the relation derivation (16) related time:

$$\{\varepsilon_4 \times (\overline{CD} \times \overline{CS_4}) + \omega_4 \times$$
$$\times [\omega_4 \times (\overline{CD} \times \overline{CS_4})]\} \cdot \overline{G_4} = 0$$

or $\qquad (20)$

$$\{\overline{CD}(\varepsilon_4 \cdot \overline{CS_4}) - \overline{CS_4}(\varepsilon_4 \cdot \overline{CD}) +$$
$$+ \omega_4 \times [\overline{CD}(\omega_4 \cdot \overline{CS_4}) - \overline{CS_4}(\omega_4 \cdot \overline{CD})]\} \cdot$$
$$\cdot \overline{G_4} = 0$$

For the numeric computation utilizes the relation:

$$-(y_D - y_C)[\varepsilon_{4x}(x_{S_4} - x_C) +$$
$$+ \varepsilon_{4y}(y_{S_4} - y_C) + \varepsilon_{4z} \cdot z_{S_4}] +$$
$$+ (y_{S_4} - y_C)[\varepsilon_{4x}(x_D - x_C) + \qquad (20')$$
$$+ \varepsilon_{4y}(y_D - y_C) + \varepsilon_{4z} \cdot z_D] - E_y = 0$$

in which E_y is the projection on journal y of equation:

$$E = \omega_4 \times [\overline{CD}(\omega_4 \cdot \overline{CS_4}) - \overline{CS_4}(\omega_4 \cdot \overline{CD})]$$

(Maybe I was acting also, via the acceleration projection theorem practice, making $\overline{a}_D$ besides the computation deploys as it showed).

4. The fixing back strokes

4.1 Poise kinetostatic equations [2]

Pursuant to the journal system of co-ordinate Oxyz, the poise kinetostatic equations are:

3 scalar equations:

$$\overline{F}_{01} + \overline{F}_{21} + \overline{F}_m + \overline{F}_1 = \overline{0} \qquad (21)$$

$$\overline{AB} \times \overline{F}_{21} + \overline{M}_{21} + \overline{AS}_1 \times \overline{F}_1 + \overline{M}_1 = \overline{0} \qquad (22)$$

4 scalar equations:

$$-\overline{F}_{21} - \overline{F}_m + \overline{F}_{32} + \overline{F}_2 = \overline{0} \qquad (23)$$

$$-\overline{M}_{21} + \overline{BS}_2 \times \overline{F}_2 + \overline{M}_2 = \overline{0} \qquad (24)$$

$$\overline{F}_{21} \cdot \overline{AB} = 0 \qquad (25)$$

6 scalar equation:

$$-\overline{OB} \times \overline{F}_{32} + \overline{OC} \times \overline{F}_{43} + \overline{M}_{03} +$$
$$+ \overline{OS}_3 \times \overline{F}_3 + \overline{M}_3 = \overline{0} \qquad (26)$$

$$-\overline{F}_{32} + \overline{F}_{43} + \overline{F}_{03} + \overline{F}_3 = \overline{0} \qquad (27)$$

5 scalar equations:

$$-\overline{F}_{43} + \overline{F}_{54} + \overline{F}_4 = 0 \qquad (28)$$

$$\overline{CD} \times \overline{F}_{54} + \overline{CS}_4 \times \overline{F}_4 + \overline{M}_4 = 0 \qquad (29)$$

7 scalar equations:

$$\overline{F}_{05} - \overline{F}_{54} + \overline{F}_4 + \overline{M}_4 = 0 \qquad (30)$$

$$\overline{M}_{05} + \overline{DS}_5 \times \overline{F}_4 + \overline{M}_5 = 0 \qquad (31)$$

$$\overline{F}_{05} \cdot \overline{u}_5 = 0 \qquad (32)$$

in which:

S_i (i = 1÷5) represents the centre of mass of elements 1÷5.

$\overline{F}_k, \overline{M}_k$ (k = 1÷5) represents the torsor of active and inertia forces, whence it acts over element k calculated in c.d.g.

In the described equations considered negligible scrubs.

The kinetostatic computation for the element 1 and 2 can do considering it the coplanar forces systems and, therefore, putting down for each element in part, only three poise scalar equations.

The back strokes from joint of A, slyder and the joint from B will appear therefore in computation only with two unknown scalar.

Essential, is of observed as the equation (29) is equivalent with only two scalar equations and not with three, as in the general case. This situation explains in that the fact as can entail a direction thereto it is verified equal.

Indeed, it can put down:

$$(\overline{CS}_4 \times \overline{F}_4 + \overline{M}_4) \cdot \overline{CD} = \overline{0} \qquad (33)$$

This equation constitutes the ground rule of method for the kinematic computation, as it saw.

4.2 Fixing static back strokes

In a first approach can entail the back strokes without to take inaction, with so more with how the real movements of mechanism are dull. In this case, $\overline{F}_k, \overline{M}_k$ (k = 1÷5) represents the torsor of active forces

(engines force, useful resistance force; it disregards the own weights).

Unknown problem are:

$F_m, x_{01}, y_{01}, x_{21}, y_{21}, M_{21}, y_{32}, x_{32}, x_{03},$

$y_{03}, z_{03}, M_{x_{03}}, M_{y_{03}}, x_{43}, y_{43}, x_{54}, y_{54},$

$z_{54}, x_{05}, y_{05}, z_{05}, M_{x_{05}}, M_{y_{05}}, M_{z_{05}}$

The ones 25 of unknown entail themselves through the system solution of 25 of derived poise equations from the relations (21) ÷ (32).

Considering as the mechanism is made aut from a plan kinematic chain and a spatial kinematic chain, further, enters a particular solution.

It solves the elements 1, 2, 3 in the plan xOy.

From the element poise 1, it was figuring 2

Fig. 2. The element poise 1.

$-\overline{F}_m + \overline{F}_{01} = \overline{0}$ (34)

From the moments equation toward the point of A

$\overline{F}_{21} = \overline{0}$ (35)

From the element poise 2, it was figuring 3

Fig. 3. The element poise 2.

M_{12} (back stroke) = 0, as it sees from the moments equation, where $B \equiv B'$.

$\overline{F}_m + \overline{F}_{32} = \overline{0}$ (36)

$\overline{F}_{32} = -\overline{F}_m$

The element poise 3

$\overline{F}_m + \overline{F}_{03} + \overline{F}'_{45} = 0$ (37)

$\overline{OB} \times \overline{F}_m + \overline{OC} \times \overline{F}'_{43} = 0$ (38)

where it noted with $\overline{F}'_{43}$ the force projection $\overline{F}_{43}$ in the plan xOy.

For the numeric computation equations (37), (38) put down themselves respectively

$F_m \dfrac{\|AB\|}{L_{AB}} + \|F_{01}\| + \|F'_{43}\| = \|0\|$ (37')

$\dfrac{F_m}{L_{AB}} \begin{vmatrix} \bar{i} & \bar{j} & \bar{k} \\ x_B & y_B & 0 \\ x_B - x_A & y_B - y_A & 0 \end{vmatrix} +$

$+ \begin{vmatrix} \bar{i} & \bar{j} & \bar{k} \\ x_C & y_C & 0 \\ F'_{43x} & F'_{43y} & 0 \end{vmatrix} = 0$ (38')

From the element poise 4 can put down:

$\overline{F}_{54} + \overline{F}_{34} = 0$ (39)

$\overline{F}_{43} = -\overline{F}_{34}$; $\overline{F}_{54} = -\overline{F}_{45}$ (40)

It takes from $\overline{F}_{45}$ only F_{45x} and F_{45y}.

$F_{45x} = 0$, being undertaken structure even joints.

Therefore,

$F'_{45} = \begin{Vmatrix} F'_{45x} \\ F'_{45y} \\ 0 \end{Vmatrix}$ (41)

The element 5 solves independent, putting down the equations

$\overline{F}_{45} + \overline{F}_{05} + \overline{F}_u = 0$ (42)

$\overline{F}_{05} \cdot \overline{u}_5 = 0$ (43)

$\overline{DE} \times \overline{F}_{05} + \overline{M}_{05} = 0$ (44)

For the numeric computation equations (42), (43), (44) put down themselves respectively:

$F_{45} \dfrac{\|CD\|}{L_{CD}} + \|F_{05}\| + F_u \|u_5\| = 0$ (42')

$F_{05x} \cdot u_{5x} + F_{05y} \cdot u_{5y} + F_{05z} \cdot u_{5z} = 0$ (43')

$\begin{Vmatrix} \bar{i} & \bar{j} & \bar{k} \\ x_E - x_D & y_E - y_D & z_E - z_D \\ F_{05x} & F_{05y} & F_{05z} \end{Vmatrix} +$

$+ \begin{Vmatrix} M_{05x} \\ M_{05y} \\ M_{05z} \end{Vmatrix} = \begin{Vmatrix} 0 \\ 0 \\ 0 \end{Vmatrix}$ (44')

From the equations (42'), (43'), (44'), it results F_{45}, $\overline{F}_{05}$ and $\overline{M}_{05}$. The system (34) ÷ (40) also entails the others back strokes.

4.3 Fixing dynamic back strokes

Taking into account the inaction forces system, then in the equation (29), $\overline{F}_4$ and $\overline{M}_4$ become:

$$\overline{F}_4 = \overline{G}_4 + \overline{F}_{14} \qquad (45)$$

$$\overline{M}_4 = \overline{M}_{14} \qquad (46)$$

For the torsor computation of inaction forces of element 4 rates a journal system of co-ordinate joint with this:

$$\overline{i}' = \frac{\overline{CD}}{l_{CD}} \;;\; \overline{j}' = \frac{\overline{PS}_4}{d} \;;\; \overline{k}' = \overline{i}' \times \overline{j}' \qquad (47)$$

It obtains

$$\overline{F}_{i4} = -m_4 \cdot \overline{a}_{S_4} \qquad (48)$$

And

$$\overline{M}'_{i4} = \begin{Vmatrix} M_{i4x'} \\ M_{i4y'} \\ M_{i4z'} \end{Vmatrix} =$$

$$= - \begin{Vmatrix} \varepsilon_{4x'} \cdot J'_{11} + \omega_{4y'} \cdot \omega_{4z'} (J'_{33} - J'_{22}) \\ \varepsilon_{4y'} \cdot J'_{22} + \omega_{4x'} \cdot \omega_{4z'} (J'_{11} - J'_{33}) \\ \varepsilon_{4z'} \cdot J'_{33} + \omega_{4x'} \cdot \omega_{4y'} (J'_{22} - J'_{11}) \end{Vmatrix} \qquad (49)$$

In relations (49), the resultant moment of inaction forces $\overline{M}_{i4}$, it is expressed through its projections in the movable journals system (47), joint with the element 4.

The main inaction moments J'_{11}, J'_{22}, J'_{33} are constants.

But, to manage the computations, is needed angular speed utterance ω_4 and angular acceleration ε_4 through their projections on movable system journals (47). This it obtains through the transformations:

$$\begin{Vmatrix} \omega'_4 \end{Vmatrix} = \begin{Vmatrix} A^{-1} \end{Vmatrix} \cdot \begin{Vmatrix} \omega_4 \end{Vmatrix} \qquad (50)$$

$$\begin{Vmatrix} \varepsilon'_4 \end{Vmatrix} = \begin{Vmatrix} A^{-1} \end{Vmatrix} \cdot \begin{Vmatrix} \varepsilon_4 \end{Vmatrix} \qquad (51)$$

in which

$$\begin{Vmatrix} A \end{Vmatrix} = \begin{Vmatrix} \overline{i} \cdot \overline{i}' & \overline{i} \cdot \overline{j}' & \overline{i} \cdot \overline{k}' \\ \overline{j} \cdot \overline{i}' & \overline{j} \cdot \overline{j}' & \overline{j} \cdot \overline{k}' \\ \overline{k} \cdot \overline{i}' & \overline{k} \cdot \overline{j}' & \overline{k} \cdot \overline{k}' \end{Vmatrix} \qquad (52)$$

where: $\overline{i}, \overline{j}, \overline{k}$ are the unit vectors determinate journals system.

To obtain the resultant moment projections $\overline{M}_{i4}$ on the determinate journals, it used the transformation:

$$\begin{Vmatrix} M \end{Vmatrix}_{i4} = \begin{Vmatrix} A \end{Vmatrix} \cdot \begin{Vmatrix} M'_{i4} \end{Vmatrix} \qquad (53)$$

where $\overline{M}'_{i4}$ it calculates from the relations (49).

5. The rated programme and test data

The computations were done on a Pentium V computer, pursuant to logical draft from figure 4. The positions were entailed through method Newton-Raphson. The equations systems of speeds, accelerations and back strokes entail themselves by the agency of algorithm Gauss.

For the accurate values fixing of resultant vector $\overline{M}_{i4}$ developed a iterative process, in which, initial, does not take into consideration, the element inaction 4 $\left(\overline{F}_4 = \overline{G}4 \right)$.

In next iteration it acquaints the equation (45) the torsor of inaction forces of element 4, calculated with the determinate acceleration in previous iteration.

The computation ends when difference among concerted point S_4, determinate in two iteration series, corresponds rated imposed accuracy.

In the rated programme, the relative accuracy was imposed $\varepsilon = 10^{-4}$, being necessary 2-4 iterations for each position. The initial solution was found from chart.

So can entail the dynamic back strokes.

Further, it enters the rated ISTROM programme, for speeds positions fixing, accelerations and of mechanism back strokes in spatial variant, trap function hydraulic piston for a data input set.

In figure 5 enters trap function case speed variation piston for values sundries of managers cosines, while in figure 6 enters case acceleration variation, trap function piston for same values of versor $\overline{u}_5$.

For his values $\overline{u}_5$ ($u_{5x} = 1$; $u_{5y} = 0$; $u_{5z} = 0$), the correct assembly case, it distinguishes linearity of case speed curve, comparable with variant was planning of mechanism with case. The case acceleration for same managers cosines gives a maximum in the middle region of piston position, the

minimum value filing to fine trap, with positive bearings over mechanism functionality.

Difference of about 2 m/s^2 among maximum and the minimum acceleration in curve zone, where it takes place the steel debit settlement indicates the possibility to an automation of casting with a high accuracy degree.

Analysing it was influencing the fitting mistakes or moves oxing to intensive field temperature, observes as running uniformity mechanism to be greatly determined of these variances.

So comparing curve 1 with 4 from figure 6, observes as in the curve situation 4 accelerations advance in continuous mode, which influences the negative automation installation stability.

6. Conclusions

It distinguishes generality, accuracy and perfect adaptability of mathematical described pattern in racing solution of any concrete appeared problems in exploitation, introducing possible automatic analysis of all fitting cases in any casting container type, the constructive input parameters function.

It obtain data tables and use charts, which give a very distinct image over mechanism parameters variation effect and over physical direction much more complete and more accurate meaning than whoever can be obtained from graphic method.

Figure 5. The speed variation V_D position dependency by hydraulic piston movement.
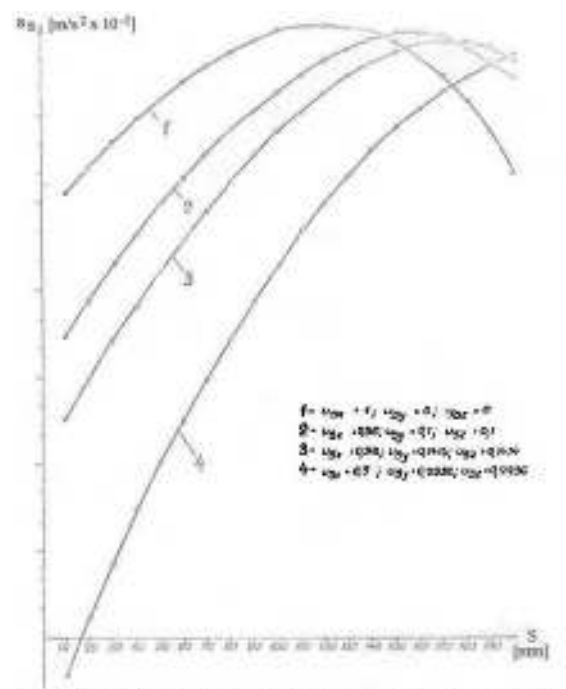
Figure 6. The acceleration variation a_S position dependency by hydraulic piston movement.

References

[1]. Munteanu V. – *Dispozitiv cu sertar glisant pentru turnarea metalului lichid din recipienții de turnare*, Brevet de invenție nr. 72729 - România;

[2]. Munteanu V., Orănescu A. - *Investigation of the Sliding Gate Nozzle Devices at Steel Casting Ladles*. Third IFTOMM International Symposium on Linkage and Computer Aided Design Method, Bucharest, July 2-7, vol. 1, pages 99-106;

[3]. Orănescu A., Munteanu V. – *Aspects Particuliers consernant l'étude technique des manipulateurs automatique dans la Metallurgie*. Sixth IFTOMM Congres – Theory of Machines and Mechanisms, 15-20 dec., New Dehli, India.
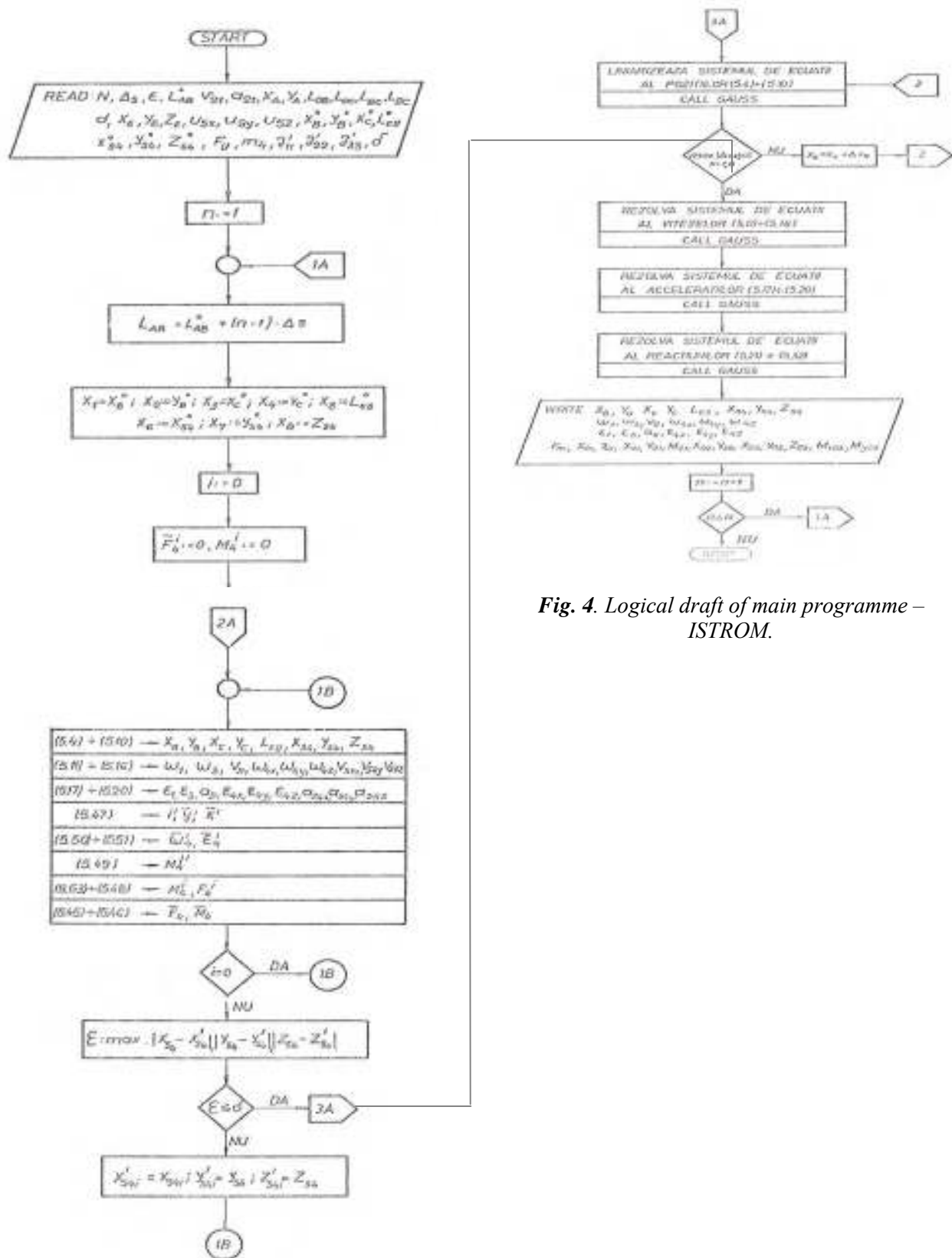
Fig. 4. *Logical draft of main programme – ISTROM.*

JASSY ACHIEVEMENTS REGARDING THE CASTING OF ART PIECES FOR ARTIFICIAL LIGHTING IN ORTHODOX CHURCHES

Florin DIACONESCU[1], Ioan CARCEA[1],
Cristian DIACONESCU[2]

[1] Technical University "Gh. Asachi" Jassy, Science and Materials Engineering Faculty
[2] Technical College "Gh. Asachi" Jassy

ABSTRACT

In this paper are presented some art pieces, used in orthodox religion for artificial general lighting. These pieces, realized at SC RANCON SRL Jassy, present a special importance, because they join harmoniously the functionality principle with the artistic and architectural concepts. Thus contribute at the achievement of sobriety, equilibrium and solemnity ambiance from spiritual service realized in Moldavian orthodox churches.

KEYWORDS: art pieces, casting, orthodox religion

1. Short history

"*God has said: To be light! And has been light.*" (Genesis 1.3 – The Old Testament). The human life, marked by two important events the birth and the death, it's indissoluble linked with light, by this divine alternative to darkness, which is associated to the sleep or the death.

The men have beginning from the very old times to use the solar light for the lighting of interior spaces, but in the interim has appeared the necessity to use both the day and night times of a new lighting sources, which can to be controlled and manipulated after the moment necessities.

In Pre-Christianity, the spiritual meetings have been interdicted by Romans and Jews, because the Christianity adepts have been regarding as the members of one dangerous sect for stability, religious, social and political interests of the Roman Empire. In these conditions, the religious cult has forced to manifested only night, in the underground conditions and consequently have appeared the necessity of the artificial lightning.

In Christianity, evening and morning prayers represent the oldest Mosaic tradition of the first adepts, recruited from Jews, as moments similar to evening and morning sacrifices prescribed by the Old Testament (Exit 29.39; 30.7; 30.8). The succession and the time of evening and morning prayers, related to those destined for Sacred Liturgy, have been systematized during the first three centuries, and in the IV-th century the hours for evening and morning prayers have been established officially through rigorous dispositions of some synods. In the manifestation of divine public orthodox cult, at evening, midnight and, sometimes, early services have been used the artificial lighting with candles fixed in chandeliers or in mural supports, candlesticks, but this method not provide a good illumination, thus in semidarkness the interior architecture has been loosed from the his artistic value of space organization. As the electrical light has become a main factor in socio-economic life the correctly choice of the illumination technique and of some adequate sources specific to each purpose has imperious necessary.

The communism period, in which the liberty of cults has just a constitutional stipulation with formal character, has mean practice a cessation of the production by lighting objects destined to orthodox cult. On the industrialization content, the artists and artisans from this domain has disappeared gradually, and the designers of lighting objects for home use have going in conceptual deadlock, given the mean attention to functionality and adaptability to industrial production. Thus has been diminished the artistic component of the creation, the beautiful industrial concepts being subordinated to the principle of products utilities, which has carried out to the adoption of an esthetic inexpressive trace, uncertain, accentuated through the using of the cheap materials with small durability. In reality, has arrived at the artistic depersonalization of the ambiance, and many interiors have acquired suddenly a slightly public aspect.

2. Illumination principles of the interior cult dwelling

The choice of the artificial lighting objects request refinement, perfect functionality, maximum

illumination efficiency, stylistic harmony and a accurate arrangement. In the case of orthodox cult dwelling the artificial illumination must assure an adequate amount of light without to tire the eye, to decorate the interior, to give him life, heat and personality, to create a specific and elaborate ambiance. This ambiance predetermined, necessary for meditation and praying, must to introduce the man in the universe of belief and love to God, to contribute at the assurance of inside equilibrium and at temporal abandonment of daily problems, to impress the man through grandness and solemnity of the religious act, through artistic images and adequate music. For the *presentation surfaces*, disposed in vertical plane and on arch, on which are exposed icons and mural paintings, must be used a constant illumination, focalized, without shades, which make evident all details, especially that the clothes of saints have usually dark colors or nuances which absorb the light. The artificial illumination from church uses a combined system to lead the light, namely a general illumination realized by chandeliers and a local illumination with the mural objects. The first kind of illumination are extended through natural sources during the day, but the windows are somewhat reduced as surface and sometime with strained-glass windows, respectively with dark colors on the interior faces, this make frequently that the light of the day to be not enough.

3. Execution technology of the artificial lighting objects

Chandeliers realize a light oriented to the top and are used to emphasize of some decorative structure and to enlarge the space through the illumination of the arch and reflection of the light by this. The great chandelier are fixed on the arch of the church (nave) by a casting "ochet" (special link), through four chains disposed in cross. The light of the great chandelier from nave symbolize the divine light which take down from the sky over all participants to the holy services of the church and to the Saint Liturgy, which stand in the middle of the public divine cult.

At S.C. RANCON S.R.L. Jassy are realized besides bells and other cult objects, the illumination objects for Orthodox Church new built in our country.

The chandelier with two levels (fig. 1) supply for artificial illumination of church with middle dimensions, because those 12 light (which symbolize the number of year months) can not assure the more lightness intensity. Sometimes such chandelier can set in pronave or in administrative interiors.

Each level is formed from disc (1) on which are fixed six ornamental arms (2) in the form of letter S. This arms, remind by Régence style (1715-1724), taken from the Rococo (1725-1800) style, thus are

reloaded the style is characterized through the suppleness and elegance of the sinusoidal line with vegetal motives, render evident the admiration of the anonymous artist for the beautiful of the nature created by God.

Fig. 1. *The chandelier with two levels and 12 lights.*

The arms (2) are casting from brass, in horizontal position, and the form are realized with monolithic cast box form aluminum, which impose the utilization a one false cast box. Between the levels are disposed the intermediate pieces (3), horizontal molting, with inside core for ulterior setting on a steel rod, respective the disc (4). These pieces, molding similar from brass, are lathed, finished and polished on felt at exterior. In the bottom part the chandelier have a little cross (5), which symbolize the Christian belief and the sacrifice of the Savior.

The cross, molding in horizontal position and worked mechanical on the both faces and finished, are fixed through the thread M10 with the pick (6) from massive metal, obtained through processing from one raw bar. The other end of the pick is also threaded for ulterior assembled with the steel rod which sustains the entire assembly.

The sphere (7), symbolizing the earth illuminated by God, is realized with an interior gauge, being formatted from two hemispheres, which are merged in equatorial plane through a threshold. The sphere is also mechanical processed at the exterior and finished. The sub-ensemble composed from the little cross (5) and pick (6) is fixed through the thread M12, situated at the inferior end of the steel rod. After are mounted the sphere (7), intermediate elements (3) and sub-ensemble formed from discs (4) and arms (2). Toward the superior ends are mounted the coronet (8), a cross disc (9) and the big cross (10), and the upper end of the threaded rod is disposed the clamping "ochet" (11).

Fig. 2. *The chandelier with four levels and 42 lights.*

The chandelier with four levels and six arms on the level (fig. 2) have 42 lights and realize an uniform illumination of the large spaces, because the multistoried and the disposing of electrical terminals follow the curvature of the arch and the acquirement of some identical light spots. In this mode are harmoniously joined the functional aspect with the artistic and emotional aspects, thus given to illumination object the grandeur and the brilliance imposed by religious service.

Also the chandelier underlines subtly the size of the room and of the presentation surfaces and help at the identification of the plastic message of icons and religious acts painted on the walls.
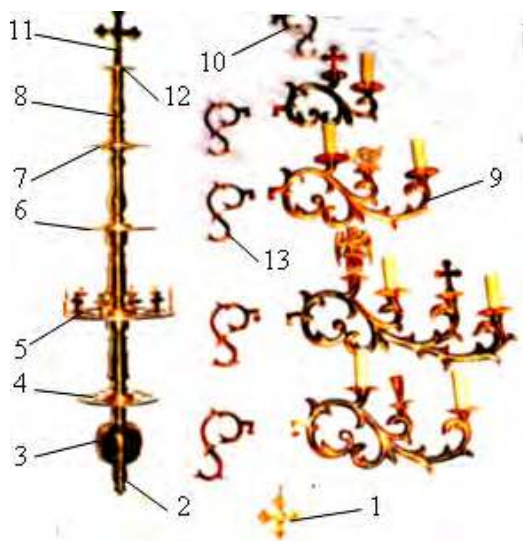
The component elements of the chandelier (fig. 3) are realized from casting brass, and mechanical processing manually or through lathing and finished. Similar with the chandelier described anterior, in the upper part is evident the small cross (1) assembled in the pick (2), in which are executed a threaded gauge for the montage of the inside rod by $\varnothing$16 mm from OL 37 steel. The sphere (3) is executed from two hemispheres with inner void, worked in equatorial plane with a threshold for a good closing. The discs (4), (5), (6) and (7) have the thickness by 10 mm and present six interradial cuttings, for the diminish from the weight. These discs have the diameters much smaller proportional with the increasing of disposed level to upper. Between the discs are inserted intermediate elements (8), casting in horizontal position with inside void, which are processed through lathing and polishing with felt. The arms (9) have the different dimensions correspondently to the level which his occupied, thus the ensemble to look like as a tree. The arms from the inferior level present elements with forms like C and S letters and vegetal motives (leaf and buds) having gracious forms, without the possibility to join in geometry rigorousness.

The next raw by arms presents at the end of a decorative vegetal element a cross, and the arms from the level immediate superior have at the end floral elements each with a seraph, which are molding separately and assembly through a thread M6 on arm. The decorative S, molding individual has a square termination which enter in a configuration slot correspondingly to the discs (5), (6) and (7). At the superior end are mounted the ornamental coronet (10) apart casting, and the great cross (11), cross disc (12) and clamping "ochet" is fixed through the thread M16 with superior end of the steel rod.

The chandelier has the maximum diameter by 1500 mm (at the bottom level), the height by 2400 mm and the mass by 125 kg.

A chandelier such as dimensions, named *the great chandelier*, is suspended at a height by some meters with four chains. These chains manufactured in industry have not even decorative element and thus can diminish the aspect and the artistic value of the illumination objects. Recently, in Jassy the producers find a solution much better, realizing elements through molting for chain (fig. 4) with floral motive, similar to decorative elements of the chandelier.

Fig. 3. *The component elements of the chandelier with 4 levels and 42 lights.*

Fig. 4. *Chain element with floral motives.*

At the chandeliers presented the central electrical conductor are situated inside of intermediate elements molding with interior void, and at the level of each level go off the insulated conductors, apparent, by yellow color, fixed on the arms with transparent adhesive tape.

4. Conclusions

Plastic and functional solutions adopted at S.C. RANCON S.R.L. Jassy for the production of these general illuminations objects, emphasize a careful preoccupation for the molting of the decorative elements components, the mechanical processing and the realization of the electrical installation, respecting the exigencies imposed by security technique of the participants at the public religious service.

The manufacturing art of the ecclesiastical ornaments and cult objects have been and is a continuous preoccupation of those believing men who understand to transform the metal in pastoral processed material and, not in the last hand, artistic. It's both a firm expression of the human talent and a adoration and respect form of the believed soul face to divinity, presents through permanently work in the human life from the earth.

References

[1]. *** *Biblia sau Sfânta Scriptură*, Editura Institutului Biblic şi de Misiune al B.O.R.. Bucureşti, 1994.

[2]. **Ene Branişte** – *Liturgica generală*, Editura Institutului Biblic şi de Misiune al B.O.R.. Bucureşti,1993.

[3]. **Vasile Drăguţ** – *Dicţionar de artă medievală românească*, Editura ştiinţifică şi Enciclopedică, Bucureşti, 1976.

[4]. **Florin Diaconescu** – *Teoria şi practica formării*, curs litografiat, vol. I şi II, Rotaprint I.P. Iaşi, 1988.

IMPROVED HARDNESS AND TRIBOCORROSION PROPERTIES OF NICKEL COATINGS BY CO - DEPOSITING ZrO$_2$ MICRO - SIZED DISPERSED PHASE DURING ELECTROPLATING PROCESS

Lidia BENEA[1], François WENGER[2],
Pierre PONTHIAUX[2], Jean–Pierre CELIS[3]

[1]Dunarea de Jos University of Galati, Romania
[2]Ecole Centrale Paris, Laboratoire LGPM, Chatenay Malabry, 92290, France
[3]Katholieke Universiteit Leuven, Department of Metallurgy and Materials Engineering,
Kasteelpark Arenberg 44, B-3001 Leuven, Belgium
e-mail: benea.lidia@ugal.ro

ABSTRACT

The tribocorrosion properties of ZrO$_2$ – nickel microstrucured composite coatings have been studied in the following conditions:

  -Solution: 0.5M K$_2$SO$_4$
  -Tribo corrosimeter: pin on disc connected with electrochemical cell.
  -Normal Force: 10N
  -Rotation Speed: 120 tours/min.

The objectives of our study in principal are to fully understanding the tribocorrosion process kinetic and mechanism of composite coatings materials. The samples with coating on a top of a cylinder were installed in a cell, containing the electrolyte and electrodes, and mounted on a pin-on-disc tribometer, with the working surface of the specimen facing upwards. The counterbody (pin) was a corrundum cylinder (7 mm in diameter), mounted vertically on a rotating head, above the specimen. The lower spherical end (radius = 100 mm) of the pin, was then applied against the composite surface (disc) with an adjustable normal force. When rotation was applied, the end of the pin draws a circular wear track (16 mm in diameter) on the working composite surface. Both continuous and intermittent friction tests were carried out. In the intermittent tests, friction was applied periodically: during each cycle, friction was first applied for 2 seconds at 120 rpm (sliding speed 100 mm/second) under 10 N (average pressure 120 MPa for hertzian contact conditions) and then stopped during a latency time (20 or 200 s.). This mechanical solicitation was repeated over 2500 cycles. Some features of these tests reproduce the wear conditions of composite coatings in the intermittent friction, K$_2$SO$_4$ 0.5M was used as corrosive and passivating electrolyte for tribocorrosion tests.

KEYWORDS: composite, coatings, dispersed particles, zirconium oxide, nickel, tribocorrosion.

1. Introduction

Composite electroplating is a method of co-depositing insoluble dispersed particles of metallic or non-metallic compounds with metals or alloy in a plating bath, to improve the material coating properties such as corrosion resistance, lubrication, hardness or wear-resistance. Such a coating features the properties of both the metal and the dispersed particles. These coatings can be considered to be metal-matrix composites (MMC), obtained through electroplating. Composite coatings obtained by metal co-deposition of various dispersed phases during electrocrystallisation have been given special attention in recent years [1-10]. Nickel, copper, chromium, iron, cobalt, silver, gold were mainly used as a metal matrix. Metals, metal oxides, carbides, borides and polymers as co-depositing dispersed particles were used. Composite Coatings are used in both aqueous and high temperature applications. Electric power generation, and waste incineration involve severe conditions and thick coatings have proved effective. Diesel and gas turbine engines are subjects of the high temperature corrosion and highly

beneficial coatings have been developed. Some nuclear power systems also rely on coatings. Factors that must be taken into account include substrate compatibility, adhesion, porosity, the possibility of repair or recoating, interdiffusion, the effect of thermal cycling, resistance to wear and corrosion, and not at last the cost.

In industry, e.g. automotive applications, there is always the risk of material touching each other under sliding conditions. In many cases, these industrial components, e.g. bearings, pumps, rolling mill bearings, are required to operate in aqueous environments (corrosive media) in which water is either deliberately introduced as a coolant or present as a working fluid. The combined action of wear and corrosion, named tribocorrosion, often results in a significant increase in the total material loss. Thus, there are required materials having the desired corrosion, friction, and wear properties. Accordingly, many efforts have been made to develop suitable materials to aqueous environment. Ni-based alloys, which are in general designed for uses at high temperature, possess some extraordinary characteristics such as excellent mechanical properties, good thermal stability, chemical inertness, and high wear resistance. The Ni-based composites are successfully used due to their capability of having self-lubricating property in a wide temperature range, for instance, the turbine engines used in aviation and electric industries, the radiator sealing systems of the automobile engines, and the mechanical devices in the atomic reactors.

However, few are reported on their friction and wear properties as well as wear mechanism in water environment. In particular, during recent years, Ni-ZrO_2 composites have been widely investigated and successfully commercialized in the automotive and aerospace industry as a result of their improved mechanical and tribological properties.

The composite materials were obtained by using dispersed micro sized ZrO_2 particles (mean diameter 10 μm). The influence of dispersed ZrO2 dispersed particles on the nickel reduction was discussed in the previous papers [4].

Prior to the wear corrosion tests, the composition and surface morphology of coatings were investigated in the scanning electron microscope with the aid of EDS. The presence of particles inside of composite coating was detected by optical microscopy.

The major challenges with the codeposition of second phase particles are the achievement of a high level of codeposition and avoiding the agglomeration of particles suspended in the electrolytes.

However, in the literature, there is very limited study in the dispersion of inert particles in the metallic matrix and its influence on the mechanical and tribological properties [3, 11].

The aim of this work is to investigate the influence of ZrO_2 particles dispersion in the Ni matrix on the tribocorrosion behavior of Ni-ZrO_2 composite coatings in aqueous environment.

2. Experimental

2.1. Preparation of nickel zirconia microstructued composite coatings

Pure nickel and nickel zirconium oxide co-depositions were made in common nickel plating electrolytes (sulfate and chloride). The electrolyte was prepared from p.a. chemicals and distilled water, which provided the required purity for the potentiodynamic investigations and characterizations of the coatings obtained. Pure dispersed zirconium oxide (ZrO_2) at different concentrations (50 - 100 g/l) was suspended in the electrolysis bath. The average particle size was 10 μm. Thickness of metal and composite deposits were obtained between 50 and 150 μm and were verified by measuring the weight before and after deposition and also by light microscopy on cross section. The particles were kept in suspension by mechanical or magnetic stirring at a rotation rate between 100 and 1500 r.p.m. A saturated calomel electrode was used as reference electrode (SCE) in order to determine the influence of the dispersed phase on nickel electrodeposition.

2.2. Structural and chemical analyses

Weighing the electrodes on a microbalance and stripping the deposit we could determine the amount of dispersed phase in the composite coating. The particles were filtered, dried and weighted. The weight percentage of the particles in the composite deposition was calculated by the formula:

$$p\% = \frac{m_p}{m_s} 100 \qquad (1)$$

Where: $p\%$ - represents the weight percentage of the particles in the composite coating;

m_p is the particles mass, in grams;

m_s is the total composite coating mass, in grams.

The uniformity of dispersed phase distribution in the composite coatings was examined by light microscopy in cross section. Scanning electron microscopy (SEM) revealed the comparative surface morphology of coatings and the uniformity of zirconium oxide particles in the composite deposit.

The micro sized composite coatings were deposited on a top of a cylinder having the dimensions: high = 25 mm and diameter = 25 mm (Fig. 1).

2.3. Wear corrosion studies

For electrochemical measurements (open-circuit potential, potentiodynamic polarization) a three-electrode set-up was used, with the sample as working electrode, a circular platinum gauze as counter electrode and a "Hg/Hg$_2$SO$_4$/saturated K$_2$SO$_4$ solution" as reference electrode (SSE = +670 mV/ NHE), see Fig. 1. The electrodes were connected to a PAR273A potentiostat controlled through a computer by using Corrware 2.2 (Scribner) software.
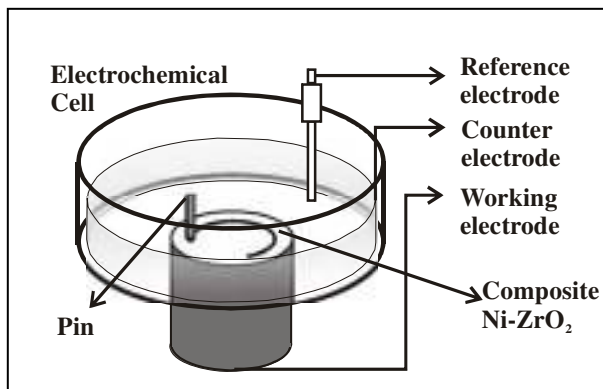
Fig. 1. *Schematic set-up for electrochemical measurements on a working electrode as Ni-ZrO$_2$ composite coating (WE)*

The tribocorrosion properties have been studied in the following conditions:
Solution: 0.5M K$_2$SO$_4$.
Tribo corrosimeter: pin on disc connected with electrochemical cell.
Normal Force: 10N.
Rotation Speed: 120 tours/min.

The samples were then installed in a cell, containing the electrolyte and electrodes, and mounted on a pin-on-disc tribometer, with the working surface of the specimen facing upwards.

The counterbody (pin) was a corrundum cylinder (7 mm in diameter), mounted vertically on a rotating head, above the specimen. The lower spherical end (radius = 100 mm) of the pin, was then applied against the composite surface (disc) with an adjustable normal force. When rotation was applied, the end of the pin draws a circular wear track (16 mm in diameter) on the working composite surface (Fig. 1). Both continuous and intermittent friction tests were carried out. In the intermittent tests, friction was applied periodically: during each cycle, friction was first applied for 2 seconds at 120 rpm (sliding speed 100 mm/second) under 10 N (average pressure 120 MPa for hertzian contact conditions) and then stopped during a latency time (20 or 200 s.), see Fig. 2. This mechanical solicitation was repeated over 2500 cycles. Some features of these tests reproduce the wear conditions of composite coatings in the

intermittent friction. K$_2$SO$_4$ 0.5M was used as corrosive and passivating electrolyte for tribocorrosion tests.

Fig. 2. *Schematic tribocorrosion tests*

After triboccorosion tests the surface of samples was analysed by SEM and EDS systems.

Local wear in the wear track was also measured. It was deduced from surveys of the wear track recorded with an optical high resolution microtopograph, with a lateral resolution of 1 µm and a vertical resolution of 30 nm: the volume of the wear track was measured and the corresponding weight loss was calculated.

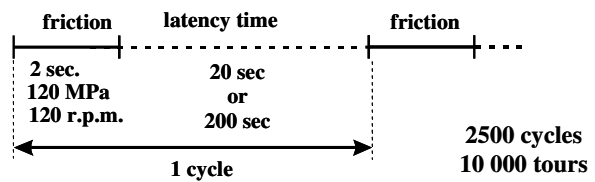## 3. Results and discussion

3.1. Structural aspects of zirconia nickel matrix composite coatings

Micrographies presented allow comparison between a pure nickel coating (Fig. 3) and nickel with zirconium oxide composite coatings (Figures 4, 5, 6 at different magnification), carried out with 100 gl^{-1} of ZrO$_2$ in the plating bath.

The pure nickel deposit has a rather regular surface, whereas the composite coating develops in a nodular disturbed surface structure. The zirconium oxide particles are clearly visible on the surface with a homogeneous distribution (white particles). The X-ray disperse energy analysis spot on a white particle have revealed a spectra with zirconium but also with nickel (Figure 7). This can suggest that particles are not free on the coating surface but they have a thin layer of nickel. The nickel layer can be done from the reduced nickel ions at the cathode. The surface structure morphology of composite coating obtained by two scanning electronic microscopy techniques is presented on the Figure 8. The surface analysis of composite coatings is not the most suitable method to determine the presence of zirconium oxide in the nickel matrix, but it is appropriate to observe the morphology and surface structure changes. One of the most reliable methods to observe the distribution of zirconia particles in the nickel matrix consists of studying the cross section of a deposit.

The microstructure performed shows the presence and distribution of zirconium oxide particles (8 mass %) in the nickel matrix see Figure 9.
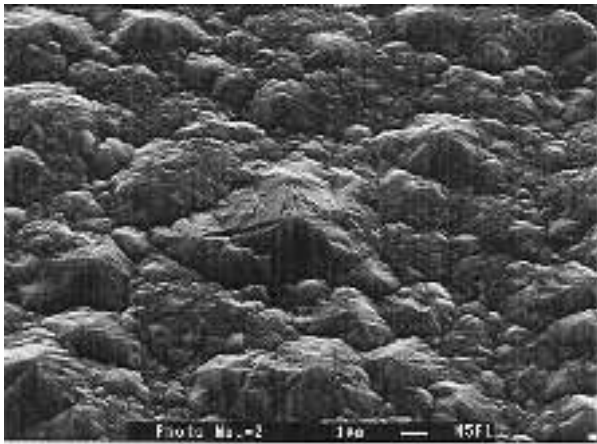
Fig. 3. *SEM morphology of pure nickel coating*
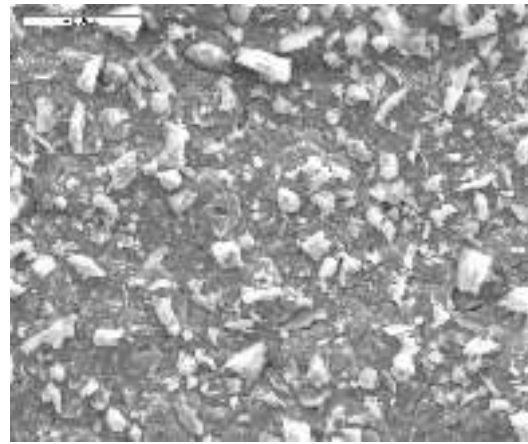
Fig. 4. *SEM Surface morphology of ZrO$_2$ + nickel composite coating*
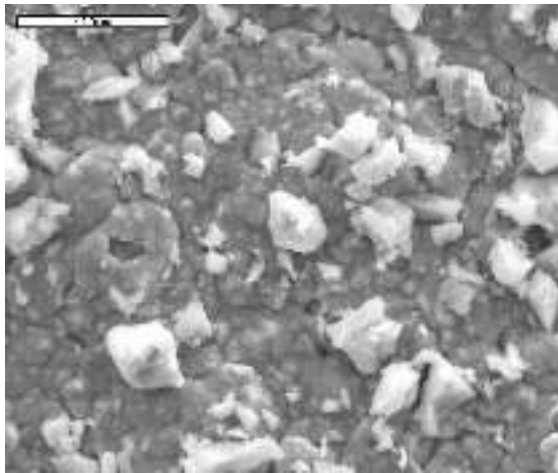
Fig. 5. *SEM Surface morphology of ZrO$_2$–Ni composite coating*
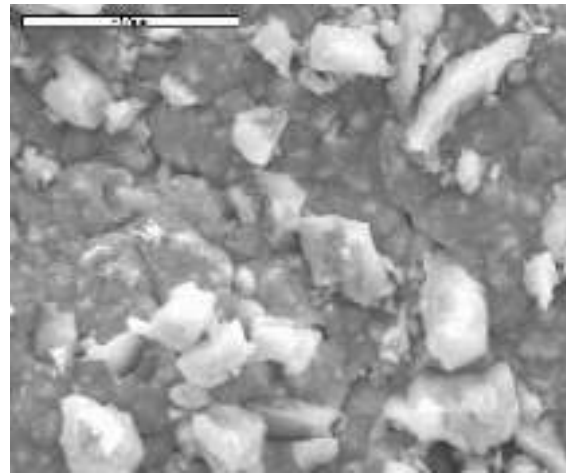
Fig. 6. *SEM Surface morphology of ZrO$_2$–Ni composite coating*
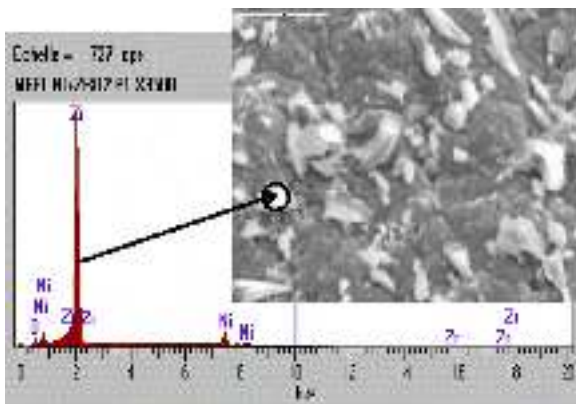
Fig. 7. *X-ray spectra analysis on a zirconium oxide (white) particle embedded in a nickel matrix*

(a)   (b)
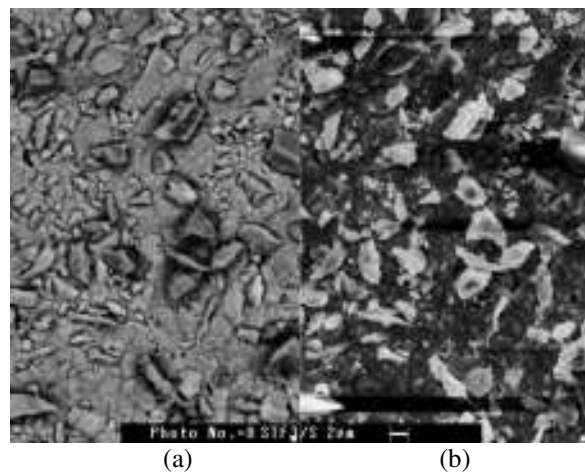
Fig. 8. *(a) Back - scattering SEM image; (b) Diffuse electron image*
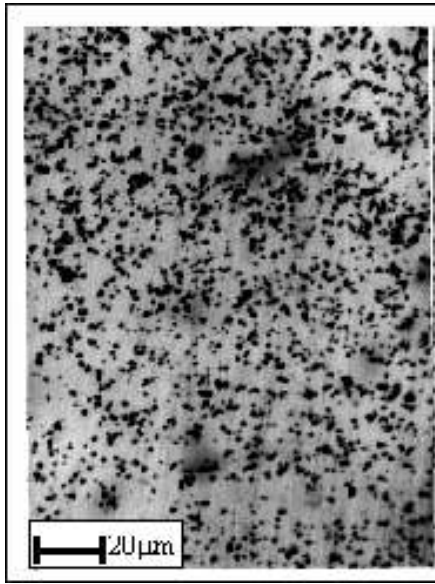
Fig. 9. *Optic microstructure of composite coatings with 8% ZrO$_2$. Cross section of the coating, magnification 500x*

On optic microscopy the zirconium oxide appear as black points and are uniform distributed inside of the composite coating. The corrosion and tribocorrosion properties of composite coatings could be improved comparative with pure nickel coating.

3.2. Microhardness of nickel – zirconia composite coatings

The microhardness of the plated layers of composite coatings have been determined by optic microscopy on the samples surface. The Vickers microhardness of zirconium oxide composite coatings comparatively to pure nickel electroplating is presented on Table 1.

Table 1. *Results of Vickers microhardness testing on pure nickel and nickel matrix composite coatings with ZrO$_2$ particles.*

Type of coating	Load grams	D$_1$ μm	D$_2$ μm	HV
Pure Ni	200	42.3	41.5	211
	100	24.9	32.4	226
	200	41.3	41.4	217
Ni+ ZrO$_2$ 20% mass.	300	25.4	27.1	808
	300	22.5	31.5	763
	300	26.9	26.7	775
Ni+ ZrO$_2$ 46 % mass.	300	20.5	29.0	909
	300	20.3	25.5	1059
	300	24.5	20.3	1110

3.3. Tribocorrosion studies

Open circuit potential measurements

This method gives information on the electrochemical state of a material, for example active or passive state. However, open circuit potential measurements provide limited information on the kinetics of surface reactions.

The open circuit potential recorded during uni-directional pin-on-disk sliding tests in which the disk is the material under investigation, is a mixed potential reflecting the combined state of the unworn disk material and the material in the wear track.

One must be aware that a galvanic coupling between worn and unworn parts on the disk surface may take place [12, 13, 14]. Consequently, the open circuit potential depends on the following parameters:

-The respective intrinsic open circuit potentials of the materials in worn and unworn areas. These open circuit potentials are different because the electrochemical state of the metal is disturbed by the removal of the surface films that may consist of adsorbed species, passive films, or corrosion products, in the sliding contact, and by a mechanical straining of the metal,

-The ratio of worn to unworn areas. In particular, if the extent of the worn area increases, the open circuit potential of the disk will shift depending on the controlling electrochemical processes, being either the anodic (e.g., the dissolution of the metal matrix) or the cathodic reaction (e.g., the reduction of hydrogen or dissolved oxygen),

-The relative position of worn and unworn areas. As a result of the galvanic coupling, a current is flowing between anodic and cathodic areas. The ohmic drop may induce a non-uniform distribution of potential and current density over the disk surface.

The measured open circuit potential is thus an average value depending on that distribution,

-The mechanism and kinetics of the anodic and cathodic reactions in worn and unworn areas.

The evolution of the open circuit potential is shown in Figures 10. The evolution of the open circuit potential was measured under unloaded and mechanically loaded conditions.

During the latency time, a competition between repassivation and dissolution occurs.

At the end of the periods of friction, during the stages of latency, the increase of E$_{OC}$ indicates the restoration of the passive film on the areas where it was removed by friction
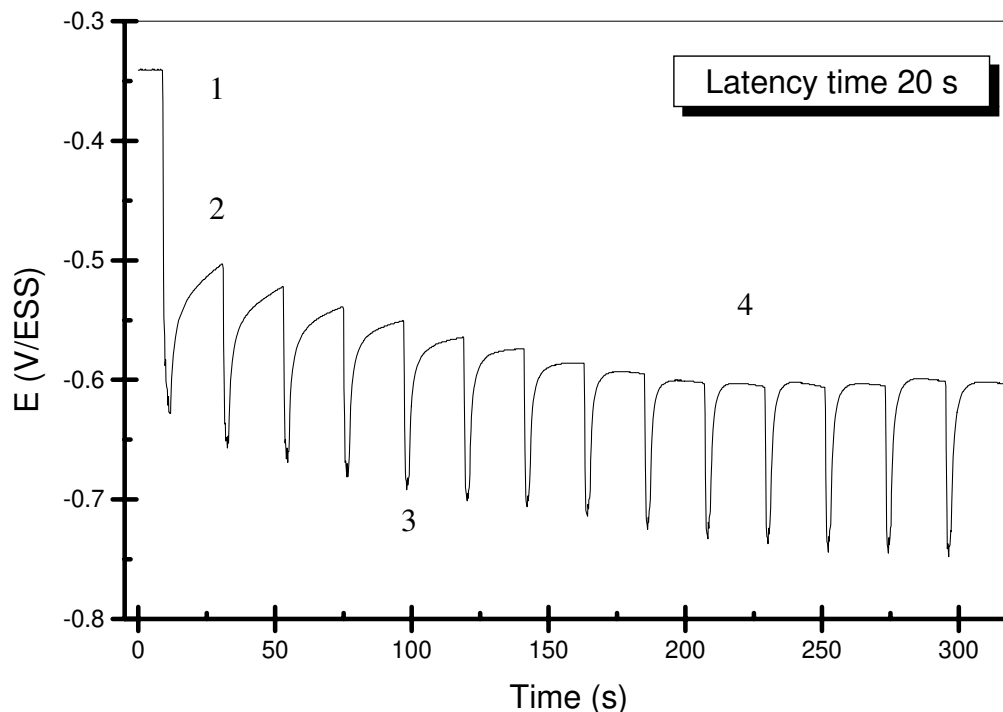
Fig. 10. *Variation of the open circuit potential of Ni-ZrO2 composite coating immersed in 0.5 M K$_2$SO$_4$ before (e.g. area 1 and 2), during (e.g. area 3), and after loading (e.g. area 4), during intermittent friction tests.*

Polarization diagrams

The polarization curves of ZrO$_2$-Ni composite coatings in 0.5 M K$_2$SO$_4$ were recorded under continuous friction (10 N; 120 rpm), and without applied friction, by direct potentiodynamic scan from the hydrogen evolution potential domain up to the beginning of transpassive dissolution domain. These curves are presented in Figure 11.

If the composite surface of the sample is not subjected to rubbing (black curve no rubbing), hydrogen evolution and oxygen reduction are the only reactions detected in the potential domain A. In domain B and C, the composite surface is passivated, the current remaining very small and the zero-current potential lying between -0.8 and -0.6 V/SSE. After domain C the anodic current must increases with the applied potential, revealing the dissolution of the alloy, induced by oxydation of the passive film, giving soluble species.

When friction is applied (red curve), the shape of the polarization diagram changes: hydrogen evolution on composite surface is not modified in domainA, but an anodic current of about 3 mA appears in the potential range from [-0.5 ; -0.3] V/SSE, indicating a dissolution of the coating. A first approch for interpreting the polarization curve under friction can be developed on the following considerations, based on a concept of "*active wear track*" [13].

The measured current, I can be considered as the sum of two partial currents I_t and I_p ($I=I_t+I_p$). I_t is the current originated from the wear track areas where the passive film is destroyed and metal is active, and I_p the current linked to the surface not subjected to friction and that remains in passive state.

-At the zero-current potential where I=0, a galvanic coupling is established. I_t and I_p are different from zero, and $I_p=-I_t$. These partial currents flow between the active wear track areas and the rest of the surface. On the wear track, where dissolution of the material and the formation of a new passive film occurs, I_t is anodic. On the remaining surface, I_p is cathodic and is related to reactions as dissolved oxygen reduction or hydrogen reduction.
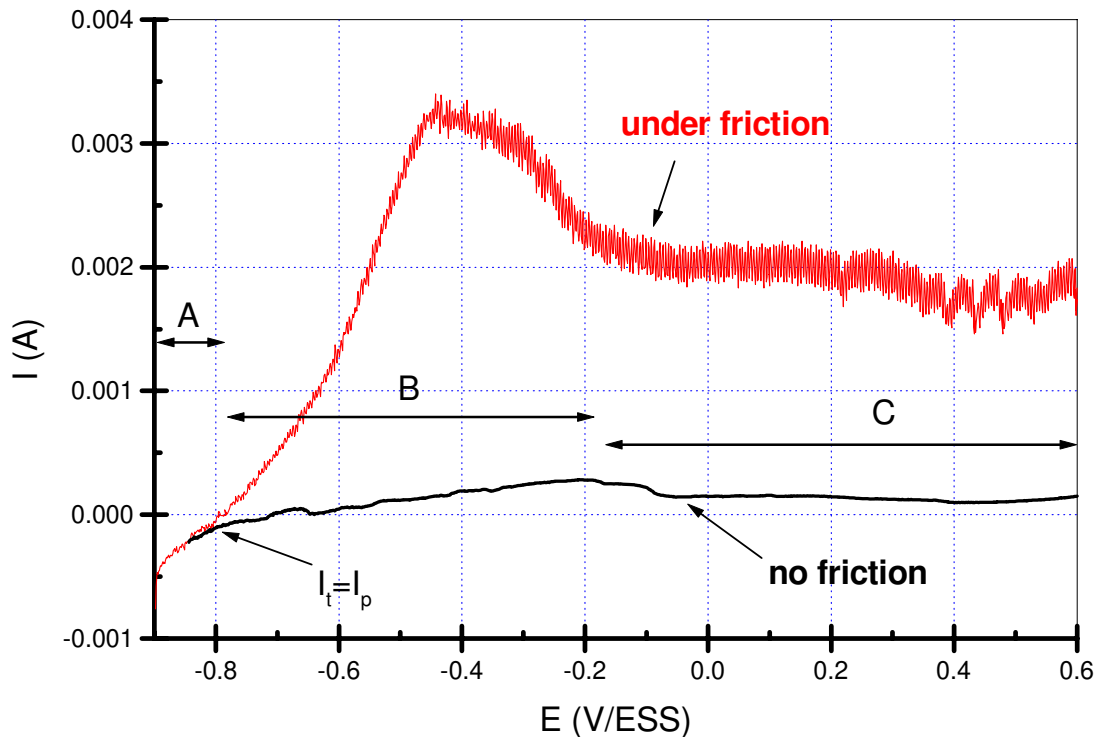
Fig. 11. *Potentiodynamic polarization curves of Ni-ZrO2 composite coating immersed in*
0.5 M K$_2$SO$_4$ recorded by direct potential scan at 0.1 V per minute.
Black Curve: no friction applied; Red Curve: continuous friction (10 N ; 120 rpm).

-When the potential increases, the galvanic coupling is broken and I_t is no longer equal to -I_p. Both I_t and I_p increase. As a result, the measured current I, flowing between the specimen and the counter electrode increases. On the surface not subjected to friction and in passive state, I_p can not exceed the value of the current measured at the same potential on the unrubbed specimen. By comparing the values of I in both conditions (see figure 10), it can be deduced that, under friction, I = I_t (from -0.78 to 0.6 V/SSE). The total current measured under friction and its evolution with applied potential, are characteristic of the behaviour of composite surface in the wear track. The steep increase of the current with potential around the zero-current potential, indicates that a rapid dissolution occurs in the wear track.

-The further decrease of the dissolution current above -0.3 V/SSE reveals the effect of repassivation in the active wear track. The rate of this reaction, occurring in the areas where the passive film is removed, increases with potential. This induces a lowering of the total depassivated area, and thus a decrease of the dissolution current.

Thus, polarization curves reveal the occurrence of depassivation and dissolution of the composite surface induced by friction in the wear track, and give the opportunity of quantitative measurements concerning the variation of the active wear track area with tribological parameters (normal load, sliding speed, etc.).

The depassivation of these areas along the wear track was interpreted as the result of the potential distribution generated over the surface of the specimen by the galvanic coupling between the anodic active wear track areas (having low specific corrosion potential) and the cathodic passivated surrounding surface (having higher specific rest potential).

SEM surface morphology after continuous and intermittent friction fretting

After triboccorosion tests the surface of samples was analysed by SEM and EDS systems. On Figs 12 and 13 there are the SEM images (at different magnifications) of wear track after continuous (Fig. 12) and intermittent friction (Fig. 13) tests with a

latency time of 20 seconds.

The chemical analysis after tribocorrosion tests on continous friction (FC) evidenced a different content of zirconium particles on the area near of the wear track compared with the wear track area. On the unrubbed surface the content of zirconium was 13, 07 % (mass percent) whereas inside of the track was around 22,18 %. This can suggest a preferential dissolution of nickel matrix on the surface in the narrow area along the trace.

The mechanical damage of the sample surfaces induces an activation of the metal structure, which is well described by the corrosion potential. However the trend with time shows a further increase in the corrosion potential towards more noble values. The equilibrium between the mechanical damage and the electrochemical processes at the metal surface needs some time to be reached. At the beginning, the mechanical wear induces a rapid deterioration of the protective surface layers, which causes a drastic decrease of the corrosion potential.

Narrow area along the track
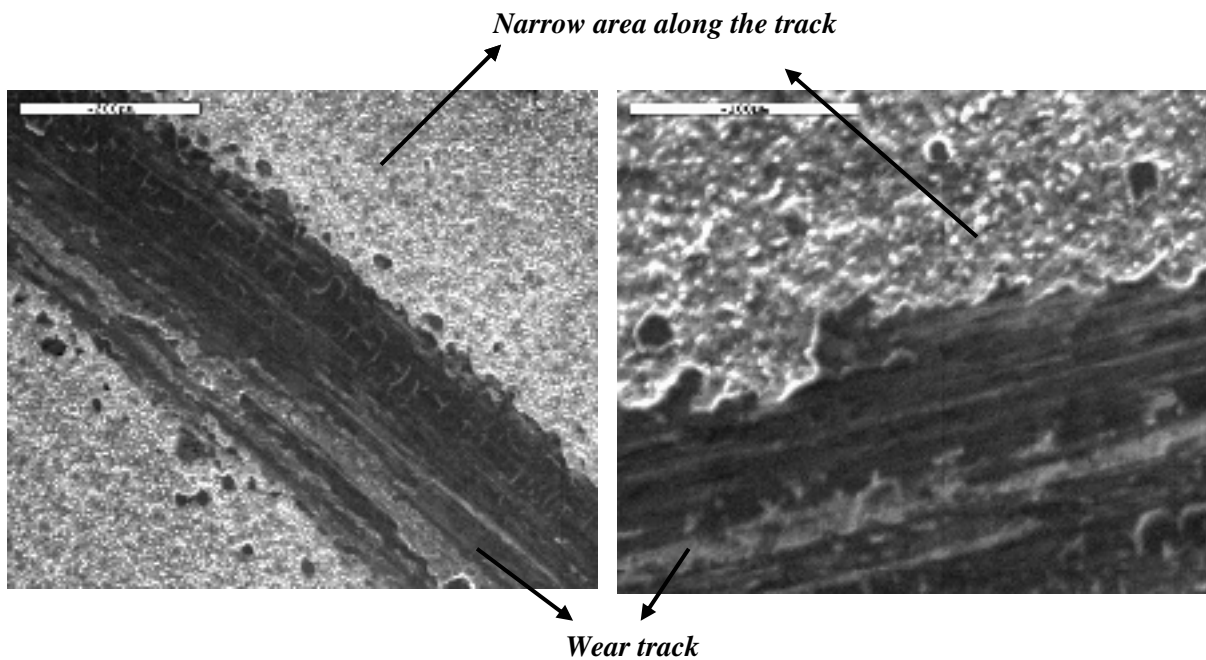
Wear track

Fig. 12. SEM Structure of composite surface after continuous friction tests (FC)

Fig. 13. SEM surface morphology of Ni-ZrO$_2$ composite coating after intermittent friction tests (latency time 20s)
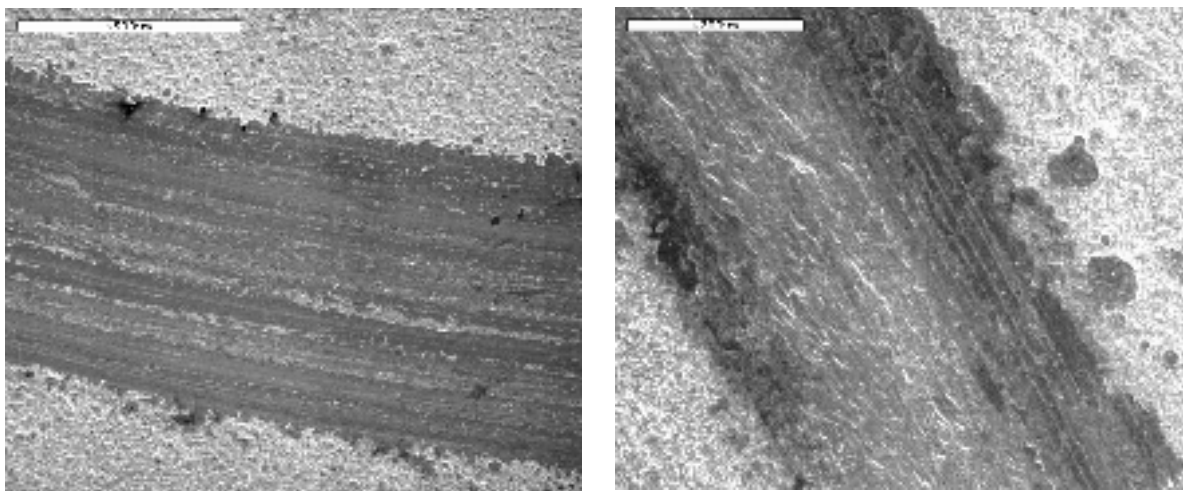
Microtopographic survey of the worn surface

Local wear in the wear track was also measured. It was deduced from surveys of the wear track recorded with an optical high resolution microtopograph, with a lateral resolution of 1 µm and a vertical resolution of 30 nm: the volume of the wear track was measured and the corresponding weight loss was calculated. On Figures 14 and 15 are presented a 3D surface and a profile measured after intermittent friction test on Ni-ZrO$_2$ composite coating.
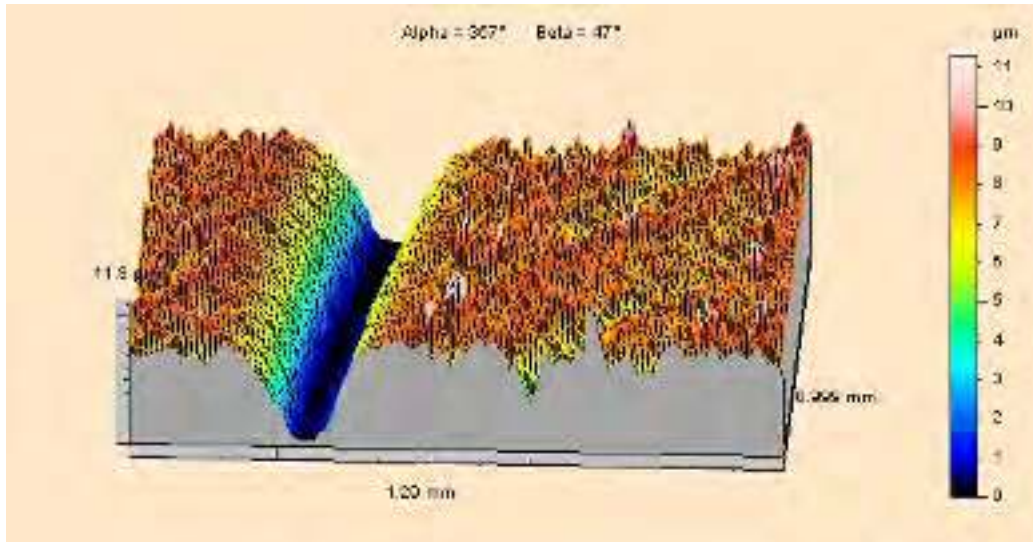
Fig. 14. *3D Microtopograph image of wear track area after intermittent friction (20s latency time) of Ni-ZrO$_2$ composite coating*

When a tribo-element is made of a ductile element such as Al, Cu, Ni, Fe or an alloy with a combination of them, material in the contact region plastically deforms severely under the combined stresses of compression and shear.

Large plastic deformation generally introduces large wear rate since wear surface tends to become rough and protective surface layers are easily destroyed. Scar surface profiles of pure Ni coating showed higher debris and higher roughness parameters [15].
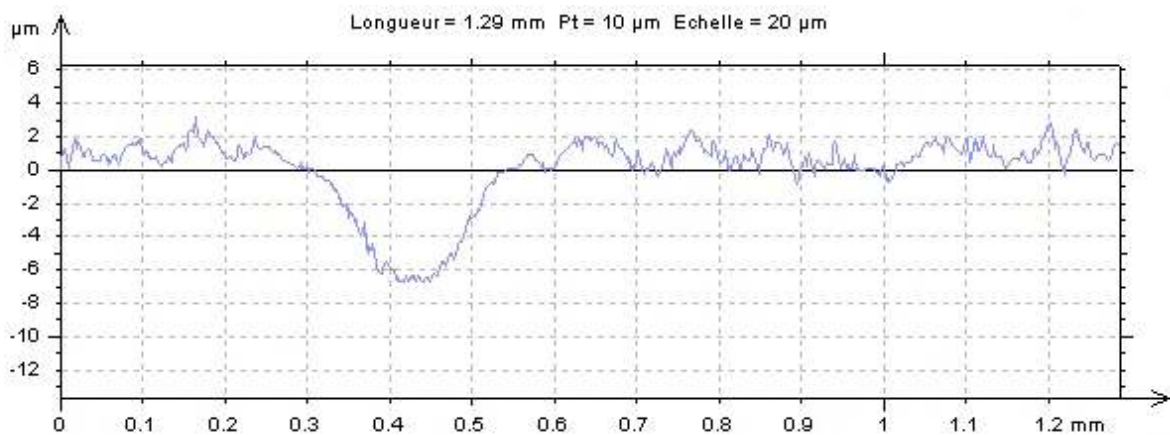
Fig. 15. *2D Microtopograph profile of wear track area after intermittent friction (20s latency time) of Ni-ZrO$_2$ composite coating*

Surface roughness parameters in the middle of the scar (mean value) presented in the paper [15] are: R_a= 8.19 µm; R_q= 9.67 µm; R_p= 28.50 µm; R_v= 29.50 µm. In the case of ZrO_2-Ni composite surface these values are under 1 micron as we can see on Fig. 15.

The introduction of a harder reinforcing phase in the ductile matrix by a certain volume fraction can reduce ductility of the matrix material in the contact region and wear of the matrix can be reduced as a result.

4. Conclusions

The tribocorrosion behaviour of Ni-ZrO_2 microstructured composite coatings in a pin on disk sliding system in 0.5 M K_2SO_4 solution was investigated combined with *in-situ* electrochemical (potential and polarization diagrams) measurements and *ex-situ* SEM –EDS and microtopographic surveys.

This overview points out the capabilities of electrochemical methods like open circuit potential measurements, polarization curves measurements, for the *in situ* investigation of materials used under tribocorrosive conditions in sliding contacts. They can provide not only essential information on the surface conditions of composite surface in sliding contacts, but also on the kinetics of reactions that control the corrosion component in the material loss during tribocorrosion tests.

Aspects of the tribocorrosion mechanism that can be clarified in this way are the nature of electrochemical reactions, the formation of protective passive surface films, the interactions between electrochemical reactions and friction. Information can also be gained on kinetics such as corrosion rate, rate of depassivation by mechanical action in the contact area, and rate of repassivation.

Nickel – zirconia microstructured composite coating is affected by a tribocorrosion process when subjected to intermittent friction in 0.5 M H_2SO_4. This tribocorrosion process involves mechanical destruction of the passive film on the contact areas by friction, and subsequent restoration of the film (repassivation) when friction stops.

The surface morphology of composite layers are different compared with pure nickel coating.

The surface structure is disturbed by dispersed particles. The crystal growth of nickel matrix result in a preferentially random than, in an oriented one.

Acknowledgements

References

[1].N. Guglielmi, *J. Electrochem. Soc*. **8**, 119 (1972) 1009-1012.

[2].L. Benea, P. L. Bonora, A. Borello, S. Martelli, F. Wenger , P. Ponthiaux, J. Galland; *J. Electrochem. Soc.*., **148** (7) C461-C465 (2001).

[3].Benea L., Bonora P.L., Borello A., Martelli S.; *Materials and Corrosion,* **53**, 23-29 (2002).

[4].L. Benea, P. L. Bonora, F. Wenger, P. Ponthiaux, J. Galland; "*Processing and Properties of Electrodeposited Composite Coatings: Results and Perspectives*", *KEY NOTE Lecture, CD-ROM Proceeding:* 15TH International Corrosion Congress -Frontiers in Corrosion Science and Technology, Granada, Spania, 22-27 Septembrie 2002.

[5].L. Benea, *Composite Electrodeposition -Theory and Practice*, Ed: PORTO FRANCO, Romania, ISBN 973 557 490 X, (1998).

[6].S. W. Watson; *J. Electrochem Soc*., **140,** 2235 (1993).

[7]. G. Maurin and A. Lavanant; *J. Appl. Electrochem*., 25, 1113-1121 (1995)

[8].J. Fransaer, J. P. Celis and J.R.Roos; *J. Electrochem. Soc*., 139, 413-425 (1992).

[9].J. Fransaer, J. P. Celis and J. R. Roos; *Metal Finishing*, 91, 97-100 (1993).

[10].L. Benea and G. Carac, *Metallurgy and New Materials Researches* V No 2, 1-19(1997).

[11].K. H. Hou, M.D. Ger, L.M. Wang, S.T. Ke, *Wear* **253** (2002) 994-1003

[12].R. Oltra, in "*Wear-Corrosion Interactions in Liquid Media*" edited by A. A. Sagües and E. I. Meletis, Minerals, Metals and Materials Soc. (1991) 3.

[13].Garcia, D. Drees and J.P. Celis, Wear, **249**, p.452-460 (2001).

[14].L. Benea, P. Ponthiaux, F. Wenger, J. Galland, D. Hertz, J. Y. Malo; *Wear, Special Issue Wear Modelling,*256 (2004) Issues 9-10, p. 948-953.

[15]. Benea, P. L. Bonora, A. Borello, S. Martelli; *Wear,* 249, Issue 10-11, Nov-2001, p. 995-1003.

RESEARCHES CONCERNING THE CORRELATION OF THE SEMIPLANETARY ROLLING PROCESS FACTORS

**Nicolae CĂNĂNĂU, Petrică ALEXANDRU,
Gheorghe GURĂU, Adriana PREDA**
Dunărea de Jos" University of Galati
e-mail: **cananau.nicolae.ugal.ro**

ABSTRACT

An available solution of the elimination of the superficial cracks network at the continuous cast slabs is the semiplanetary rolling. The application of a semiplanetary rolling mill at the exit of slab from the curve zone of the continuous casting machine leads at the slab unbending. For real constructive conditions of the geometry of casting machine, the establishing of the factors of semiplanetary rolling process, is necessary. The researches showed in this paper, worked at a lab semiplanetary mill, demonstrate that the bending of the linear body or the unbending of the curve body is possible. At the same time is establishing a correlation between the geometrical factors of body and the semiplanetary rolling factor – the relative reduction of thickness.

KEYWORDS: continuous casting, semiplanetary rolling, unbending process

1. Introduction

Semi-planetary rolling is an interesting deformation process. The rolling process is performed in a rolling stand mill consisting by a planetary cylinder and a massive cylinder what determines a non-uniform strain repartition into the thickness of rolled body [1].

The penetration of the satellite cylinder is much greater then the penetration of the massive cylinder [2].

The non-uniformity of the strain induces a compression stress field with the intensity of the stress greater in the proximity of the planetary cylinder and smaller in the proximity of the massive cylinder because the diameter of the satellite cylinder is much smaller then the diameter of the massive cylinder.

Consequently, into the deformation zone is developed a bending moment as result of the variation of the stress intensity.

This bending moment induces the curving of the deformed body or the unbending of the curved body.

An example of the semi-planetary rolling application may be the unbending of the continuous cast slab in the on-line regime.

Also, through the semi-planetary rolling may be worked curved pieces. The obtaining of the adequate quality of the rolled product the correct leading of the rolling process is necessary.

The factors of the semi-planetary rolling process (figure 1) are the reduction of the thickness, geometrical ratio b/h of the body, the radius R of the rolled product or the ratio R/h (we denote b the width h the thickness).
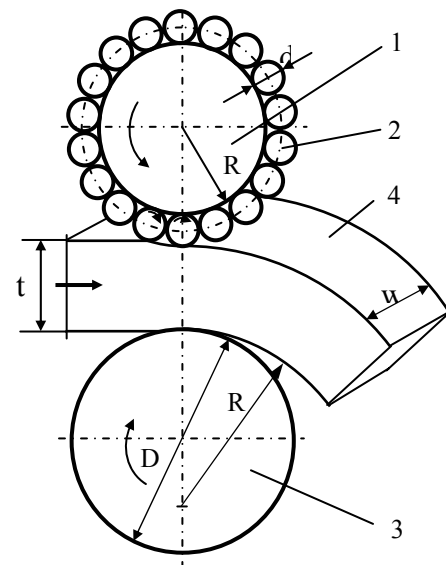
Fig. 1. *Scheme of semi-planetary rolling:
1-planetary cylinder, 2-satellyte cylinder,
3-massive cylinder, 4-semi-product.*

The paper objective is the establishing of the link among the relative thickness reduction and curvature radius for different values of the geometrical ratios of body. The establishing of this correlation is necessary to evaluate the practical possibilities of application of this procedure at the unbending process of continuous cast slabs.

2. Experimental conditions

The experimental researches have been effectuated at a semi-planetary rolling stand mill (fig.2) composed by a massive cylinder (diameter of 80mm) and a planetary ensemble, composed by 18 satellite cylinders (diameter of 12mm) and a support cylinder (diameter of 56mm). The length of the active surface of rolling cylinders is of 50mm.

In the aim of the simulation of semi-planetary rolling process the samples have been worked of lead. The dimensions of the samples are rendered in table 1. They were programmed for various values of the initial thickness and width, i.e. various values of the geometrical ratio b/h.

The experimental process consists in the measuring of the sample dimensions, programming the value of the thickness reduction, semi-planetary rolling and measuring of the effective value of thickness and radius of the rolled samples.

Table 1. *Dimensions of the samples, [mm]*

Length	Width	Thickness
100	10	6, 9, 13, 16
	20	6, 9, 13, 16
	30	6, 9, 13, 16
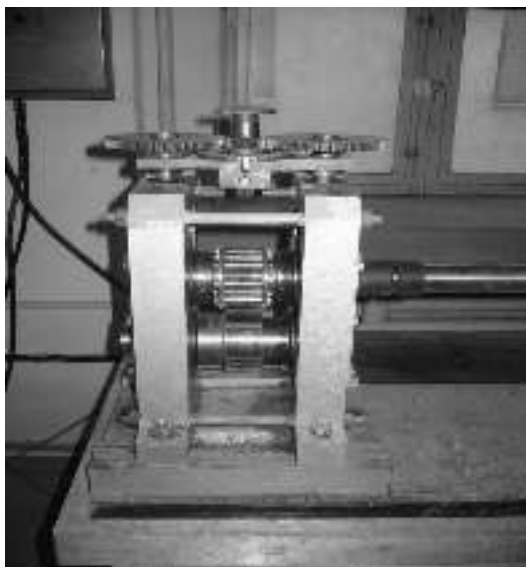
Fig. 2. *Semi-planetary rolling stand mill (experimental model).*

3. Results and interpretation

In figure 3 are showed some examples of semi-planetary rolled samples.
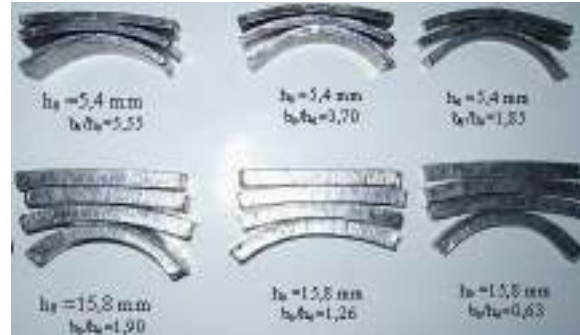
Fig. 3. *Semiplanetary rolled samples.*

The results of the experimental researches are systematized in graphic form in the figures 4, 5.

In figure 4 is showed the variation of the curvature radius of semi-planetary rolled samples, in absolute values, in the all cases of their geometrical factors, in function of the relative reduction of thickness.

In figure 5 is showed the variation of the ratio - curvature radius/initial thickness of semi-planetary rolled samples, in the all cases of their geometrical factors, in function of the relative reduction of thickness.
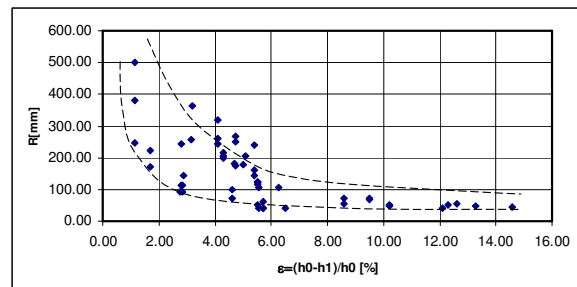
Fig. 4. *Variation of curvature radius with relative thickness reduction.*
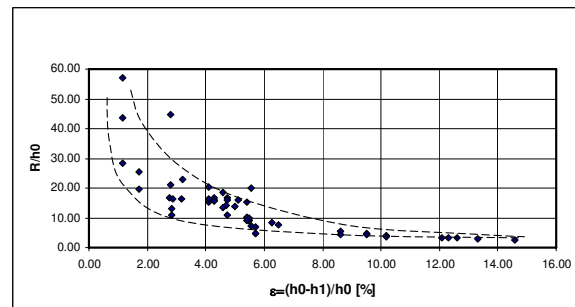
Fig. 5. *Variation of R/h_0 ratio with relative thickness reduction.*

It observes a smaller dispersion of experimental data in the second case, in case of small deformations as effect of the measuring precision of the curvature radius.

Consequently, the ratio *R/h* allows a better evaluation of the deformation degree (relative reduction of the thickness) what is necessary at the unbending of a continuous cast slab with a date curvature radius and date thickness.

4. Correlation of the results

The influence of the reduction of thickness on the curvature radius is certitude.

The increasing of the thickness reduction determines the adequate increasing of the curvature radius. For establishing a truthful correlation we made the refining of experimental data using a specializing soft (DATAFIT).

As result the regress equation has been established.

$$\frac{R}{h_0} = 41,89 \cdot \varepsilon^{-0,846} \cdot 1,05^{\frac{b_0}{h_0}} \quad (1)$$

The comparative representation of the experimental results and regression surface, conform the equation (1) as showed in figure 6.
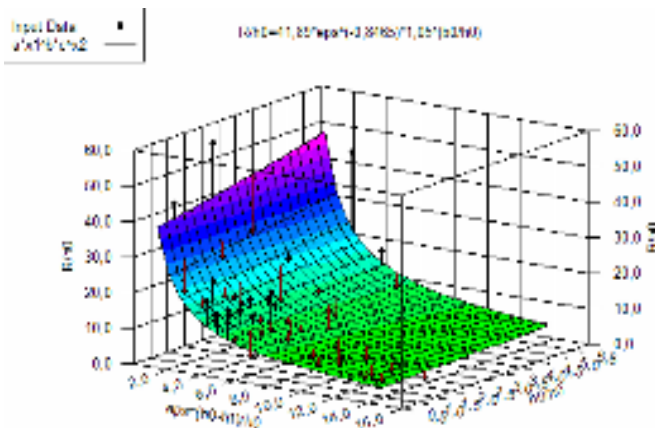
Fig.6. The regression surface.

The influence of the b/h ratio of the R/h ratio for different values of the relative thickness reduction is presented in figure 7.

Is evident the b/h ratio has grater influence for reduced values of deformation degree and at the greater values of R/h ratio (fig.7.)
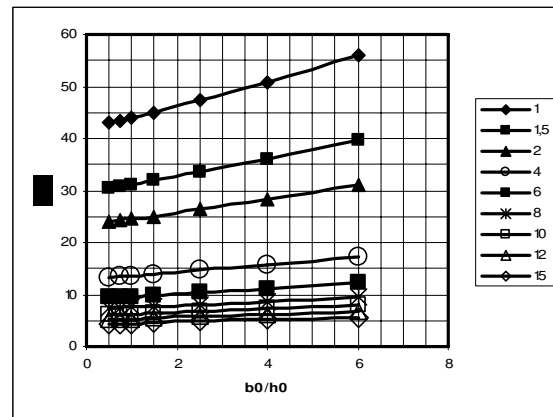
Fig.7. *The influence of the b/h ratio of the R/h ratio for different values of the relative thickness reduction.*

The variation of the R/h ratio with relative reduction of thickness (ε), is presented in figure 8. This graphic may be used at the evaluation of the deformation degree necessary for unbending of cast slabs.

Thus, for known R/h ratio and b/h ratio, in function of the geometry of continuous casting machine and geometry of crystallizer we can establish the value of the relative thickness reduction.
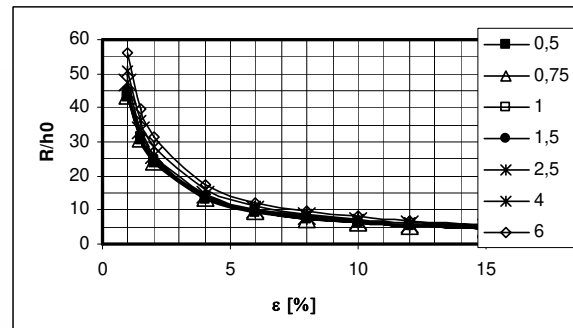
Fig. 8. *The variation of the R/h ratio with relative reduction of thickness (ε).*

5. Conclusions

The experimental researches demonstrated:

1. Semiplanetary rolling is a deformation method what induces a non uniform deformation in the thickness of rolled body. This phenomenon determines the curving or unbending of rolled body.

2. In case of semiproduct with certain value of geometric ratio b/h, in aim of obtaining a certain curvature radius by semiplanetary rolling the establishing an adequate value of relative reduction is necessary.

3.   Unbending a continuous cast slab may be realized by semiplanetary rolling selecting the adequate value of relative reduction correlated with geometrical ratio b/h and R/h ratio (R being the radius of curve thread).

4.   The researches demonstrated at the geometrical ratio b/h greater two in the body section is developed a plane deformation state. In this case the base factor for programming of semiplanetary rolling process is the thickness reduction.

Consequently the semiplanetary rolled may be applied at the exit of continuous cast slab of curve thread of casting machine in the aim of unbending with out tensile stresses.

This fact will have as effect the elimination of cracks on the superior surface of continuous cast slab.

Finally it will assure the quality of metallurgic products and decreasing of production costs.

References

[1]. **Wiesenfeld, D.**, 1999, "*Thread and form rolling - planetary (rotary) versus flat die machines*", Steel Time Intern., Sept. 1999.

[2]. **Anon**, 1995, "*Thin Hot Strip Using Planetary Mill*", Steel Time Intern., Sept. 1995, 33-35.

[3]. **Cănănău, N., Ivănescu, A.**, 2001, "*Study on the Relation between the Quality of Continuous Cast Slabs and the Surface Discontinuities of the Steel Thick Sheet*," 'International Conference on Advances in Materials and Processing Technologies", September 18-21, Leganes, Madrid, Spain, vol. 2, p.949-954.

[4]. **Cănănău, N., Gurău, G.,** 2005, "*Semi-planetary rolling process and experimental simulation*" Buletinul Institutului Politehnic Iasi, tom LI, Fasc.2, p.59-65.

[5]. **Moussy, F., Franciosi, P.**, 1990, "*Physique et mechanique de la mise en forme des metaux*", Presses de CNRS, IRSID, Paris.

[6]. **Gelin, J., Oudin, J., Ravalard, Y.**, 1984, "*Influence de quelques parametres metallurgiques sur la rupture ductile des acieres a bas de moyen carbone*", Mem. Et. Sci. Rev. Metall. 81.

[7]. **Cănănău, N., Ivănescu, A.,** 1999, "*Cercetari în vederea optimizarii procesului de turnare continua în scopul eliminarii fisurilor superficiale*". Universitatea din Galati.

[8]. **Cănănău, N.,** "*Cercetari privind comportarea sub tensiune a unor oteluri turnate continuu, la temperaturi de 850 - 1200 ^{0}C*". Contract de cercetare, Universitatea din Galați, 2002.

MERCURY DETERMINATION FROM INCIDENTALLY POLLUTED WATERS BY *COLLECTING GRAVIMETRY IN ORGANIC STAGE* METHOD

Olga MITOŞERIU[1], Dan T. LEVCOVICI[2],
Gabriela FILIP[2]

[1] „Dunărea de Jos" University of Galati
[2] S.C.Uzinsider Engineering S.A. Galati
e-mail: olga.mitoseriu@ugal.ro

ABSTRACT

Determination of mercury in incidentally polluted waters, presented in CALIST Program, was carried out using tiobis-β-naphthol as a reagent. The method proposed for mercury determination, named "collecting gravimetry in organic stage" is original, thus being superior to other simpler methods used in laboratory.

KEYWORD: Mercury, tiobis-β-naphthol, quantitative analysis, incidentally polluted waters

1. General considerations

Polluting by heavy metals is considered to be a major issue. Mercury concentration increasing in water is a consequence of both industrial pollution (specially by mineral derives) and agricultural one (organic-mercurial derives). In water, these derives decompose in organic products which progressively change in methyl-mercury, the simplest but the most toxic derive.

The methods for determination of mercury from waters, found in the technical literature, including those standardized, are laboriously, and require a large quantity of work intended for achieving of each stage. At the same time, they use different reagents as well as separation and shielding methods as a result of negative foreign water ions interference and sufficient non-specificity of reagents.

Researches carried out by CALIST program propose an original method intended for determination of mercury from incidentally polluted waters.

Therefore, tiobis-β-naphthol (proposed reagent) forms by Hg (II) insoluble compounds, both in water and in mostly usually solvents tested.

As a result of researches carried out it was settled that the reagent, dissolved in n-propyl carbinol, extracts these ions from solution as steady in time precipitates and constant chemical composition.

Method called "collecting gravimetry in organic stage" focuses a lot of qualities:

- The got precipitates are distinctly pure; so, tiobis-β-naphthol being soluble in n-propyl carbinol and the possibility of polluting the precipitate by reagent is excluded.

- Operation methodology suggested in this paper decreases very much each of gravimetry determination stages. In this way, determination methods proposed for copper (II), mercury (II) and lead (II) join the accuracy and simplicity of gravimetrical methods with analyses performing rapidity by other procedures;

- Metal exhaust from watery medium and adjusting the suitable pH increase the selectivity;

- Increasing the local precipitate quantity the reaction sensitivity enlarges very much. As a result of extraction, the metallic ion from diluted solution is lumped in a small solvent volume, therefore, getting the conditions of reaching the solubility product and so the precipitation.

- solubility of precipitates formed in n-propyl carbinol is smaller than in partly watery solvents; the smaller dielectric constant decreases the dissociation degree and therefore the solubility.

2. Determination of mercury in waters

The suggested method intended for mercury determination is selective; in running conditions given in the paper, Hg(II) only precipitates. Therefore, it proves to be better then other usual methods applied in laboratory.

2.1. Required conditions for operation mode set up

> *Compound raw formula set up*

As compound between tiobis-β-naphthol and Hg (II) was discovered by the professional university staff, several additional researches were required to set up its structure and formula in order to be used in chemical analysis. Aiming this goal the researches given below were performed.

a) Hg (II) ion forms together with tiobis-β-naphthol a yellow colored compound in acid medium, a few soluble in water and in usually solvents. When tiobis-β-naphthol dissolves in n-propyl carbinol this one has the capacity of exhausting the Hg (II) ions from watery solutions and forms a light yellow precipitate in organic solvents.

It is supposed that a neutral compound by general composition forms:

$$[HgR_n \cdot (m-n) \, HR]$$
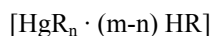
with extraction equilibrium described by equation:

$$Hg_{ap}^{n+} + m(HR)_o \rightleftharpoons [HgRn \cdot (m-n)]_o + n[H^+]_{ap}$$

where:

HR corresponds to the reagent with the raw formula :

$$C_{20}H_{13}O_2S$$

ap index – watery phase;
o index – organic phase.

In order to set up the Hg (II) exhaust by tiobis-β-naphthol using n-propyl carbinol as water non-miscible solvent, the experimental and calculation model was used in case of extraction system by chelate compounds.

Therefore, it was set up that Hg (II) extraction by tiobis-β-naphthol at pH = 1 – 2 is made based on the following equilibrium.

$$Hg_{ap}^{2+} + 2(HR)_o \rightleftharpoons (HgR_2)_o + 2H_{ap}^+$$
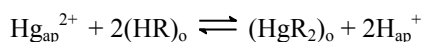
b) The precipitate formed in organic phase was separated, washed by acetone and dried in air. Chemical analysis emphasized a new compound forming with raw formula: $Hg (C_{20}H_{13}O_2S)_2$.
Its results are shown in table1.

Table 1

Chemical analysis	C [%]	H [%]	S [%]
Calculated	57.31	3.14	7.68
Experimentally found	58	3.20	8.01

> *Influence of pH*

Following the variation of repartition coefficient and exhaust percentage implicitly, depending on pH value, it may be noticed that for ratio C_{HR}/C_{Hg}^{2+} = 10/1 (where: C_{HR} – reagent concentration in organic phase and C_{Hg}^{2+} - Hg^{2+} ion concentration in watery phase), the extraction percentage increases by pH. A larger exhaust percentage than 99% is obtained beginning with pH = 1.7 (fig.1).

Practically quantitative extraction, as a steady composition precipitate of Hg^{2+} ion existing in watery solution, suggested the idea of using this operation system in order to set up a separation method of Hg^{2+} ion from these watery solutions and gravimetrical processing of the extract obtained.

$$C_{Hg}^{2+} = 1,2 \cdot 10^{-3} \, m \, / \, l$$

$$C_{HR} = 1,6 \cdot 10^{-2} \, m \, / \, l$$
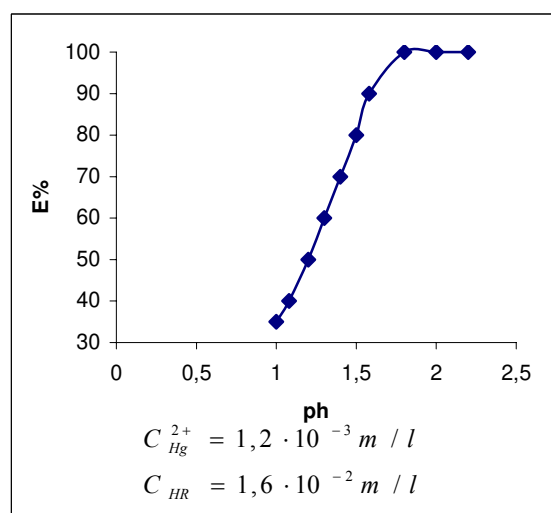
Fig. 1. *Variation of the exhaust percentage by the watery phase pH.*

> *Temperature influence*

In order to characterize the compound obtained with mercury, intended for use in quantitative analysis by the proposed method (collecting gravimetry in organic stage), the heating behavior was studied by derivative-graphical analysis.

Thermal-gravimetrical study made in dynamic temperature conditions by steady heating speed allowed to get some information about thermal stability of the investigated combination , chemical composition and thermal decomposing kinetics.

At the same time, as a result of experiments, it was set up that at 102ºC the compound (mercury tiobis-β-naphthol) begins to decompose; so, drying in the oven will be made up to 90ºC, that is enough temperature to eliminate the acetone used as flushing agent.

2.2 Checking the proposed method – experimental

Operation mode. The following will be supplied in a 250 ml separation hopper: 100 ml solution to be analyzed brought to pH = 1 ÷ 2 which contain a known quantity of mercury ions (2.4÷3.4 mg Hg^{2+}), 10 ml solution of reagent in n-propyl carbinol, $1.6 \cdot 10^{-2}$ mole/l (5.088 g tiobis-β-naphthol / l), 5 ml solution of potassium nitrate 1 n, 2 ml buffer solution, then 5 minutes stirring. After phases separation, the precipitate got in organic solvent is filtered on vacuum spout by G_4 filtering crucible.

Precipitate traces which remain sticky on the hopper walls will be entirely passed in crucible helped by 2-3 stirrings and washing by acetone. The crucible with precipitate dries in oven for approx. 10 minutes at 80 ÷ 90 ºC temperature, cools down in special vessel and is weighed.

Experimental determinations proved that compound formation and extraction are performed in high speed, therefore, in order to settle down the equilibrium, a few minutes are sufficiently.

Total precipitation checking is traced by repeating the extraction operation from watery solution, separated from the first solution.

Using for extraction 10 ml solution of tiobis-β-naphthol in n-propyl carbinol, $1.6 \cdot 10^{-2}$ mole/l respectively, good results got for a precipitate weighed in 0.0100 ÷ 0.0160 g range.

Experimental determination are alike the provisions made, the lower limit being conditioned by analytical balance accuracy where the weighting were performed, and the upper limit of maximum reagent solubility in n-propyl carbinol, being that one required for providing the ratio C_{HR}/C_{Hg}^{2+} = 10/1 (where: C_{HR} – reagent concentration in organic phase and C_{Hg}^{2+} - Hg^{2+} ion concentration in watery phase), favorable for extraction and precipitation.

In order to calculate the accuracy of gravimetrical method the procedure of comparison of pair samples was used. This procedure may be used also for adjusting a new method, making determinations in a wide range of concentrations and comparing the pair values, "the found" value against 'the taken" one– exactly known.

In conclusion, the precipitate with formula HgR_2 got by this method is pure, has a steady composition and may be processed by quick gravimetric determination. The gravimetric factor (f = M_{Hg}/M_{HgR2} ; f = 0.2401 respectively) is convenient for this kind of determinations. The method offers very good selectivity and small execution time.

Filtering and washing of precipitate, separated in a small volume of organic solvent is quickly, and thus allows the performance, in a short time of large watery solution volumes having small mercury content (II). For example, at 10/1 phases ratio,

mercury (II) may be separated and determined, with good results, from 0.02 mg/l concentration solutions.

2.3 The method application - mercury determination from incidentally polluted waters

Usually, mercury from natural waters is either lacking or may be found in small concentration (< 0,1 µg/dm³). The danger of increasing the mercury concentration in water is due to both industrial and agricultural pollution. The permitted mercury limit allowed in industrial and domestic waste water exhausted in natural receivers, according NTPA–001/2002, is 0.05 mg/l. Because of this, it was required to determine the mercury even in small quantities, in water, in order to prevent some incidentally contamination.

In case in which the mercury quantity from analyzed sample is beneath 0.02 mg/l the *additions method* will be used, which is often used in chemical analysis practice of element traces.

Operation mode. In order to apply the method proposed in hereby stage, a reaction is made previously for mercury ion identification in water.

In a 500 ml separation hopper a necessary and sufficiently water analyzing volume is feed (depending on the probably mercury content in water) which is noted as V_1. Solution is brought to pH = 1 ÷ 2 and 10 ÷ 50 ml solution of reagent in n-propyl carbinol, $1.6 \cdot 10^{-2}$ mole/l (5.088 g tiobis-β-naphthol / l), 5 ml solution of potassium nitrate 1 n and 2 ml buffer solution are added and stirred for 5 ÷ 10 minutes.

After the phases separation, the precipitate got in organic solvent is filtered in vacuum spout by G_4 filtering crucible. The precipitate traces which remain sticky on the hopper walls will be entirely passed in crucible, helped by 2-3 stirrings and washing by acetone. The crucible with precipitate dries in oven for approx.10 minutes at 80 ÷ 90 ºC temperature, cools down in special vessel and is weighed.

● *Calculation of mercury quantity from analyzed sample*

$$X_{Hg} = 1000 \cdot p \cdot f / V_1 \ [g/l]$$

where: f – gravimetric factor, p = 0.2401;

p – precipitate quantity got, g;

V_1 – water volume taken in sample

The method was checked on two samples where known quantities of Hg (II) together with ions of Ag(I), Pb(II), Fe(II), Ca(II), Ba(II), Mn(II), Mg(II) and Cu(II) were added and which form chemical compounds with tiobis-β-naphthol but not at pH used for determination of Hg(II).

The compound formed by Fe (III), at pH = 2, is extracted in n-propyl carbinol but is soluble; for the excessive reagent used, it does not prevent the

mercury (II) determination up to the ratio Fe(III)/Hg(II) = 10/1 studied.

Statistically processing of experimental results (table 2) got on samples with known composition shows that the proposed method is accurate ($t_{exp} <$ $t_{95\%;9}$) and is not affected by systematically errors (table 3 for specimen 1 and table 4 for specimen 2).

The real mercury content, in samples that simulate a polluted water, frames in the experimentally determined trusty range limits.

Table 2

Sample code	Average content (mg Hg/ sample)	
	Specimen 1	Specimen 2
n_1	2.90	3.86
n_2	2.92	3.78
n_3	2.89	3.80
n_4	2.86	3.94
n_5	2.82	3.82
n_6	2.85	3.88
n_7	2.94	4
n_8	3.02	3.72

Table 3

Statistical parameters	Parameter	Analyzed sample
		Specimen 1
Real content (mg Hg/sample)	A	2.95
Number of determinations	N	8
Average content (mg Hg/ sample)	$\overline{x}$	2.9
Dispersion of selection	S^2	0.0038
Standard deviation	S	0.616
Quadratic average error of mean selection	$S_{\overline{x}}$	0.02177
t_{exp}	t_{exp}	2.29
$t_{p\%}$ k = (n-1)	$t_{95;7}$	2.37
Individual values spreading	$\overline{x} \pm \Delta X$	2.9 ± 0.141 (3.041 – 2.759)

Table 4

Statistical parameters	Parameter	Analyzed sample
		Specimen 2
Real content (mg Hg/sample)	A	3.83
Number of determinations	N	8
Average content (mg Hg/ sample)	$\overline{x}$	3.85
Dispersion of selection	S^2	0.008

Standard deviation	S	0.09
Quadratic average error of selection mean	$S_{\overline{x}}$	0.0318
t_{exp}	t_{exp}	0.629
$t_{p\%}$ k = (n-1)	$t_{95;7}$	2.37
Individual values spreading	$\overline{x} \pm \Delta X$	3.83 ± 0.056 (3.886 - 2.774)

where:

$$\overline{x} = \frac{\sum_{i=1}^{n} x_i}{n} ; \qquad S^2 = \frac{\sum_{i=1}^{n}\left(\overline{x} - x_i\right)^2}{n-1}$$

$$S = \sqrt{S^2} ; \qquad S_{\overline{x}} = \frac{S}{\sqrt{n}}$$

$$t_{exp} = \frac{\left|A - \overline{x}\right|}{S_{\overline{x}}} ; \quad \Delta x = \pm t \cdot S$$

$$\Delta x = \pm t \cdot S_{\overline{x}}$$

2.4 Conclusions

• A solution of tiobis-β-naphthol in n – propil carbinol extracts Hg (II) from watery solution; in organic phase, a pure steady precipitate forms with well defined composition .

• The obtained compound may be processed by „collecting gravimetry in organic stage". Filtering and washing the precipitate, in a small volume of organic solvent, are quickly and allow, in a short time, lumping of mercury from large volumes of watery solutions.

• Extraction and variation of pH allowed to increase the sensitivity and selectivity of determination.

• The method was applied for quickly analyzing of Hg (II) from incidentally polluted waters.

References

[1]. **Mitoşeriu O.**, 1980, „*Doctor's degree thesis*", Jassy Polytechnic Institute.
[2]. **Seracu Dan I.,** 1989, "*Analytical chemistry reference book*", Technical Publishing House, Bucharest
[3]. **Ceauşescu D.,** 1982, „*Use of mathematical statistics in analytical chemistry*", Technical Publishing House, Bucharest
[4]. **Liteanu C.,** 1964, „*Volumetric quantitative analytical chemistry*", Didactic and Pedagogic Publishing House, Bucharest
[5]. **Odochian L., Mihai E., Fişel S., Mitoşeriu O.,** 1981, Rev. Roumain Chim. R.S.R, 26, 3, p. 383.
[6]. **Mitoşeriu O., Hartopeanu A., Cioroi M.,** 2001, „ *Analytical chemistry. Separation and identification of cations*", Ed. "Ars Docendi" University from Bucharest , ISBN (973-8118-51-4)
[7]. **Holzbecher Y., Divis L., Kral M., Lucha L., Vlacil F.,** 1979**,** „*Organiceschie reagenti v neorganicescom analize*", Izd., Mir, Moscova, p 427.

INDUSTRIAL ELECTRON-BEAM EQUIPMENT ON BASE OF NOBLE AND NON-FERROUS METALS

**N.GRECHANYUK, P.KUCHERENKO,
P.SHPAK,G.KROITORU**
Kiev National University of Building and Architectures
Kiev, Ukraine

ABSTRACT

Method of obtaining of metals and alloys by melting – is basic. By this way make in practice the majority of metals, alloys and ligatures. The essence of a method is, that in special melting device (furnace) to melt metal or basic component of an alloy and overheat it. After that, to liquid will add alloying elements in solid or liquid condition. Temperature of liquid lead up to necessary level, make metallurgical processing (refining, modifying), and then alloy spill to the foundry forms or crucible.

KEYWORDS: electron-beam equipment, noble and non-ferrous metals.

Depending on purpose of metals and alloys necessary degree of cleanliness, economic reasons connected to reduction of losses of metal and the charge of fuel (electric power), character of initial materials and their physical-chemical properties them make by the following ways:

a) direct melting of pure metals and elements;

b) by joint restoration of components of alloy (ore-thermal melting);

c) by electrolyze of liquids or solutions;

d) by replacement of one element by another element (thermal-metallic);

e) by diffusion's way with use firm, liquid and vapor of substances;

f) by the combined way with application two-three above-stated.

Method of obtaining of metals and alloys by melting – is basic. By this way make in practice the majority of metals, alloys and ligatures.

The essence of a method is, that in special melting device (furnace) to melt metal or basic component of an alloy and overheat it. After that, to liquid will add alloying elements in solid or liquid condition.

Temperature of liquid lead up to necessary level, make metallurgical processing (refining, modifying), and then alloy spill to the foundry forms or crucible.

In quality of scrap's materials for manufacture of metals and alloys by the melting's method use as pure metals, and re-scraps, secondary metals and alloys, ligatures. High efficiency and opportunity of reception of high pure alloys, impurity from metal- and non-metal inclusions (oxides, gases, slag) with the strictly certain chemical structure both necessary physical-chemical and mechanical properties - basic advantages of this method way.

Preparation of liquid carry out in melting's devices (furnaces) of various designs. The widest application now have open melting's furnaces working at atmospheric pressure and environment. Thus quality of metal liquid and its chemical composition depend on processes occurring in melting furnaces:

1) heating and melting of metals;

2) boiling and evaporation ;

3) interaction with oven gases;

4) interaction of metals with inner surface of furnace. Thus one of the named processes are necessary for reception of metals and alloys, others are extremely undesirable, as are accompanied by an intoxication of components, oxidation, pollution of liquid by not metal inclusions and gases. For translation of metal from solid state to liquid it is necessary to spend quantity of heat (energy) determined by melting point temperature, thermal-capacity and latent heat of melting.

Thus the various sources of heating and, accordingly, various melting furnace and equipment are used. Also more and more wide application find in practice use re-melting processes of special electric metallurgy, in particular vacuum. The comparative characteristic of methods of melting of metals and alloys are given in table 1.

Table 1. *Comparative characteristics of different method of metal's melting*

Method's name:		Furnace's environmental	Input materials:	Refining environmental	Method of ingot's obtaining
full	short				
open melting in burning furnace	OM	air, products of fuels burning	scrap, re-scrap, (pure metals and alloys), ligatures	slag	casting (foundry) to the form or crucible
open melting in electrical resistive furnace	OM	air		slag	
open induction melting	OIM	air		-	
open arc melting	OAM	air		slag	
plasma melting in ceramic crucibles	PM	protective (Ar)		slag	
vacuum-induction remelting	VIR	vacuum		vacuum	
vacuum-arc remelting	VAR	vacuum	spending electrode	vacuum	solidification in crucible
electric-slag remelting	ESR	air		slag	
electron-beam remelting	EBR	vacuum	spending electrode, scrap	vacuum	
plasma-arc remelting	PAR	protective (Ar)		-	

From analysis of the data, given in the table 1, follows, that for reception of high-quality metals and alloys of high purity (especially refractory) certain advantages and prospects there is use of the method electron-beam melting.

Also it is necessary to emphasize complete ecological safety of realization electron-beam melting, as all processes thus occur in vacuum without contact with environment.

The basic lacks of a method limiting its wide circulation, are: difficult of melting of metals with high elasticity pair; relative dearness of the equipment and its limited productivity.

Today Research-production enterprise "GEKONT" has a wide experience of development, introduction and application of technology electron-beam melting of metals and alloys, and also industrial equipment for realization of technological processes. In particular, the technologies electron-beam melting chromium and aluminum bras, alloys on nickel basis, and also platinum are developed.

The characteristics of industrial electron beam installation B 5 for melting of noble metals developed in "GEKONT" is given in table 2. The scheme and general view of this facility are showed on figure 1.

The equipment represents the vacuum technological chamber with connected to it by horizontal mechanisms of scrap's loading and withdrawal of ingot. The facility is equipped with three EB-heaters with independent control by each. It allows to carry out of melting under the circuit with use of intermediate capacity, that, in turn, allows effectively and separately to operate processes of scrap's melting, overheating and refining of liquid in vacuum, their solidification in copper vater-cooling crucible and formation of the ingot.

***Table 2.** Technical parameters of the EB-melting unit B 5*

No.	Technical parameters:	
1	Total power, kW	280
2	Accelerating voltage, kV	20
3	Input voltage, 50 Hz (3 phases), V	380
4	Quantity and power of EB-heaters, n x kW	3 x 100
5	Level of vacuum, Pa	1×10^{-2}
6	Discharge of cooling water (15°C), m^3 per hour	8
7	Pressure of cooling water, Pa	$3\text{-}4 \times 10^5$
8	Diameter of melting ingots, mm	74
9	Maximal length of melting ingots, mm	500
10	Velocity of ingots withdrawal, mm/min	0.15-300
11	Maximal size of re-melting billet, mm	150x130x500
12	Velocity of billet's feeding, mm/min	0.15-300
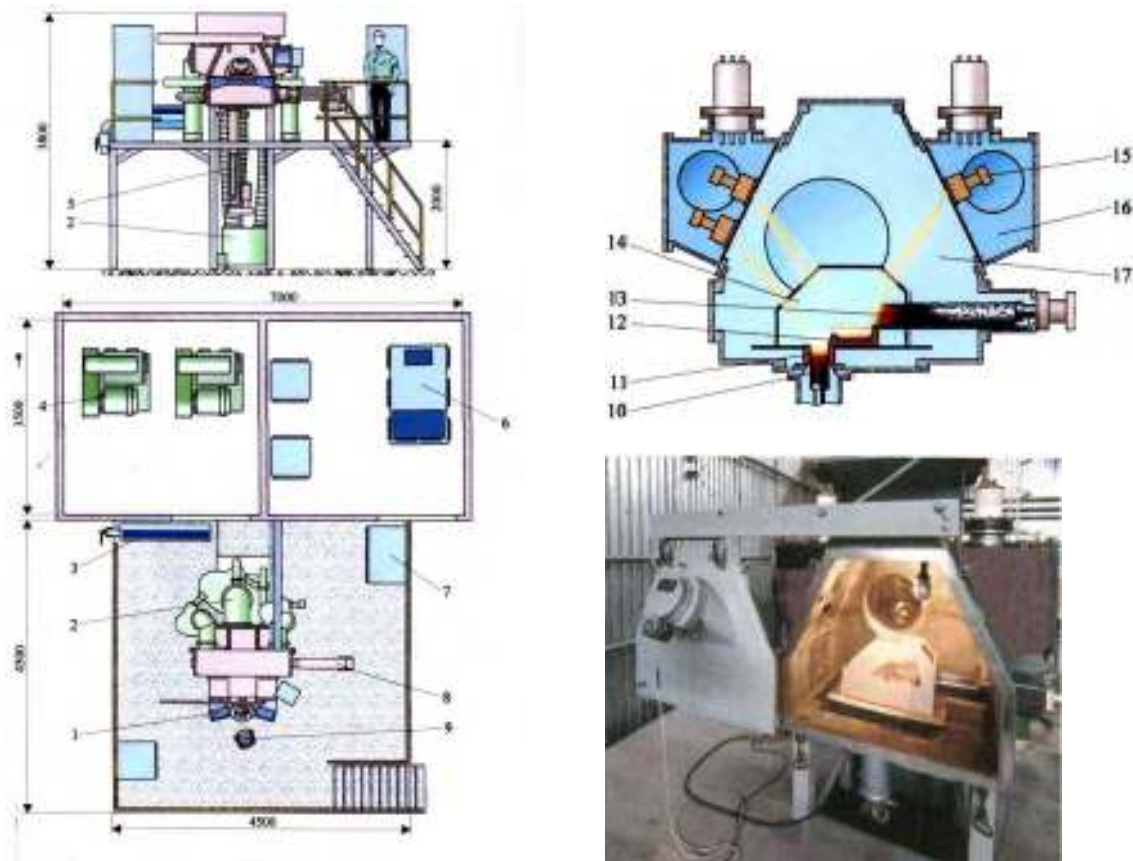
***Fig. 1.** The scheme and photo of EB-melting unit B 5. The EB-facility is equipped
by automatic system of registration of technological parameters of melting.*

References

[1]. **Schiller S., Heisig U., Panzer S.** *Elektronenstrahltechologie.* - VEB Verlag Technik: Berlin, 1976.

[2]. **Choundhury A., Hengsberger E.** *Electron Beam Melting and Refining of Metals and Alloys.* / ISIJ International, Vol. 32 (1992), No. 5, pp. 673-681.

THE AUTHENTIFICATION OF OLD BRONZE COINS AND THE STRUCTURE OF THE ARCHAEOLOGICAL PATINA

Ion SANDU[1], Florin DIACONESCU[2], Ioan Gabriel SANDU[2], Adrian ALEXANDRU[2], Andrei Victor SANDU[3]

[1] "Al.I.Cuza" University of Iasi, Department of Cultural Heritage
[2] "Gh. Asachi" Technical University of Iasi
[3] Romanian Inventors Forum

ABSTRACT

This paper presents comparative results concerning the chemical composition and mineralogical distribution of the main compounds from the structure of the archaeological patina of ancient bronze coins, which were determined by the corroboration of microchemical, IR spectrophotometry, SEM/EDAX and Colorimetric methods. The stratigraphical distribution of the chemical components in the structure of patina is caused by the pedological processes from the archaeological sites and which represents main elements used in the authentication of ancient bronze artifacts.

KEYWORDS: ancient bronze coins; pedological transformation; primary, secondary and contamination patina; archeological patina; stratified structure; authentication elements

1. Introduction

Coins and other metallic numismatic pieces often have various casuistic of *preservation state* and can be taken as valid samples for experimental analyses during the research activities. Except the *treasures* made of noble metals, the pieces made of other metals have the disadvantage of a precarious preservation state, in the worst case of *pre-collapse* – as the pieces with a very thin metallic bulk that merely preserves their shape – or of *collapse* – when the metallic bulk is completely absent and the shape can't be recognized, their authentication being almost impossible [1-7]. Among these, those made of **ancient bronze** have a *very complex composition* of the corrosion products, resulted from the reactions with *corrosion agents* (of chemical, electrochemical or microbiological nature), or by *contamination*, during the various *pedological processes* (*disgregation, segregations, cementations, monolithisations, recrystallizations etc.)*. The most important problems arise for the *pieces without metallic bulk*, that during the *preliminary classification* in the yard (excavation place) were destinated to the „grey fund", in the most of cases abandoned. At the present, these pieces are a very important source of information, often being unique proofs of a technique or metallurgical tradition/period.

According to the previous studies [1-7], for the pieces of ancient bronze, both the ones with metallic bulk and the ones without it, coming from disturbed sites or not, three types of products can be differentiated in the structure of the archaeological patina: the first ones resulted from the corrosion processes, the other ones from the acid-base processes, mainly through hydrolyses and ionic exchange, and the last ones from the processes of contamination (diffusion, segregation, deposition, etc.). These products are formed in different tapes, being characteristic to certain types of patina: the oxides and sulphides, formed since the utilization period, constitue *the primary patina*; the halogenides, oxyhydroxides, carbonates, sulphates, phosphates etc., resulted in the last period of utilization and in the first step of pedological period, define the *secondary patina;* finally those resulted from physical processes of diffusion-segregation-deposition-recrystallization are forming the *contamination patina*.

Their study allows the explanation of the inner mechanisms of formation but also the evaluation of some chronological parameters, that offers a series of elements used in authentication, such as: alloy's nature, mineral's type, technology (elaboration of the alloy and of the coin), provenience of the coin (period and place of creation), way and period of utilization and other data concerning the „time's emprint" [8, 9]. The continuous stratigraphical deepness of the site in time, from the surface, where the action of the climatic, microbiological and antropological agents is strong and cyclic, to the internal zones, where the aerobically or anaerobically conditions of the soil

alternates and the oxygen and water in soil have oscillations in time creating another different system of cyclic variation, has a very important role in the structuring of the corrosion products, of the ionic exchange or contamination products.

The last cyclic processes, although occur with a very slow rate during centuries, provoque important structural modification of the ancient patina of an object, creating a stratigraphical distribution of the three groups of products. The cyclic property of the pedological processes determine the characteristic stratification of the three patinas, that can be easily put in evidence through known stratigraphical methods.

If we compare the microstratigraphies of the archeological patinas of two coins coming from different sites - one non-disturbed and with low humidity, almost constant, and the other site situated in an area with a great mobility of subterranean water and a complex chemism - we observe the stratigraphical distribution, under the form of deposits of products specific to the three types of patina: primary, secondary and of contamination (fig. 1a) for the first coin and a deposition of the micro-crystals, not uniform in the volume phase of the archaeological patina for the second coin (fig. 1b).
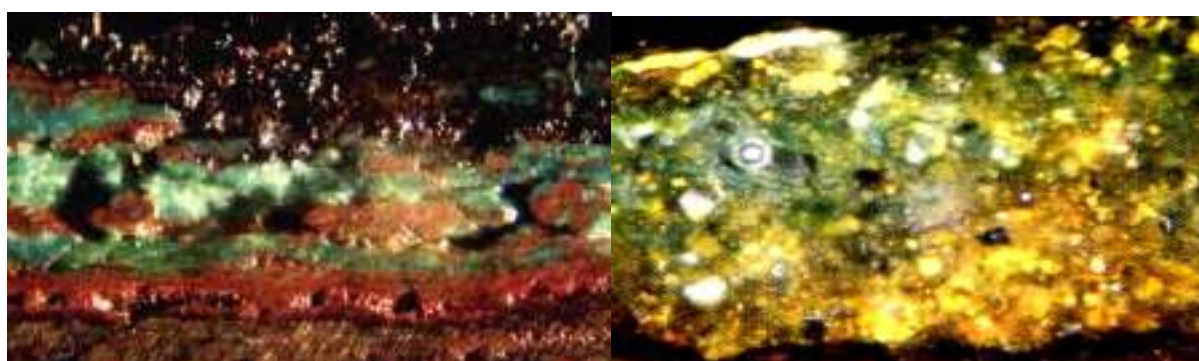
Fig. 1. *Microstratigraphical structure of the archaeological patina:*
a – patina for the coin coming from an archaeological non disturbed site and with low humidity;
b – patina for the coin coming from an archaeological site with a fluctuant chemism provoqued by the abundant subterranean water.

If in the case of a non-disturbed site, we can easily draw up structural-phenomenological correlations for chronological evaluations, for the second one, the study of the parameters implied in such correlations requires complex analyses through co-assisting systems or corroboration of new methods and techniques, of great resolution.

So, the stratigraphical morphology of the most of the archaeological patinas of the ancient bronze pieces have a *sandwich* structure, characteristic to the *Liesegang effect* [9], in which the layers of primary patina are overlapped or partially interposed with the ones of the secondary patina. The layers of contamination products, formed during chemical chronological processes that occur in the heterogeneous systems liquid-solid, with a sequential formation of products with characteristic morphology, are also named „*Liesegang rings*". In the case of bronze coins, the primary patina contains layers of *cup rite* or *cuprite/tenorite* and *sulphides*, the secondary patina of *malachite/azurite,* overlapped or alterned with layers of *athacamite/parathacamite and brochantite/anthlerite* and of contamination products*: ankerite, gypsum, silicates and caolinite*

interposed with *cassiterite*, resulted from the segregation and diffusion processes in the inferior layers.

The paper studies the comparative chemical and mineralogical distribution for two bronze coins of the byzantine period - one with metallic bulk and the other one without it - with the help of *modern methods of microstratigraphical analysis*, such as: microchemical tests, IR spectroscopy, SEM/EDAX and reflection colorimetry, that allow the determination of chronological characteristics used for their authentication.
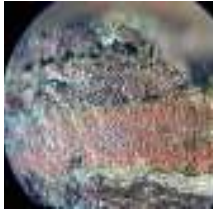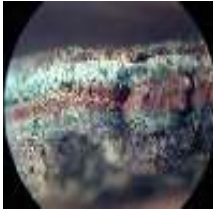
2. Experimental

2.1. Coins taken into study

The study was done on two ancient coins (IV-V century) – M1 and M2 - discovered in the archaeological site Nufărul, Tulcea county, in 2000, initially classified for the *grey fund*; one of them conserves the metallic bulk and the other one is without it.

The table 1 gives the images and the shape of the two coins, together with the microstratigraphy of the sections in the break and polished, observed with the optical microscope at a magnifying power of 40X.

Table 1. *State and aspect of the coins and metallic bulks*

	Image of the coin	Shape of the coin	Cross-section in break/polished (40X)	State of the metallic bulk
M1		Flat, thick		Thick, affected by corrosion after the removal from the site; advanced segregation processes with holes and fissures between phases
M2		Flat, thick		Thick, discontinuous, sponge shape, strongly affected by corrosion after the removal from the site; nonuniform distribution of the pores and small holes

2.2. Micro-chemical and stratigraphical analysis

Both the cross-sections and the surfaces of the coins were analyzed by optical microscopy using a OLYMPUS CX21 microscope under reflected light (Vis), followed by micro-chemical tests.

The micro-photographies were taken with an OLYMPUS C990zoom digital camera, adapted to the microscope.

The nature of the corrosion products and of the contaminants was established by micro-chemical reactions on surfaces or cross-sections, in a native state or after mechanical or chemical cleaning (nital attack).

The nature of the structural components of the corrosion products and contaminants, formed in concentrated areas as beautifully colored crystals, was directly attributed, based on color and crystallographic system [9].

2.3. Colorimetry by reflection

The colorimetric study was done by selecting on the surface of the coins the areas with corrosion products and the area with an uniform passivated patina.

A digital colorimeter with two types of optical devices (based on optical fibers) with different illumination geometries and observation angles, coupled with a computer with which the values R G B of the CIE colorimetric triangle were established. The analyzed areas were covered with *mylar* (PET), foreseen of small holes that delimit the measuring areas.

The number of 3-5 points is corresponding to the comparison areas (basic alloy and patina). In each point the transducer was positioned directly on the material, protecting in this way its color from the contact.

Because the colorimetric analysis was applied on a non-shining surface, with rough areas, using the same light spot projected in one point, 3-5 determinations were done, in order to eliminate the errors of the measure.

The colorimetric calculation was done on the average spectrum of each point, for which the

standard deviation was successively determined. It has to be said that the analyzed areas were first cleaned with aqueous and alcohol solutions and for the alloy a side area with active corrosion was chosen for being treated with nitric acid (40%) in order to remove the corrosion layer from the metal.

After the nital attack with acid, the coin was attentively cleaned with water and acetone and afterwards desiccated on filter papers.

2.4. IR Spectroscopy

The IR analysis was done using fine dispersed samples as KBr pellets. The IR spectra were registered in the field of 200-4000 cm^{-1}, using a SPECORD M80 Carl Zeiss Jena spectrophotometer [10 - 14].

2.5. Scanning Electron Microscopy and Xray Spectrometry (SEM/EDAX)

Scanning Electron Microscopy was done with an electron microscope HITACHI S2600N with EDAX spectrometer, with two functions:

- Image analysis with secondary electron detector (SE): resolution: up to 4.0 nm;
- Element mapping with energy dispersive x-ray spectrometer (EDAX): up to 8 elements simultaneously are displayed and automatically overlaid.

The present study was done at an accelerating power of 15,0 kV, in the field of magnifying orders of 250-300x, with the distribution mapping of 8 elements from the surface composition of the two coins [15].

3. Results and discussions

As we saw, during the deposition in an archaeological site, the metallic pieces degrade and deteriorate, under the action of two types of pedological processes [19 - 23]:

- *chemical interactions* (chemical, electrochemical and microbiological corrosion; ionic exchange; hydrolyses; carbonatations; phospatations, etc.), that lead to *surface products* creating the *primary and secondary patinas*;

-*physical-mechanical interactions* (osmosis, segregation, recrystallization, hydration/dehydration of physically-bounded water, monolithysation, deposition, erosion, deformation, fessuration etc.), among which the physical ones lead to *contamination products* as adherent deposits, that are called *contamination patina*.

Both the products of the first two patinas and those of the contamination patina, are subject in time to various processes, with formation of new phases, that can be used for a chronological evaluation. From these points of view, the differentiating analysis of the compounds resulted from the primary and secondary patina and of those from the contamination patina, indicates important clues in the authentication of ancient metallic artefacts.

The formation of heavily soluble compounds as consequence of the chemically charged subterranean or meteoric waters actions leads to contaminations with uniform dispersion in the volume phase of the surface layers of compounds, as in the case of double salts.

There is also another series of processes, such as monolithisations, that can create zonal concentrations of contamination products, easily determined through instrumental methods, such as in the case of cassiterite.

The metals with a pronounced amphoterous character, such as Sn and Pb, by transformation in saline oxides, acquire the capacity of ionic exchange, forming masked deposits of mixed products (saline oxides) resulted from corrosion and by contamination, being hardly observed by optical methods.

3.1. Mineralogical composition of the surface structure of ancient bronze coins

3.1.1. Micro-chemical qualitative analysis

During the formation of the *archaeological patina* each metal of the ancient basic alloy (copper, zinc, tin, lead, iron etc.) forms specific products resulted from pedological processes and the bronze coins are characterized by a great number of mineral species, that are given in the table 2. The chemism of these products is quite well differentiated, in function of *exogeneous* agents, related to the climatic environment, to the site's place and its agressive character etc., but also of the *endogenous* ones, related to the alloy elaboration, to the originary mineral and the metallurgical technology.

Analyzing data from the table 2, it can be observed that from a mineralogical point of view and as concentration and distribution of the products in the volume phase of the archaeological patina is concerned, there is a correlation for the two coins – with a basic alloy made of Cu, Sn and Pb – subject to redox processes with formation of Cu(I), Cu(II), Sn(IV), Pb(II), Pb(III) oxides and Cu(I), Sn(II) suplhides and afterwards to acid-base processes with formation of hydroxycarbonates, hydroxyhalogenides and hydroxysulphates and finally to processes of contamination with gypsum, calcite and quarz.

Table 2. *Chemical compounds determined by IR spectroscopy and XRD*
in the corrosion products and contaminants

Mineral phase	Chemical formula	Color and aspect	Density (g/cm^3)	Relative Molar Volume	M1	M2
Cup rite	Cu_2O	Brick-Red, with gray-brownish or yellowish to orange tones	6,00	1,67	++++	+++
Tenorite	CuO	Black-gray to brown	6,40	1,75	+++	++
Calcocite	Cu_2S	Pb-like gray, with metallic brightness	5,60	1,99	+	++
Tin sulphid	SnS	Black	5,22	1,77	+	++
Malachite	$CuCO_3 \cdot Cu(OH)_2$ or $Cu_2(OH)_2CO_3$	Green, with a characteristic vitreous aspect	4,00	3,88	+++	+++
Azurite	$2CuCO_3 \cdot Cu(OH)_2$ or $Cu_3(OH)_2(CO_3)_2$	Dark blue	3,88	4,16	+	++
Athacamite	$Cu_2(OH)_3Cl\ nH_2O$ or $CuCl_2 \cdot 3Cu(OH)_2 \cdot nH_2O$	Emerald-green with more or less dark tones in function of n and with a vitreous aspect	3,75	5,32	++	+++
Cassiterite	SnO_2	Shiny white	6,95	1,33	+	++
Minium	Pb_3O_4	Red	9,10	1,37	++	+++
Gypsum	$CaSO_4 \cdot 2H_2O$	White-gray	2,32	2,84	+	++
Quarz	SiO_2	Translucid gray	2,653	1,94	+	++
Calcite	$CaCO_3$	White-gray	2,71	1,43	+	++

3.1.2.Colorimetric analysis by reflection

Based on the experimental results of microchemical analysis, regarding the chemical nature of the corrosion products mainly as beautifully colored minerals, the areas for the colorimetric analysis by reflection were selected under an OLYMPUS CX21optical microscope (fig. 4).
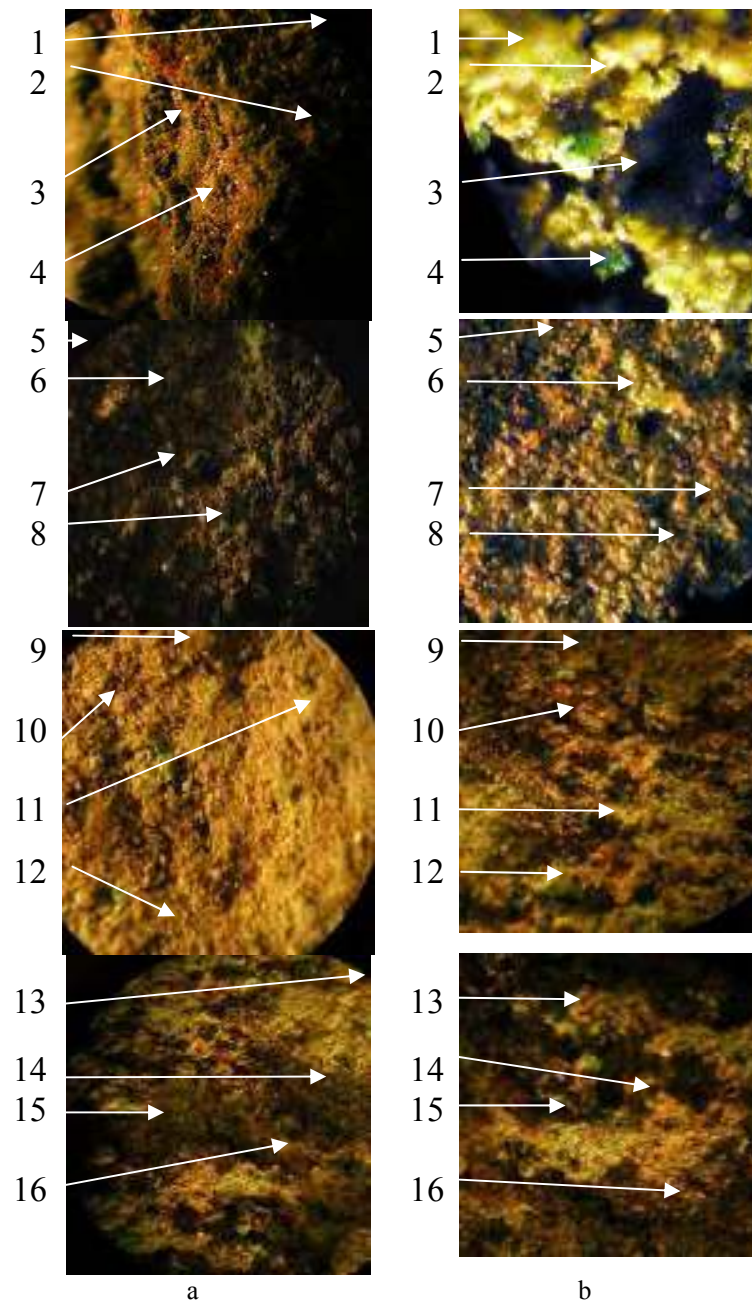
Fig.4. *Sampling areas for the colorimetric analysis: a – M1, b – M2*

The points selected for analysis are represented by mineralogical entities more or less unpurified, both during the corrosion processes and by contamination after the pedological processes (recristallizations, dehydrations, segregations, osmoses, carbonations, sulphations, chlorination etc.).

The colorimetry has the advantage that allows a punctual analysis of the color of the microcrystallites. In this respect, the mineralogical phases, studied also with other methods, were identified in their major part (table 3).

Table 3. *The colorimetric results (RGB) for the minerals in the structure of the patina analyzed by groups of coins*

Nr. crt.	Mineral	M1			Mineral	M2		
		R	G	B		R	G	B
1	Quartz	231	241	123	Calcite	231	246	57
2	Cup rite	137	52	8	Malachite	75	140	14
3	Malachite	64	126	22	Malachite	58	117	51
4	Cup rite	141	47	6	Calcite	251	241	109
5	Anglesite	106	83	0	Cup rite	211	55	0
6	Gypsum	246	258	142	Cup rite	215	82	15
7	Tenorite	214	107	27	Calcite	255	236	209
8	Calcite	211	181	61	Quartz	216	157	39
9	Tenorite	182	102	6	Minium	220	125	41
10	Cup rite	192	65	18	Tenorite	175	88	9
11	Gypsum	247	253	152	Calcocite	125	114	22
12	Cup rite	151	47	0	Tenorite	160	116	7
13	Gypsum	244	252	120	Malachite	84	108	24
14	Cup rite	181	52	17	Thin sulphide	32	54	12
15	Tenorite	186	107	12	Cup rite	142	68	17
16	Cup rite	139	58	7	Gypsum	240	251	115

3.1.3. Analysis through IR spectroscopy

Figure 5 gives the IR spectra for the two coins taken into study and the table 3 attribute the fields of characteristic group vibrations to the predominant chemical species from the composition of the archaeological patina. In this case, a certain similitude can be observed for the two coins.
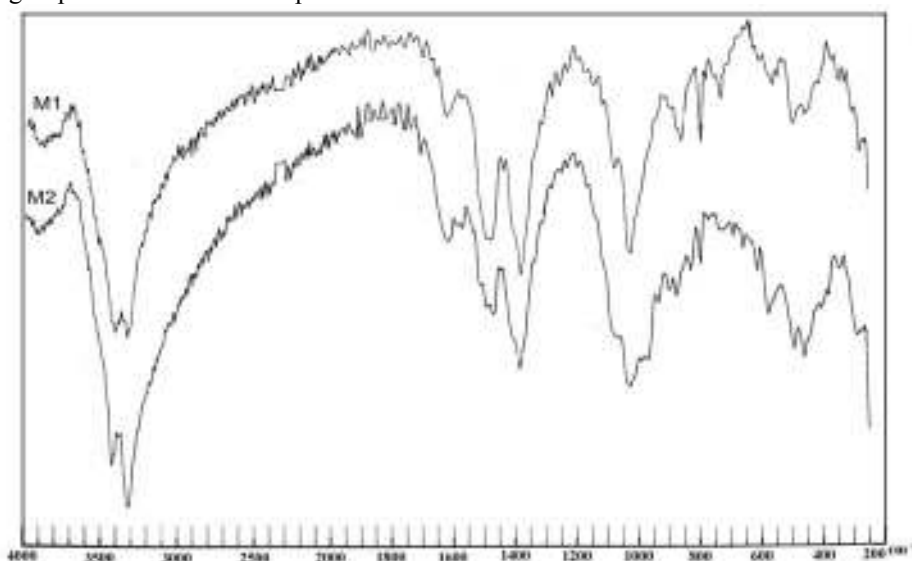
Fig. 5. *IR spectra of the two coins.*

Table 4. *Characteristic group vibrations for the main chemical species*

Sample	Mineral	Predominant species	Characteristic vibrations of group (cm^{-1})
MA1	Sulphide/Stannate Cuprite Tenorite Silico-aluminate Athacamite/Parathacamite Quartz Malachite Gypsum Malachite	S^{2-} / SnO_3^{2-} Cu_2O CuO SiO_3^{2-} / AlO_2^{-} SO_4^{2-} SiO_2 CO_3^{2-} $CaSO_4 \cdot 2H_2O$ HO^{-}	270 – 310l, 330l, 400s, 500s, 790m, 800l, 1050vs, 1100s 1400p, 1500s, 1610s, 3370p, 3450s
MA3	Sulphide/Stannate Cuprite Tenorite Silico-aluminate Athacamite/Parathacamite Quartz Malachite Gypsum Malachite	S^{2-} / SnO_3^{2-} Cu_2O CuO SiO_3^{2-} / AlO_2^{-} SO_4^{2-} SiO_2 CO_3^{2-} $CaSO_4 \cdot 2H_2O$ HO^{-}	250 – 270m 330s, 400s, 500s, 630p, 850m, 1000p, 1050s, 1100s, 1400p, 1500s, 1640s, 3350s, 3450s

Intensity of vibration: vs. – very strong, s – strong, m - medium, l – law, str – straight, br – broad.

3.1.4. SEM-EDAX analysis

SEM microscopy put in evidence for the two coins a rough structure on their surface, non-homogeneous, with uneven relief and microfessures, and mineral deposits resulted from depositions and monolithisation but also from segregation in the volume phase.

The coin M2 has many pores and micro-crystals non uniform distributed on the surface.

On the same surface area where the SEM microphotography was taken, EDAX microanalysis was done, the results indicating the presence, together with copper, of some other alloy elements of the originary minerals specific to the ancient bronze, such as Pb, but also of anions resulted from corrosion and ionic exchange processes, such as carbonates, sulphates and chlorides and the contamination products based on Si, Ca, K, Mg.

The difference between the two coins consists of a different distribution of the elements specific to anions and contamination products.

Analyzing the comparative distribution of atoms in the surface structures, it can be done a clear distinction between atoms from alloy and those resulted from corrosion and ionic exchange or the ones of contamination. The first ones have an uniform distribution (Cu, Sn, Pb, Cl etc.) but the other ones have a zonal concentration (Si, Ca, Al, Cl etc.).

The apparent uniformity in the distribution of atoms of Ca and Cl is explained as effect of segregation, ionic exchange and insolubilization under the form of double salts.
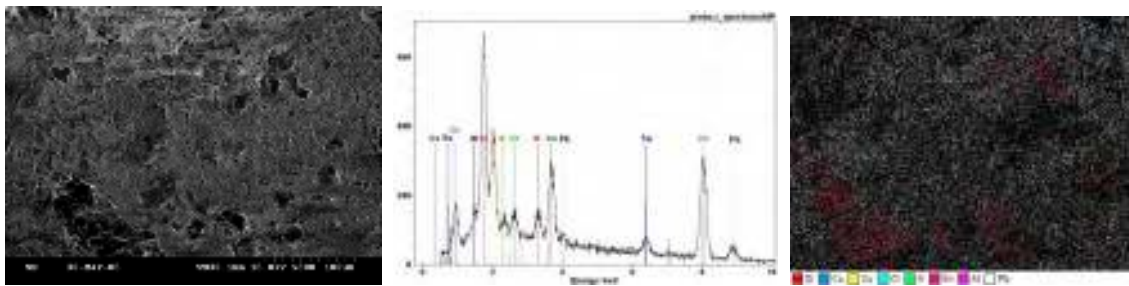
Fig. 6. *SEM microscopy coupled with EDAX microanalysis for coin M1*
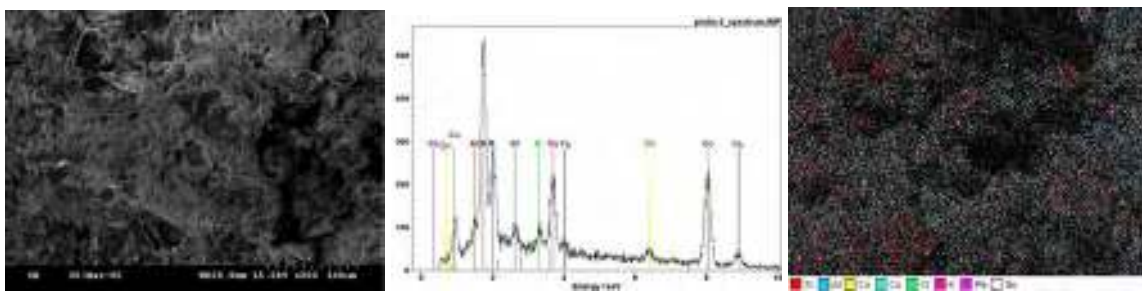
Fig. 7. *SEM microscopy coupled with EDAX microanalysis for coin M2*
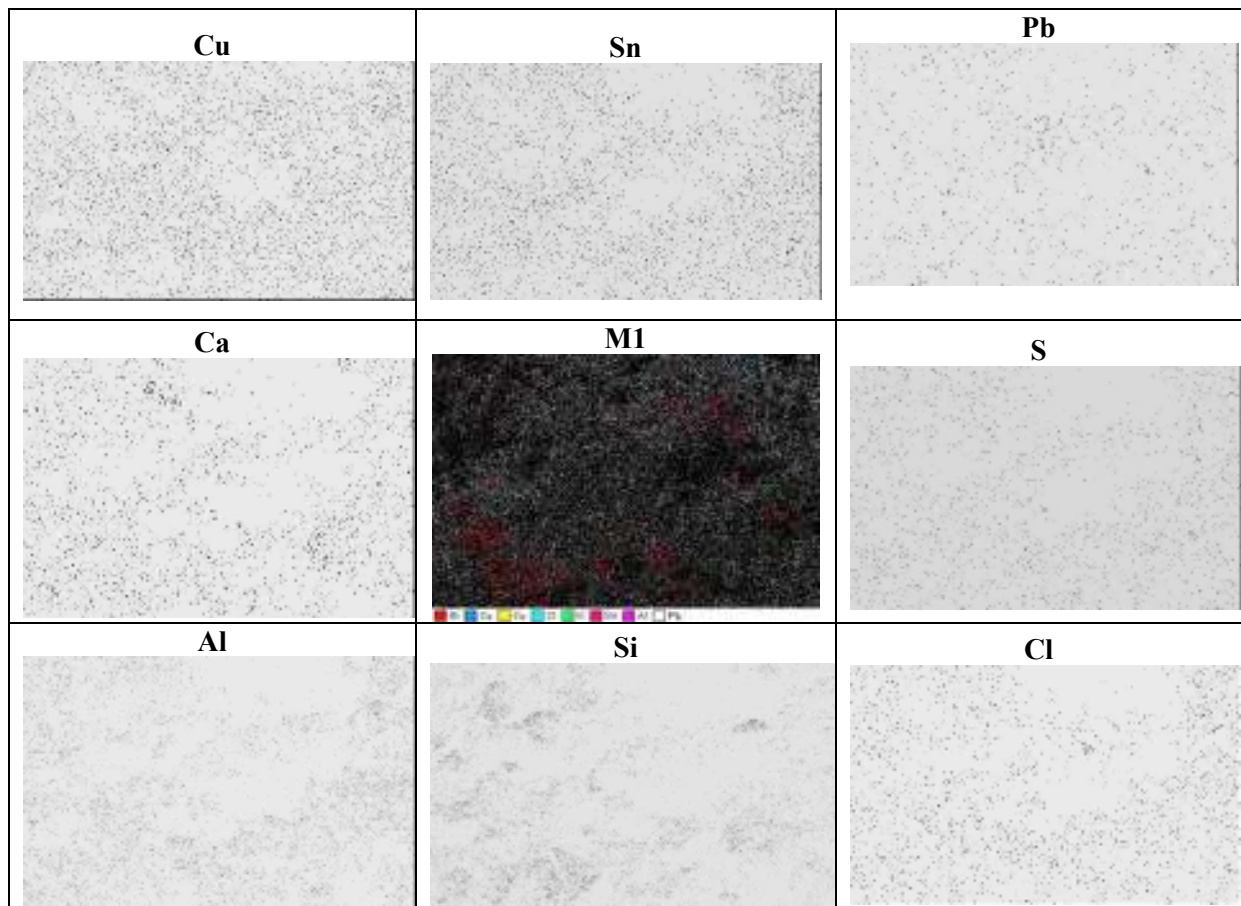
Fig. 8. *Comparative distribution of atoms on the surface of coin M1*
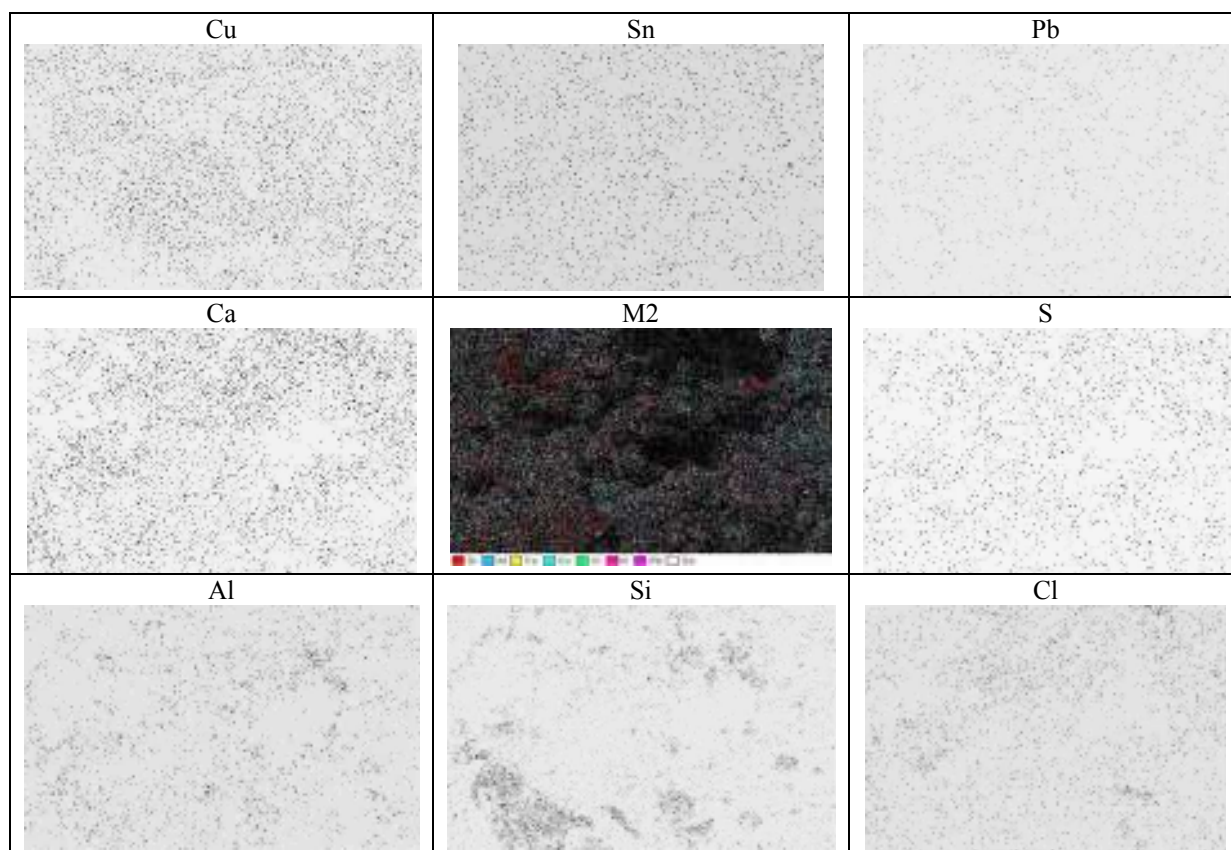
Fig. 9. *Comparative distribution of atoms on the surface of coin M2*

Based on these observations, the SEM microscopy, coupled with EDAX microanalysis can be well correlated with the data obtained from microchemical and spectroscopical analyses.

4. Conclusions

For the ancient bronze coins and other metallic pieces discovered in the archaeological sites, a detailed analysis can put in evidence a series of structural elements specific to the archaeological patina, that allow chronological evaluation and differentiations as the alloy, area of creation and period of utilization etc. are concerned.

Each piece, at the abandon or when lost, has a *specific ancient patina*, that contains only the *primary patina* (for the objects in the utilization period) or only the *primary patina* interposed *with the secondary one* (for the objects out of use but non-abandoned). During the permanence in the site, the pedological processes are causing continuous physical and chemical transformations to the surface of the piece, the contamination patina being overlapped on the primary and secondary ones.

When the processes are on surface, under the influence of climatic agents, the ancient patina conserves quite well the shape of the object, but when the stratigraphical deepening begins, the pedological cyclic processes lead to the segregation into different layers of the compounds resulted from the three types of reactions: redox, acid-base and physical-mechanical, that create a monolithic complex of the three patinas: primary, secondary and of contamination. In function of the mechanical fluctuations of the site (non-distrubed or disturbed), the archaeological patina can have compositions and mineralogical distributions with specific dispersions: stratified or not. The detailed study of the structural characteristics of the archaeological patina allows the identification of structural-phenomenological correlations.

The present study analyses two coins of IV-V century d.C, discovered in 2000, in the site of Nufărul, Tulcea county, intially classified for the *grey fund*, because of their precarious preservation state (thin and fragile metallic bulk or very thin, discontinuous and even absent). These coins were discovered separately in the site. The main question about them is to establish the emission period and the circulation area.

Using a system of four modern techniques: optical microscopy, reflection colorimetry, IR spectroscopy and SEM/EDAX, the following aspects were put in evidence:

- The coins are part of the same lot, because of the basic alloy composition, and have the same age, even the preservation state of the metallic bulk is different, this aspect being considered a result of the different aggressivity of the soil;
- The correlation of data resulted from the microchemical analyses coupled with the mineralogical and colorimetric ones with the data obtained from the IR spectroscopy and SEM/EDAX allowed to establish the similitude between the two coins, with a basic alloy made of the same mineral, as for the byzantine coins of Dobrogea, containing in their composition Cu, Sn and Pb;
- Furthermore, the method of scanning electronic microscopy (SEM) coupled with the X ray spectrometry, EDAX type, has proved successful to differentiate the chemical products from the primary and secondary patinas versus the contamination ones, using the dispersion mapping of atoms.

The study will allow, after a deeper analysis of the composition, structural and thermal behavior of the main components of the archaeological patina, the determination of other chronological characteristics, that will be the object of further papers. The analyses will include the techniques coupled with SEM/EDAX for the microstratigraphical sections and the use of thermogravimetry for establishing the evolution of kinetic parameters in function of temperature and transformation degree.

References

[1]. **Sandu I.G., Stoleriu S., Sandu I., Brebu M., Sandu A.V**., "*Authentication of ancient coins by the study of archaeological patina*" Rev. Chim. (Bucureşti), 56, nr. 10, (2005), p. 981;

[2]. **Sandu, I., Dima, A., Sandu, I.G**., *Conservation and Restoration of Metallic Artifacts*, Ed. Corson, (ISBN 973-8225-24-8) Iaşi 2002, p. 152;

[3]. **Sandu, I., Sandu, I.G**., *Modern Aspects Concerning the Conservation of Cultural Heritage*, vol.I, Ed. Performantica (ISBN 973-730-048-3), Iaşi, 2005, p.261;

[4]. **W. Mourey, *Conservation of Metallic Antiquities – from the Site to the Muzeum**,* Ed. Tehnică, (ISBN 973-31-1180-5), Bucureşti, 1998, p. 28;

[5]. **Sandu, I., Găluşcă, D.G., Carcea I., Ştefan, M., Sandu, A.V**., "*Authentication of ancient bronze coins. I. Aspects concerning the composition of the patina*", in Bul. Inst. Polit. Iasi (ISSN 1453-1690),

tom LI (LV), Fasc. 2, Section Science and Engineering Materials, 2005, p. 157;

[6]. **Sandu, I. G., Sandu, I.C.A., Dima, A., Sandu I., Neacşu, I.,** "*Authentication of ancient bronze coins.II. Microchemical, IR and XRD analyses*", in Bul. Inst. Polit. Iasi (ISSN 1453-1690), tom LI (LV), Fasc. 2, Section Science and Engineering Materials, 2005, p. 167;

[7]. **Sandu, I. G., Stoleriu S., Sandu, I., Dima, A., Sandu, I.C.A., Neacşu, I.,** "*Authentication of ancient bronze coins. III.Colorimetric and thermogravimetric analyses*", in Bul. Inst. Polit. Iasi (ISSN 1453-1690), tom LI (LV), Fasc. 2, Section Science and Engineering Materials, 2005, p. 177;

[8]. **Sandu, I.G., Dima, A., Sandu, I., Diaconescu, F., Sandu, A.V.,** "*The conservation level of metallic artefacts. I. Acient coins and other metallic numismatic pieces*", in Bul. Inst. Polit. Iasi (ISSN 1453-1690), tom LI (LV), Fasc. 2, Section Science and Engineering Materials, 2005, p. 197;

[9]. **Mazzeo, R**., "*Patine su manufatti metallici*", în Le Patine. Genesi, Significato, conservazione - Kermesquaderni, Ed. Nardini, Firenze, 2005 p.29;

[10]. **Bellamy, L.J**., *Infrared Spectra of Complex Molecules*, Ed. Chapman and Hall, London 1975;

[11]. **Nakamoto, K**., *Infrared Raman Spectra of Inorganic and Coordination Compounds*, Ed. Wiley, New York, 1978;

[12]. **Nyquist, R.A., Kagel, R.O**., *Infrared Spectra of Inorganic Compounds,* Academic Press, New-York and London, 1971;

[13]. *** * , *The Sadtler Standard Spectra***, Ed. Stadler Research Laboratories, Philadelphia PA, 1972;

[14]. **Bentley, F.F., Smithson, L.D., Rozek, A.L**., *Infrared Spectra and Characteristic Frequences. A collection of spectra, interpretation and bibliography,* Ed. John Wiley & Sons, New York – London – Sydney, 1988, p. 1515-1566;

[15]. **Hodges, G.M., Hallowes, R.C**., *Research applications of scanning electron microscopy, vol*. I şi II, Academic Press, New York, Toronto, Sidney, 1980;

[16]. **Mackenzie, R.C., Mitchell, B.D.,** *Differential Termal Analysis*, Academic Press, New York, 1980;

[17]. **Vasile, C., Calugaru, E.M., Stoleriu, A., Sabliovschi, M., Mihai, E**., *Comportarea termică a polimerilor*, Ed. Academiei RSR, Bucureşti, 1980;

[18]. **Llopiz, J., Romero, M.M., Jerez, A., Laureiro, Y**., *Thermochimica Acta*, **256**, 1995, p. 205;

[19]. **Chiavari, G., Mazzeo, R**.,, "*Chemical Characterization of Surface Corrosion Products Present on outdoor Bronze Monuments*", în Proceedings of the 4th International Symposium on the Conservation of Monuments in the Mediterranean, Rodhos, 6-11 Maggio 1997, vol. 1, p. 111;

[20]. **Graedel, T.E**., "*Copper patinas Formed in the Atmosphere. I. A Quantiative Assessment of Mechanism*", in Corrosion Science – Special issue, **27**, (7), 1987, p. 721;

[21]. **Marabelli, M., Mazzeo, R.,** "*La corrozione dei bronzi esposti all'aperto: problemi din caratterizzazione*", în La metallurgia italiana, 85, (4), 1993, p. 247;

[22]. **Mazzeo, R., Chiavari, G., Morigi, G**., "*Identificazione ed origine di patine ad ossalato su monumenti bronzei: il caso del Portale Centrale del Duomo di Loreto (AN)*", în Atti del Convegno: le pellicole ad ossalato: origine e significato nella conservazione delle opere d'arte, Ed. Centro G. Bozza, 1989, p. 271;

[23]. **Scott, D.A.,** *Copper and Bronze in Art. Corrozion, Colorants, Conservation*, Ed. The Getty Conservation Institute, Los Angeles, 2002;

PROCESSING SMART WIRES FROM CU-AL-NI SYSTEM

Carmela GURAU, Gheorghe GURAU

Dunărea de Jos" University of Galati

e-mail: carmela.gurau@ugal.ro

ABSTRACT

In this paper we present some results concerning plastic deformation applied to shape memory alloy and two most direct characterization methods for shape memory. We work with a copper based alloy- Cu Al13Ni 4. Over eight percent in aluminum the plastic deformation on the copper aluminum alloys is very difficult to do. Our purpose was to obtain the thin wires. The first material shape was cast ingots very fragile. We choose to work with a direct extrusion method because the high fragility of this material required a three dimensional stress compression scheme.

KEYWORDS: smart memory alloy, extrusion

1. Introduction

The motivation for this research is the market requirement for a new materials class Shape Memory Alloy (SMA). This materials are expensive because use the expense elements also use expense technologies. In these conditions our purpose was to choose an easy obtain smart material and to find adequate processing. We chose the copper based SMA using the former team experience in cooper alloys [1], [2], [5].

Shape Memory Alloys is a designation that is applied to that group of metallic materials that demonstrate the ability to return to some previously defined shape or size when subjected to the appropriate thermal procedure. Generally, these materials can be plastically deformed at some relatively low temperature, and upon exposure to some higher temperature will return to their shape prior to the deformation.

A shape memory alloy may be further defined as one that yields a thermoelastic martensite.

In this case, the alloy undergoes a martensitic transformation of a type that allows the alloy to be deformed by a twinning mechanism below the transformation temperature.

The deformation is then reversed when the twinned structure reverts upon heating to the parent phase. [6]

2. Melting conditions

The melting process has been developed in a tipping furnace graphite melting pot. The maximum charge weight: 100 kg. For the charge composition we used electrolytic copper plates, nickel and titanium plates.

Practically in burning melting pot was introduced protection material. When this material came incandescent the electrolytic cooper preheated at 200 ^{0}C was introduced.

The method supposes ingot casting followed melting to avoid pre alloys for purity reasons. At same time we had a special attention for melting bath protection. In this way we used $Na_2B_4O_7$ and NaCl. Deoxidation was made with CuP_{10} and degasification with Cl_2Mn.

The melting scheme is:

CuP_{10}	Stop Furnace		CuP_{10}		Casting Ingot	Casting samples
Cu_E	Ni	Cu_E		Al	alloy	re melting
——— alloy ———	————	————	————	————	————	———
First Deoxidation		Second Deoxidation				
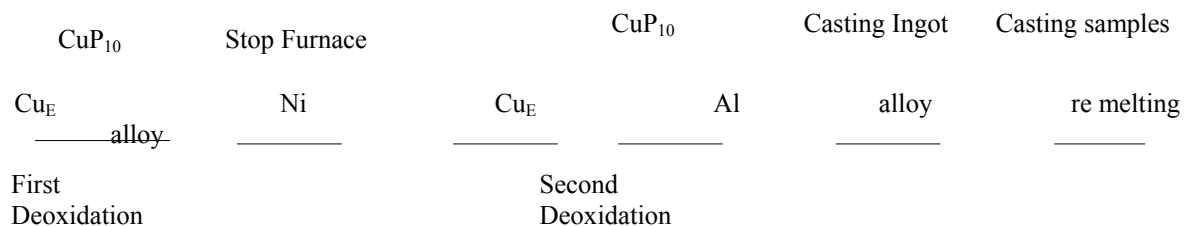
The melting conditions were managed so that cooper fusion to be faster. Final temperature was 1150^0C. In this moment was made a first deoxidation with CuP_{10}. Nickel also pre heated was added in small parts. In this time a bath agitation was made. From initial weight 10% was retained and is used in this moment for reduce the bath temperature.

This reduce is necessary for aluminum addition. The second deoxidation followed.

The chemical composition was determined using a Qantovac device based on the optical spectral analysis. The result is presented in table 1.

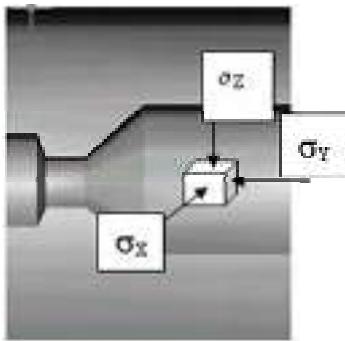The structure for this alloy (fig.1) and a classic bronze microstructure are very different.

alloy 1									
Nr.crt	Sn	Pb	Zn	Mn	Fe	Ni	Si	Al	Cu
4.1	0.02	0.01	0.79	0.09	0.27	4.00	0.04	12.88	Rest

Fig.1. *Alloy with 13%Al and 4% Ni,*
Alloy: Cast aluminium bronze
Chemical composition: 13 %Al, 4 Ni, rest Cu
Magnification: 50x
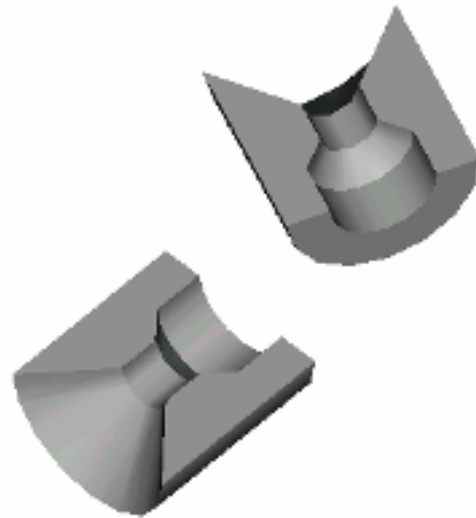
Fig.3. *Direct extrusion die*

The direct extrusion is only plastic deformation method which assures tri dimensional compressive stress (fig. 2) indicates for such hard deformable alloy.

In this sense was designed a direct extrusion dies (fig. 3) to assure plastic deformation from 35 mm diameter to 3mm diameter wires (fig. 4). The 13 % Al extruded semi products microstructure show a martensitic aspect (fig. 5).

Fig.2. *Stress scheme direct extrusion*

3. Plastic Deformation

Before the plastic deformation technology was choose necessary behavior plastic deformation study was made [1], [2], [4]. All those study confirm that upper 10% Al plastic properties of alloy are pronounced decrease.

In these conditions direct hot extrusion process was designed. This deformation process must resolve problem to obtain cylindrical shapes 10 mm diameter and 120 mm length starting from normal conic molded ingot (Φ25-Φ40)x 150 mm, aluminum bronze 4%Ni.

Fig.4. *A- ingot, B- 20 mm extruded shape, C-10 mm extruded shape*

Smart memory alloy deformation degree 111%
Chemical composition 12.88%Al, 3.84% Ni, rest Cu
Microstructure: γ_1'
Magnification: 100x

Smart memory alloy deformation degree 111%
Chemical composition 12.88%Al, 3.84% Ni, rest Cu
Microstructure: γ_1'
Magnification: 100x

Fig. 5. Microstructure 13% Al smart memory alloy

The last plastic deformation was made from 10 mm diameter to 3 mm wires.

In figure 6 is presented the semi product and the extrusion dies.

Fig.6. Extrusion die, punch, 3 mm extruded wire

Fig.7. Extruded SMA wires

Our next step study has been concentrated on aged and quenched specimens of Cu-Al-Ni alloy, solubilized and we performed, the Differential Scanning Calorimetry and Electrical Resistivity characterization techniques.

The specimens were solubilized in austenitic domain at 850°C for 30 minutes. Homogenized specimens were immediately quenched in iced water in order to obtain β-type martensite.

After these treatments the calorimetric experiments were performed by means of SETARAM 92 instrument at a rate of 10°C per minute, between -50°C and 250°C. The cooling treatments were acted by using liquid nitrogen. The electrical resistivity to identify the crystalline phases present in materials and to measure the structure properties was made with a THERMO ELECTRON COOP HAAKE DC50-K40

4. Characterization methods

There are two major methods of characterizing the transformation in SMAs and a large number of minor methods:

Differential Scanning Calorimetry

Electrical resistivity

The objective of the present work is to analyze the variation of the temperature with thermal cycling using the Differential Scanning Calorimetry (DSC), and the electrical resistivity to identify the crystalline phases present in materials and to measure the structure properties.

The most direct method is by DSC. This technique measures the heat absorbed or given off by a small sample of the material as it is heated and cooled through the transformation temperature range. The sample can be very small, such as a few milligrams, and because the sample is unstressed, this is not a factor in the measurement. The endotherm and exotherm peaks as the sample absorbs or gives off energy due to the transformation, are easily measured for the beginning peak, and end of the phase change in each direction.

Fig.8. DSC SETARAM 92

The second method often used is to measure the electrical resistivity of the sample as it is heated and cooled. The alloys exhibit interesting changes and peaks in the resistivity (by up to 20%) over the transformation temperature range; however, correlating these changes with measured phase changes or mechanical properties has not always been very successful. Also, there are often large changes in the resistivity curves after cycling samples through the transformation a number of times. Thus, resistivity is often measured as a phenomenon in its own right, but is rarely used to definitely characterize one alloy versus another.

The technical importance of most engineering materials is based on their mechanical, electrical or magnetic properties, which should, normally, be as independent as possible from environmental influences.

5. Experimental results
DSC analysis

A sample weighting 0.0347g was cut from a Cu-Al-Ni wire, etched with a solution of 1:1 HNO_3 and H_2O for 13 minutes to remove the layers affected by the cutting. The calorimetric experiments were performed between -50°C and 250°C at a heating rate of 10°C/min. The cooling treatments were carried out by using liquid nitrogen.
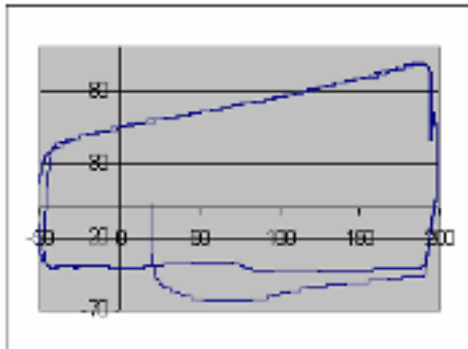
Fig.9.

The curve from (fig 9) was a closed one with no phase transformation, with no peak on the reverse martensite transformation, between 73°C and 159°C present a large peak.

The quenched curves (fig.10) showed a phase transformation both on forward and reverse direct martensitic transformation.
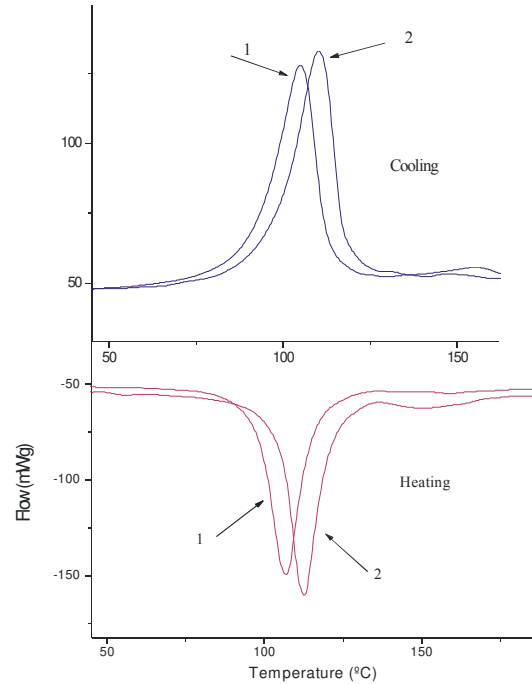
Fig.10. DSC curves for a solubilized alloy at 850ºC

6. ER analyses

We can observe a straight line, the resistivity is increasing with the temperature rising, showing that there is no phase transformation at the 9 months aged at room temperature specimen.

Fig11. ER aged sample

At 850°C solubilised sample there is a phase transformation that starts around 85°C, the resistivity starts to decrease until 103°C when the phase is finished and the resistivity has the tendency to increase. On cooling a reverse phase transformation takes place.

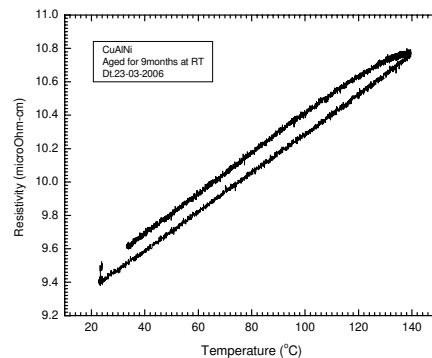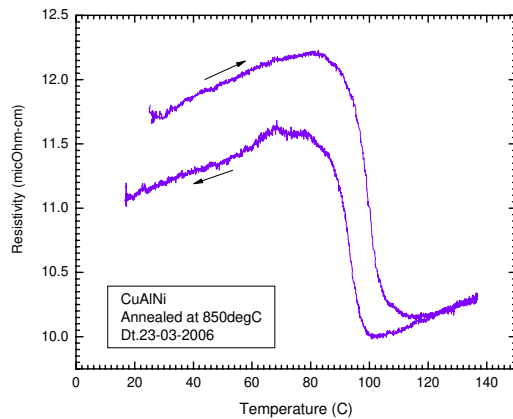*Fig.12*. *ER quenched sample*

In table 2 we have transformation temperatures obtained from DSC and ER measurements.

Table 2

Transformation temperatures	Solubilized at 850°C	
	DSC	ER
As	92	80
Af	138	103
Ms	152	90
Mf	84	60

7. Conclusions

The extruded wires have a martensitic structure to the normal temperature. Dimensions and micro structural aspect allow continuing to the next step establishing thermo mechanical treatments to induce the shape memory effect.

The Cu-Al-Ni, after solubilization followed by quenching, showed the phase transformations that are typical of the Shape Memory Effect (by DSC and Electrical Resistivity).

References

[1]. Gheorghe,G., *Teza de doctorat*, Universitatea Dunarea de Jos Galati

[2]. Cănănău,N., *Teza de doctorat*, Universitatea Dunarea de Jos Galati

[3]. Cananau, N, Gurau, G., *Comportarea la deformare a materialelor metalice. Ecuatii constitutive*, Editura Evrika, 1996

[4]. Cănănău, N, Mitoşeriu, O., *Researches concerning the heat treatment at special aluminium bronze for shiping propellers*, Euromat, Lisabona, Portugalia, 1998, vol.2, pag.293-298

[5]. Vlad, M., *Teza de doctorat*, Universitatea Dunarea de Jos Galati

[6]. Darel Hudgson, Ming H.Wu and Robert J. Biermann *"Shape memory alloys for power connector apllications"*

[7]. Z.G. Wei' H.Y. Peng; D.Z.Yang\ C.Y Chung and J.K.L.Lai *"Reverse transformations in CuAlNiMnTi alloy at elevated temperatures"*

[8]. G.M Loughran; T.W Shield, P.H Leo *"Fracture of shape memory CuAlNi single crystals"*

[9]. V.Recarte; J.I. Perez- landazabal, A. Ibarra, M.L. No *" High temperature β phase decomposition process in Cu-Al-Ni SMA"*

[10]. J.Font, E,Cesari, J. Muntasell, J.Pons *" Thermomechanical cycling in Cu-Al-Ni-based melt-spun shape memory ribbons"*

[11]. **R.Gastien, C.E.Corbellani, M.Sade** *" Thermomechanical aspects of martensitic transformations in CuAlNi single crystals"*

[12]. **Ganesh Ganapardy, Abhijit Bhattacharyya** *"The effect onf isothermal mechanical cycling on Cu-Al-Ni shapememory alloy single crystal wire"*

[13]. K.Otsuka and C.M. Wayman *" Shape memory materials"*

[14]. J.Gui, W.H.Zon, D.Zang *" X-RAY diffraction study of the reverse martensitic transformation in Cu-Al-Ni-Ti shape memory alloy"*

[15]. A.S. Paula, J.P.H.G. Canejo, R.M.S. Martins, F.M. Braz Fernandes *" Effect of thermal cycling on the transformation temperature ranges of Ni-Ti shape memory alloy"*.

COMPOSITE-DECORATIVE TILES
WITH GRANITE

Octavian POTECAŞU, Florentina POTECAŞU,
Elena DRUGESCU
"Dunarea de Jos" University of Galati
e-mail: **fpotec@ugal.ro**

ABSTRACT

The paper presents the results of the authors' scientific research on a composite material with polymeric matrix, hardened with rock particles. It was studied the influence of the quantity of the hardening phase on the compression resistance of the product. These weather resistant materials have a long period of ageing, a permanent finishing and require almost no maintenance.

For the research was used granitee from the Măcin Mountains, Dobrogea România with greenish shade, which was crushed and then granulometric sorted. Granitee is an acid volcanic rock, with over 65% SiO_2; it has granular structure and massive texture. Polyesteric thermorigid resin was used for the matrix.

These resins can be characterized by: easy obtaining and accessibility of the raw materials, quick strengthening without side-off products, good chemical resistance at acids and alcohols. Composite samples were made through shaping in steel mould. After shaping and maturation, the samples were tried at compression.

KEYWORDS: polymeric matrix, composite material, rock particles, Dobrogea

1. Introduction

Dynamic development of the consumer's goods manufacture has imposed new materials to be setting up.

From the advanced materials with great usage expectation are the Composites, named in reference material as Future's Materials.

Composites answer to every industrial demands and almost all human needs. Composites can be obtained by suitable staples association and they can have simultaneous new combinations: rigidity, resilience, toughness, refractoriness, corrosion resistance, dimensional steadiness, absorption of vibration, electrical and thermal conductibility, and, unlike other building traditional materials, composites' price is lower. Today, Composite Materials applications cover very different fields, such as: aeronautics, naval-building industry, electronics, radio-location, machine-building industry, industrial equipments, light industry, industrial and civil – building industries. In buildings field, composites prefab are either even elements or technical ingots. These bad weather resistant materials have long life seasoning, facing continuous and they require almost no maintenance.

Mechanical properties concerning building industry are: compression strength, abrasive resistance, impact, bending strength,, traction resistance, dimensional steadiness, modulus of elasticity and yield impact resistance.

Composite materials are generally made from a hardening phase and a binding compatible matrix. In building industry the most used matrix is polymeric and reinforcement phases could be mineral rocks, like granite, basalt, marble, pumice, and a wide range products can be made from the outcome materials.

The hardened rocks composites offer buildings personality and style being in the same time very practical due of their easier maintenance, being used in various purposes, such as exterior platting and floors for public institutions or areas with intensely traffic, either in ornamentally purposes, for fitting out the indoor of private houses. The raw materials used for obtaining the composites were granite and polyester thermo rigid resin. The granite is a volcanic rock made up from over 65% SiO_2, CaO, MgO, R_2O_2, Mn_2O_3, TiO_2, Fe_2O_3, etc., in different percentage; it has granular structure and massive texture. Due these integrant elements, the granite can be white, grey, yellowish, pink, auburn –brown, greenish, or bluish. Sometimes, presence of feldspath crystals wide grown dents the rock a freckless structure. The granular structure can be characterized by mineral grains crystallized which are visible with naked eye. This structure is formed in earth depth, where the cooling magma is made very slowly, and mineral crystals have enough time for growing. The granular structure is find

out in all depth magmatic rocks. Our country has mountainous massive all built from granite. Such mountains can be found in Măcin Mountains, Apuseni, Meridional Carpathians and running granite quarry are in Săvârşin, Cladova, Radna, Măcin, Turcoaia, Greci.

2. Experimental procedure

For the research was used granitee from the Măcin Mountains, with greenish shade, which was crushed and then granulometric sorted. Polyesteric thermorigid resin was used for the matrix. These resins can be characterized by easy obtaining and accessibility of the raw materials, quick strengthening without side-off products, good dimensional steadiness, coloring properties, transparency, good chemical resistance at acids and alcoohols.

Polyesteric usage should be aware from following restriction: increased shrinkage through shaping, decreased resistance at alkali and hot water.

3. Experimental results and discussion

Composite samples were manufactured in accordance with the recipes from table 1, through shaping in 18,6 mm steel mould diameter.

After shaping and maturation, the samples were compression tested in hydraulic press, according to diagram 1.

The results are shown in table 1 and hystogram figure 2. Macrostructure of the composites obtained concordant with recipes 2, 4 and 6 are shown in figures 3, 4, 5.
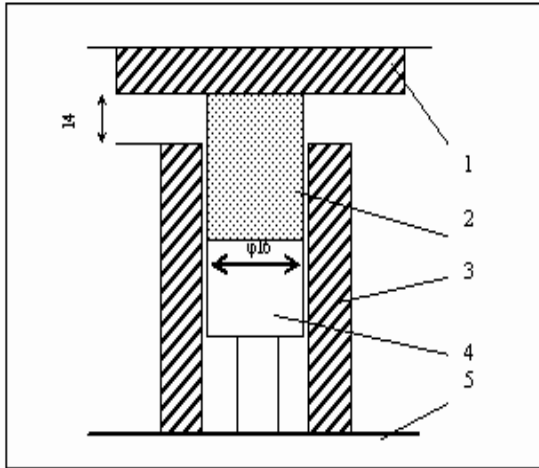
Table 1

No. recipe	Composition	Pressure (daN/cm^2)	Force (daN)	Section (cm^2)	Compression resistance (MPa)
0	**Natural Granite**	11	2200	3,5	62,8
1	➢ **11 g granite;** grain size: 0,73 - 1,27mm; ➢ **resin 9%**	12,5	2500	2,7	92,5
2	➢ **11 g granite;** grain size: 0,73-1,27mm; ➢ **resin 18%**	12	2400	2,7	88,8
3	➢ **11 g granite;** grain size: 0,73-1,27mm ➢ **resin 27%**	11	2200	2,7	81,4
4	➢ **11 g granite;** grain size: 1,85-2,17mm; ➢ **resin 13%**	9	1800	2,7	66,6
5	➢ **10 g granite** grain size: 1,85-2,17mm. ➢ **1 g granite;** grain size: < 0,040 mm. ➢ **resin 22%**	12	2400	2,7	88,8
6	➢ **5 g granite;** grain size: 1,85-2,17mm; ➢ **5 g granite;** grain size: 0,73-1,27mm. ➢ **resin 22%**	10	2000	2,7	74,0

4. Conclusions

➢ During the experiments, especially effect in composite has the granite grain size. It's obvious that the composite samples 1 and 2 (with the finest grain size) have a higher compression resistance than composite 4 (with a bigger grain size).
➢ If a smaller quantity from the finest granite grain size (below 0.040 mm) is added in composite

a bigger grain size (1,85-2.17 mm) for filling the space between the particles, the compression resistance will be increased with 25% compare to the composite sample made only of the finest granulation particles. Set beside samples 1, 2 and 3 from histogram 2, the compression resistance has been decreased with 12% by increasing the amount of resin.

➢ Compression resistance of the composite obtained is higher than the compression resistance of natural rocks used for research.

Fig. 1. *The diagram of the compression test 1- anvil; 2 – cylindrical die; 3 – controlled support, 4- blank assay; 5 – the press table.*
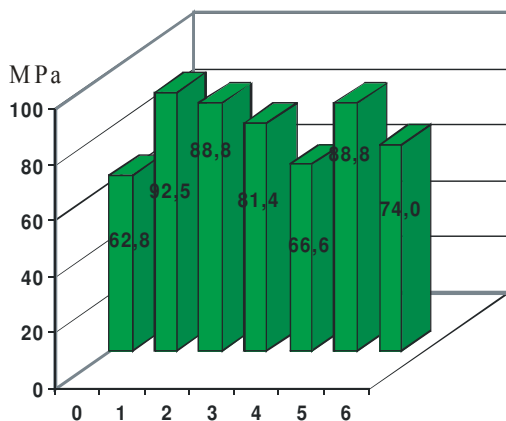
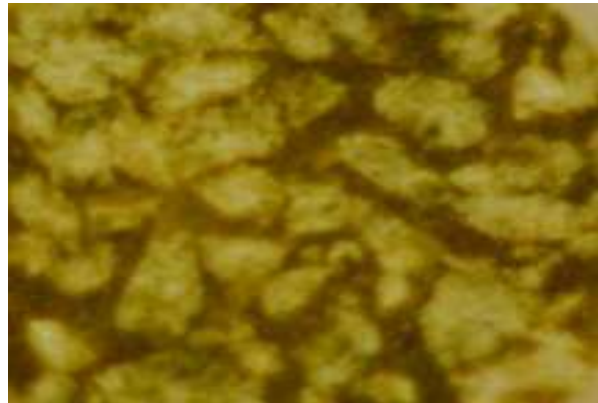**Fig. 2.** *The variation of the compression resistance varying with the granite granulation and the resin percent, compared to the granite.*

Fig. 4. *The macrostructure of the composite, recipe 4.*
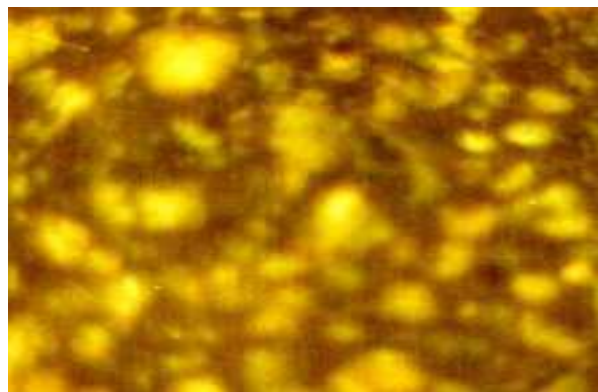
Fig. 5. *The macrostructure of the composite, recipe 6.*

References

[1]. Mihalcu M. - *Materiale plastice armate*- Editura Tehnică, Bucureşti. 1973.

[2]. Dumitraş C., Oprau C.- *Prelucrarea materialelor compozite ceramice şi minerale*- Editura Tehnică, Bucureşti,1994.

[3]. Tentulescu D., Tentulescu L. – *Fibre de sticlă*, Editura Tehnică, Bucureşti, 1994

[4]. Nica A.- *Ceramica Tehnică*- Editura Tehnică, Bucureşti, 1988.

[5]. O.Potecasu, L.Buburuzan, E.Drugescu - *Compozite durificate cu roci* - Conferinta cu participare internationala Tehnologii si Materiale Avansate, 20-22 noiembrie 2003, Galati, Romania, ISBN 966-549-916-5, p.105

SURFACE HARDENING BY NITRATION FOR SOME STAINLESS AUSTENITE STEEL TYPES

Ovidiu DIMA, Nelu CAZACU

"Dunarea de Jos" University of Galati
e-mail: dima.ovidiu@ugal.ro

ABSTRACT

Stainless austenite steel types have a good resistance to corrosion in different natural, industrial environments but their hardness and mechanical resistance are low enough. In order to assure an increased resistance to abrasion it is necessary to increase also the surface hardness. This thing is possible if the nitrogen concentration in the surface layer is increased by means of nitration.

The researches made on stainless austenite steel types pointed out a strong hardening tendency for the major part of steel types except for steel type 2CuMoNiCr200. The austenite in this has a very high degree of stability as a result of high content of alloying elements. When the nitrogen is diluted, the hardness is more reduced. Hardness strong increase in the other steel types is determined by complex nitrides separations favoured by nitrogen diffusion and increase of its concentration in the surface layer. The thickness of the hard layer increases depending on the period of nitration process from one hour to 3 hours and is influenced also by the characteristics of each sample.

KEYWORDS: austenitic stainless steel, nitration, corrosion, erosion

1. Introduction

Stainless austenite steel types have a good resistance to corrosion in different natural, industrial environments but their hardness and mechanical resistance are low enough. In man] cases industrial installations components are subjected both to corrosion and to erosion because the fluids are moving with relative high speeds, and the erosion is favoured by the presence of some hard particles in this fluids.

Such cases can be seen for example in the mining industry at the ore preparation installations, in soil fertilizers industry, in paper and cellulose industry etc.

The increase of facilities lifetime is possible by assuring a higher hardness degree that can be more resistant to erosion if this resistance to corrosion is maintained in reasonable limits.

It is well known that for normal steel types is possible to assure a surface hardness if a carburization thermo-chemical treatment followed by quenching and tempering is applied.

For stainless austenite steel types the increase of carbon content determines, in certain temperature conditions, the precipitation of chrome carbides to the limit of austenite grains and implicitly, to decrease of resistance to inter-crystalline corrosion.

In order to remove this inconvenience, it is recommended to replace the carburization with nitration.

Nitration as well as carburization, assures an increase of surface hardness without affecting the resistance to inter-crystalline corrosion.

Nitrogen alloying extends austenite stability domain even if the carbon content is higher, diminishing the danger of chrome carbides precipitation, of decreasing the chrome content in austenite and its de-homogenization, these being the main reasons for inter-crystalline corrosion.

2. Experiments

The materials subjected to research were stainless austenite steel types Cr-Ni and Cr-Ni-Mo with low carbon content %C<0.03, with higher carbon content %C=max.0.12 and even higher and stabilized with Ti or Nb. The chemical composition of these steel types is presented in table 1. The samples were made from rolled plates, the austenite structure being obtained after a quenching treatment of adding into solution. They were cut-off at 60x20x3 mm, by chipping and with abundant cooling. Samples quality surface is important because it may influence the nitration process. A polished surface assures an uniform layer but a slow development of the process.

Table 1

Steel code	Related mark	C	S	P	Mn	Si	Cu	Cr	Ni	Mo	Ti	V
		[%]										
1	12NiCrl80	0.12	0.028	0.055	1.24	1.64	0.06	23.	9.8	0.11	0.01	0.02
2	10TiNiCrl80	0.06	0.008	0.036	1.55	0.65	0.08	17.	9.3	0.05	0.60	
3	2NiCr1 85	0.03	0.005	0.028	1.27	0.42	0.19	18.	8.95	0.15	0.01	0.02
4	2MoNiCrl75	0.02	0.005	0.039	2.06	0.78	0.27	20.	8.8	2.7	0.03	0.03
5	10TiMoNiCrl75	0.045	0.012	0.031	0.96	0.54	0.16	18.	11.6	2.04	0.32	
6	2CuMoNiCr200	0.02	0.008	0.027	1.12	0.41	0.70	20.	18.1	6.1		0.2

Too much roughness may lead to a non-uniform layer. As a result of this remark, samples surface have been finely adjusted on metallographic paper with grains of 280-320, and the edges rounded.
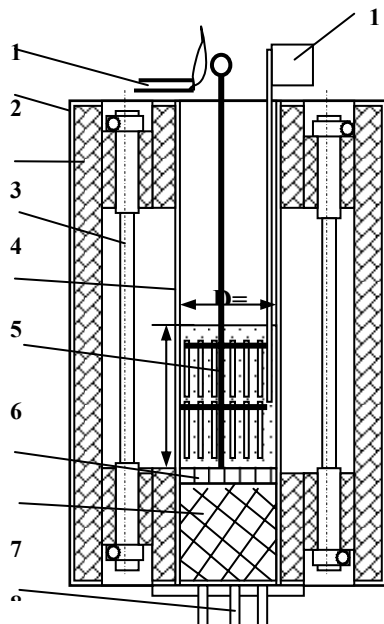
Fig. 1. Furnace for fluidized bed nitration.
1 - methane gas hose for look - out flame,
2 -plate house, 3 - insulation, 4 - heating
elements, resistors, 5 - refractory ceramic tube,
6 -wire support for suspending the samples,
7 - ceramic grid for separating the fluidized
bed, 8 -gas homogenization chamber, 9 - lower
cover for gas blast, 10 - thermocouple,
D, H -fluidized bed dimensions.

At one end, a hole was drilled into the sample so hat they can be suspended on a stainless steel wire support. This support allowed the samples o be arranged vertically inside the nitration installation, at equal distance, and this made possible for a great number of samples to be treated simultaneously in identical conditions. Before being treated the samples were washed and de-greased together with the wire support, by means of agitation and immersion in carbon tetrachloride, then dried with air.

In order to make this research, it was used the fluidized bed nitration method, made of quartz sand washed and dried, with uniform grains having dimensions between 0.1 and 0.16 mm. Like the classical methods for thermo-chemical treatment, temperature, time and nitration environment composition are the base parameters of the process.

This method assures a high speed for carrying out the process when the temperature is low, between 500 -1000°C and even at the lower limit of the interval. The trials were made at a temperature of 550°C for 1, 2 or 3 hours. The gaseous nitration environment made of N_2 mixed with dissociated 30%NH_3 was obtained directly in the fluidized bed which represents also the heating environment of the samples. This way, the properties of the fluidized bed are valorised such as: great uniformity of temperature, high coefficient of mass and heat, good dynamics of the process. A heating furnace with electric resistances was used for nitration. Its scheme is presented in Fig. 1.

3. Samples analysis

In order to point out how the hard nitrated layer is formed, a hardness trial on the exterior layer was made by Vickers method, with low loads HV_{02} for which the pressure force was 200gf. For this trial, the surfaces were polished with metallographic paper, the size of grains being 800, so as to remove the grey-brown surface layer formed by oxides and other compounds. The results have shown a great increase of hardness, so the existence of a very hard but thin surface layer. In a previous hardness trial Vickers HV_5 with the pressure force of 5Kgf, the hard layer for which the thickness increases at the same time with the process duration could be pointed out.

The values of hardness does not characterize the surface layer which has a small thickness if we compare to the prints depth and it offers only qualitative information. The results of these trials are presented in table 2.

Table 2

Steel code	Related mark	HV$_5$ hardness Kgf/mm^2				HV$_{02}$ Nitration for 3 hours
		Initial samples	Nitrated samples			
			1 hours	2hours	3 hours	
1	12NiCr180	198	246	277	317	1310
2	10TiNiCr180	202	260	289	258	1180
3	2NiCr185	188	268	296	321	1315
4	2MoNiCr175	180	244	251	336	1320
5	10TiMoNiCR175	202	286	296	362	1170
6	2CuMoNiCr200	182	190	210	270	500

For the study of hardness variation in the layer section some samples have been made in order to estimate correctly the hardness and thickness of nitrated layer. They were cut-off with an abrasive disk with abundant cooling. The samples have been incorporated in resin, grinded and polished. In order to point out the layer and the structure, in general, the samples have been subjected to electrolytic attack, in a fresh solution with 50% HNO$_3$ at a voltage of 1.5 - 2 V$_{cc}$ for 15-20 seconds.

As the thickness of nitrated layer is believed to reach tens of microns, a Vickers hardness test with very small loads was considered to be necessary, so as to obtain very small prints, respectively HV$_{005}$ for which the pressure force is 50gf. The tests were made for all the 6 types of steel, for the three nitration conditions with duration of 1, 2 and 3 hours. The results of these tests are presented in tables 3, 4, 5, 6, 7, 8.

Table 3. *Hardness variation HV$_{005}$ in the nitrated layer, sample code 1 - steel type 12NiCrl 80*

Nitration duration	Surface distance μm											
	7.5	9	10.5	12	16.5	18	22.5	30	36	46.5	55.5	Centre
1 hour	1006		486				286					251
2 hours				1144		412	340		251			243
3 hours		1313			584			412		340	276	251

Table 4. *Hardness variation HV$_{005}$ in the nitrated layer, sample code 2 - steel type 1 TiNiCrl 80*

Nitration duration	Surface distance μm											
	7.5	9	10.5	13	17.5	21	27	36	39	45	54	Centre
1 hour		643			612		353		251			251
2 hours			1144			643	317	286				268
3 hours				1054			1184	643		380	268	268

Table 5. *Hardness variation HV$_{005}$ in the nitrated layer, sample code 3 - steel type 2NiCrl85*

Nitration duration	Surface distance μm											
	7.5	10.5	11.5	12.5	20	22.5	25.5	33	36.5	42	48	Centre
1 hour				1006	557			286				251
2 hours		1224				340			259			259
3 hours			1314				1144		562	402	306	243

Table 6. *Hardness variation HV$_{005}$ in the nitrated layer, sample code 4 - steel type 2MoNiCr175*

Nitration duration	Surface distance μm											
	8	9	12.5	13.5	15	24	26	27.5	33	45	52.5	Centre
1 hour	1224				752		259					251
2 hours		1314		1144		353			350			259
3 hours			1314		1144			508		306	386	251

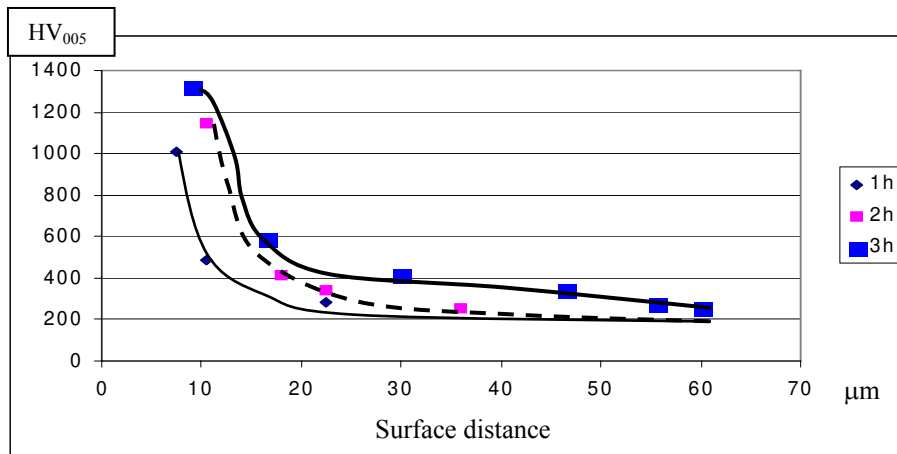**Table 7.** *Hardness variation HV$_{005}$ in the nitrated layer, sample code 5 steel type 10TiMoNiCrl 75*

Nitration duration	Surface distance μm											
	8	9	10.5	14	20	24	25.5	30	36	43.5	54	Centre
1 hour	557			713		340						268
2 hours		1006			584			340		306		270
3 hours			1172		891		584		380		286	260

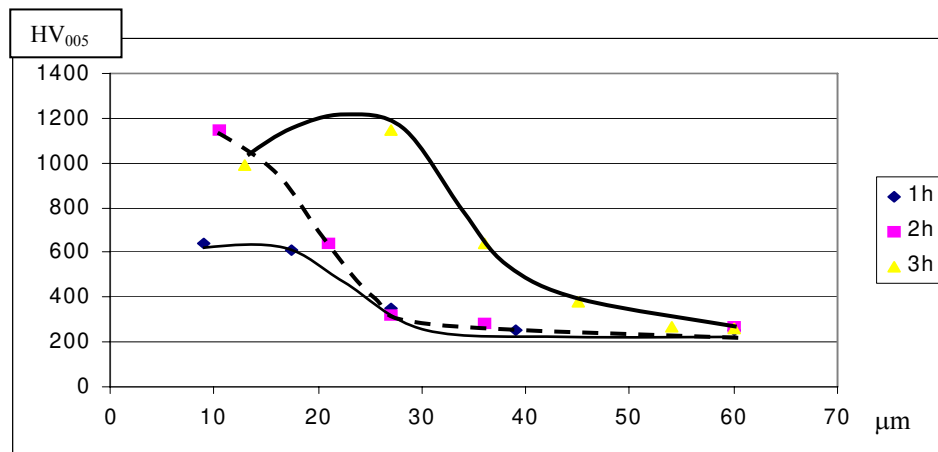**Table 8.** *Hardness variation HV$_{005}$ in the nitrated layer, sample code 6 - steel type 2CuMoNiCr200*

Nitration duration	Surface distance μm					
	9	22.5	34.5	39	55.5	Centre
3 hours	508	500	508	412	306	243

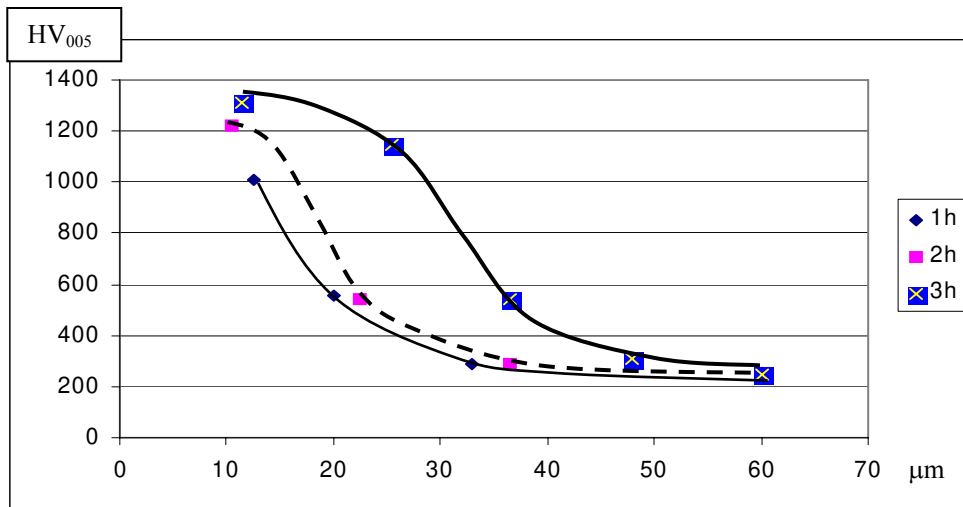Hardness variation curves on the depth of the nitrated layer are presented in fig. 2, 3, 4, 5, 6, 7, for the thermo-chemical nitration treatment of 1, 2 respectively 3 hours, in fluidized bed.
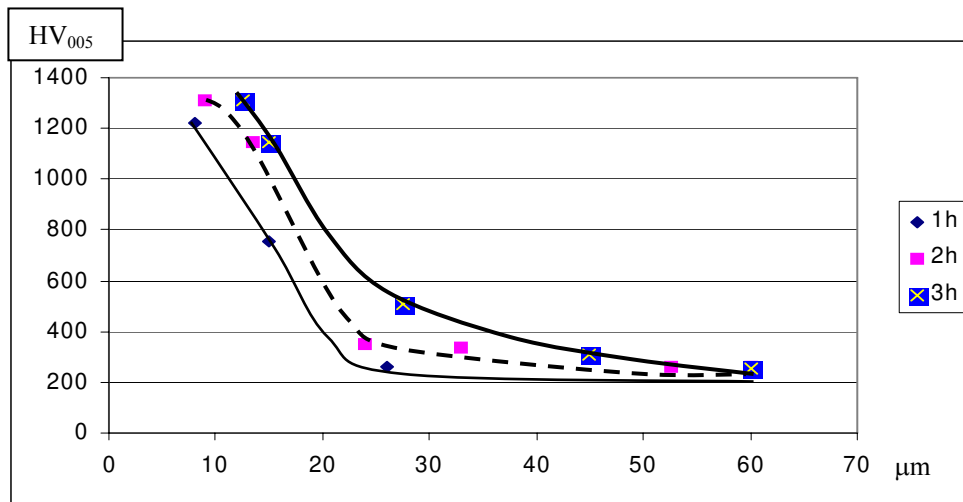

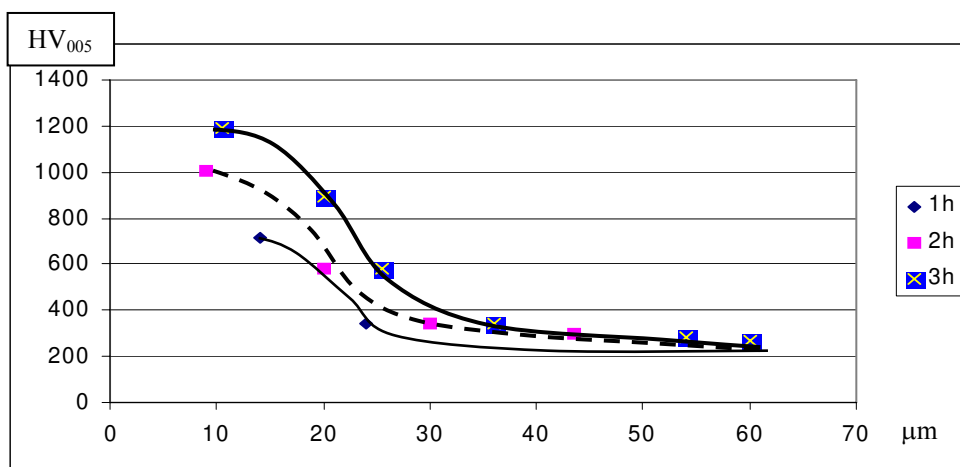**Fig.2.** *Hardness variation HV$_{005}$ in nitrated layer, sample code 1, steel type -12NiCr180*

Fig.3 *Hardness variation HV$_{005}$ in nitrated layer, sample code 2 steel type 10TiNiCr180*

Fig.4 *Hardness variation HV_{005} in nitrated layer, sample code 3 steel type 2NiCr185*

Fig.5 *Hardness variation HV_{005} in nitrated layer, sample code 4 steel type 2MoNiCr175*

Fig.6 *Hardness variation HV_{005} in nitrated layer, sample code 5 steel type 10TiMoNiCr175*
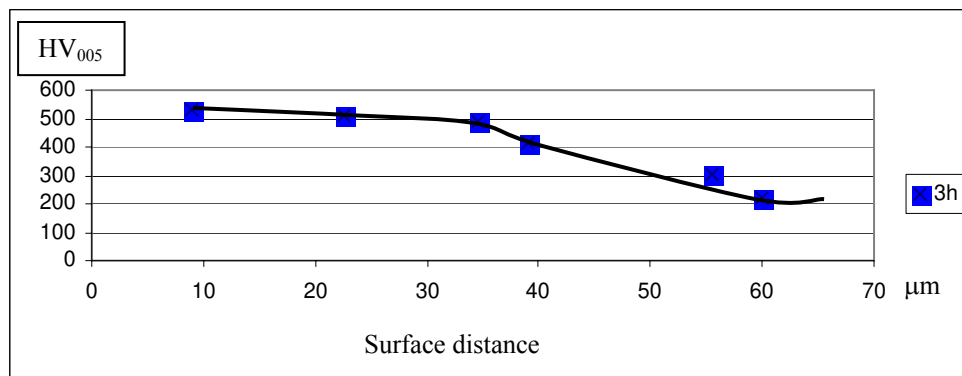
Fig.7 *Hardness variation HV$_{005}$ in nitrated layer, sample code 6 steel type 2CuMoNiCr200*

4. Conclusions

The analysis of hardness tests results shows that after one hour of fluidized bed nitration treatment the surface layer hardness reached very high values for the first 5 steel types, approx. 1000 HV$_{005}$. The layer was very thin, 10μm, discontinuous and non-uniform. In certain areas there are present only small islands of hard nitrated layer and this alternates with areas which have an austenite structure enriched with nitrogen and reduced hardness. This aspect is explained by the fact that on the surface there are more favorable dissociation, absorption and diffusion areas compared to others. After 2 hours of treatment, the layer expands to the entire surface, having the tendency to become uniform and after 3 hours of treatment the layer becomes thicker, the values are

20-40μm and even more. For steel type code 6 2CuMoNiCr200, highly alloyed with Cr, Ni, Mo, Cu, which has a very high index for austenite stability, the increase in hardness is smaller, with a value of 508 HV$_{005}$ and a layer depth of 35-40um. This shows that nitrogen diffusion process is more reduced in a highly alloyed austenite, mainly because of high nickel concentration, over 18%. At the same time, the great stability of austenite stops the separation of hard complex nitrides. Table 9 presents the values of austenite stability S indices and, in parallel, the depth of nitrated layer harder than 500 HV$_{005}$ for the steel types that have been analyzed. S=E$_{Ni}$+0.4Ec$_r$ in which:

$$E_{Ni}=30x(\%C+\%N)+0.5x\%Mn+\%Ni;$$
$$E_{Cr}= \%Cr+\%Mo+\%Si$$

Table 9. *Values of austenite stability S indices*

Steel type	1	2	3	4	5	6
S	24	19	17.5	21.6	22.6	29.8
Thickness of nitrated layer [μm]	19	40	38	3	28	35

We can see that nitrogen diffusion and formation of hard nitrated layer depends on the concentration of alloying elements present in the steel types, on the austenite stability indices. Steel types code 2 and code 3 which have the smallest stability indices have the deepest hard nitrated layer and are being followed by steel types code 3 and code 4. On the 5 position there is steel type code 1 with a very thin layer, approx. 19μm. Steel type code 6 has a special behavior and, as we showed before, has an external layer about 500 HV$_{005}$- . The small value for the achieved hardness compared to nitrated layers hardness from the other steel types is explained by the lack of combinations and nitrides layer and formation of a diffusion layer. The external layers will be pointed out in the next paper by analyses of the structure.

References

[1]. **Dobrovici S.** *Cercetări privind tehnologia carbonitrurării în strat fluidizat aplicată oţelurilor*. Teză de doctorat Galaţi 1999.
[2]. **Truşculescu M.** *Oţeluri inoxidabile şi refractare*. Ed. FACLA Timişoara 1983.
[3]. **Berns H.** *Case hardening of stainless steel using nitrogen*. Ruhr University, Bochum, Germany 2002.
[4]. **Berns H.** *Solution nitriding of stainless steel for process engineering*, Mat.-wisws. u. Werkstofftech. 31/2000.
[5]. **Mocanu D. R.** *Încercarea materialelor*. Ed.Tehnică Buc. 1982.
[6]. **Vellier M.** *Solution apportees aux problemes de la corosion-abrasion par certaines aciers inoxydables austenitiques et austenito-feritiques*. Conference internationale des arts chimiques Paris 1976.
[7]. **Dima O. Mitoşeriu O. Levcovici S.** *Studiu asupra aspectelor de coroziune evidenţiate pe table şi îmbinări sudate din instalaţiile de fabricaţie a celulozei chimice prin procedeul sulfit din cadrul combinatelor CCH Zărneşti, CCH Letea Bacău, CCH Brăila.* Tehnologii Calitate Maşini şi Utilaje 36 Ed. Tehnică Buc.1999.

CALIBRATION AND REFERENCE BLOCKS USED IN NONDESTRUCTIVE ULTRASOUND EXAMINATION, ACCORDING TO NEW EUROPEAN UNION REQUIREMENTS

[1]Cristian Stanciu, [2]Ionel Petrea,
[1]Horia Silvica

[1] S.C.Uzinsider Engineering S.A. Galati,
[2] "Dunarea de Jos"University of Galati,
e-mail: research@uzineng.ro

ABSTRACT

Pursuant international standards such of the European ones, the nondestructive examinations have to be worked out by the most possible accuracy and repeatability, that allow the difference making between the admitted indications, whatever they involve, dump or rejection.

The activity may be carried out with positive results, only, after providing :

➢ *suitable tests and settlements of assay equipment by the agency of calibration and reference blocks;*

➢ *insurance for good training of working staff.*

With the view of touch of this challenge the CALIST framework program was made.

KEYWORDS: nondestructive examination, ultrasounds, calibration blocks, reference blocks.

1. General considerations

Some foreign companies coming on the Romanian market or achieving the free circulation of products manufactured in Romania require to provide the conformity with international and European standards. Therefore, it is imperative that our country to align urgently to the new requirements for providing the stipulations fulfillment of European Union **"New Approach"** and apply Community AQIS regarding promotion of several accurate, repeatable and reproducible metering and trials.

In order to be profitable, a company has to make systematically efforts to reach the stage of fluently and rapidly offer the high quality new products or services required by market at the lowest costs. Therefore, the metering equipment is the only way to guarantee the conformity with the plan, specification or standard of products, installations or buildings made.

This paper work is of present interest, according to those written above, aiming the Romanian entry in the European Union, based on the following matters:

➢ It represents the result of a research of making the reference calibration blocks and samples for examination at international and European standards, fulfilling so the essential requirements from European Standards and Indications.

➢ Necessity of feeding the advanced methods intended to evaluation of parts and steel structures, requested by a large number of running fallen down, pursued by important material damages, serious contamination of the environment and even human losses.

➢ Observation of the low provisions regarding the manufacturer guarantee to which the nondestructive examinations submit also, of which accuracy regarding the defaults size is given by quality of calibration and reference blocks used;

➢ Requirement of increasing the Romanian products competitiveness and decreasing the volume of disputes of law between different business partners.

2. Evaluation of conformity in case of nondestructive tests

In engineering calculation the resistance characteristic values taken into calculation are statistical sizes. In order to increase the running safety it is required to check products by nondestructive examinations, which can give data regarding the material characteristics and are able to find and evaluate the areas with default. After

pointing out the discontinuities it is required to find how much these ones may be or not tolerated. Therefore, it results the importance of providing repeatability of nondestructive examination techniques which have to ensure the certitude that parts considered to be able for use (after control), do not show defaults, which previously pass over one definite evaluation threshold, by the product standards. In order to provide nondestructive examination conformity it has to be given a special attention to making the specimens as per international and European standards by manufacture, checking and control technologies rigorously standardized in procedures.

Adjusting and checking the instrumentation is to be made in order that they work in the chosen scope and by the desired accuracy. A suitable calibration may be checked by getting identically results from the same kind of instrumentation or from different type ones. hese requirements objectified by working out of a large range of calibration and reference blocks, intended for fault detectors adjustment. The scope and accuracy of the values got depend on the quality of specimens used and are influenced by:

➢ Incertitude of results;
➢ Detection limit;
➢ Method selectivity;
➢ Linearity;
➢ Repeatability limit;
➢ Reproducibility limit;
➢ Crossed sensitivity;
➢ Solidity against outside influences.

Checks required for keeping the trust in primary reference specimens condition, transfer or working and reference materials have to be accomplished according to definite procedure and planning.

Methods of providing the trust in results of nondestructive examination may be:

➢ Use of suitable reference materials, certified in order to point out the trustworthy material characterization;
➢ The specimens mutually agreed or methods which are clearly specified upon which all the interested parts agreed;
➢ Participation in a suitable program of comparison between laboratories or amplitude tests.

3. Blocs intended for the examination equipment adjustment

3.1. General data

Calibration and reference blocks have to be manufactured in MQ system, from certified materials, by manufacture, check and control technologies rigorously observed, standardized by procedures and should have certificates for quality

and metrology check. Their getting complexity results from the existence of a large range of calibration and reference blocks, that follow to be manufactured by materials with very different structural characteristics, purity, forms and discontinuities, with small building tolerances given in Nondestructive Examination Standards, generally or those specifically for each product examined.

3.2. Calibrating blocks

Calibrating consists in optimal adjustment of equipment parameters so that the indications, got by the ultrasound beam, to be correctly located. Therefore, reflecting surfaces and calibrated discontinuities with known characteristics and disposed in calibration blocks are used and have to fulfill the following conditions:

➢ To be made from a very good quality material with uniform and fine granulation;
➢ To be accurately manufactured and worked out;
➢ To allow the optimal adjustment of different types of ultrasound equipment.

Their manufacture tolerances are given in general standards for nondestructive examination.

Calibrations and checks are available only for one piece examination made of a material in which the ultrasound speed is equally to that one of the block. So, a calibration block made by S355J steel may be used only for unalloyed steel part examination for which ultrasound propagation speed is 5920 ± 20 m/s. The ultrasound speed varies depending on the steel quality, so, for a steel with 17,8% Mn and 9,6% Cr it is 5600 m/s, and for one with 18,9% Cr and 11,3% Ni it is 5735 m/s, that is leading to large errors in defaults position determination, in case of equipment calibration by calibration block presented above. Acoustically speaking, this has not to show local variations larger than ±1dB. In case of nondestructive examinations by ultrasound of light alloyed steel, material from which is made the calibration block is S355JO quality unalloyed steel. The quality corresponds to a structural steel (symbol S) with minimum value specified of flow limit and energy of breaking for hammer test for 0^0C temperature.

Trials, that have to be made in order to check the conformity with product standard stipulations are the followings:

➢ Chemical analysis;
➢ Mechanical trials:
✓ Tension;
✓ Bending by chock.

Raw by-products will be submitted to a treatment and then they have to be examined, in order to provide the ratifying requirements of material properties from ultrasound examination point of view, by:

➢ Determination of longitudinal and transversal ultrasound waves propagation speed;
  ➢ Attenuation coefficient determination;
  ➢ Material noise level measurement;
  ➢ Internal discontinuities finding.

Ultrasound propagation speeds have to be determined by more than 2% accuracy. By-product is considered to be able to further work out whether the determined ultrasound wave speeds frame within limits and tolerances given in product standards. An other parameter, that characterizes the calibration block quality is ultrasound attenuation. Attenuation determined in 4 MHz frequency transversal ultrasound weaves has to be placed around 0,05 dB/mm. According to the product standards the material noise level has not to exceed 10% of screen height of ultrasound examination equipment. Maximum amplitude of discontinuities have not to exceed the material noise level. Final work out has to provide each surface roughness less than 0,8 μm.

Each calibration block will have marked the followings:
  ➢ Items intended for identification of lengths and angles;
  ➢ Standard of product;
  ➢ Series of manufacture;
  ➢ Manufacturer mark.

Each calibration block of this type has to be delivered with:
  a. Quality certificate which certifies:
  ➢ Conformity with the product standard;
  ➢ Average value of ultrasound longitudinal waves measured speeds;
  ➢ Average value of ultrasound transversal waves measured speeds;
  ➢ Attenuation average value;
  ➢ Material noise level.
  b. Metrology control bulletin.

3.2 Reference blocks

Ultrasound equipment adjustment for working sensitivity determination and estimation of echoes amplitude is made by helping of a large number of reference blocks and aims several accurate and reproducible indications getting from discontinuities.

Reference blocks have to fulfill the following conditions:
  ✓ To be made of a very good quality material similar to that one controlled;
  ✓ To be very accurate made and worked out;
  ✓ Sizes and structural shape have to be close to the examined product;
  ✓ To offer the possibility of determination the discontinuity characteristics (position, size, nature).

For curved parts, which require the detector base adjustment, the reference block thickness and curve do not differ by more than 10% of those of the examined object. In case of control application to parts and by-products made of aluminum, Plexiglas, austenite steels, copper, bronze, bimetal, etc, suitable reference blocks will be made by these materials. By-products have to be nondestructive examined in order to provide the requirements of material properties homogeneity from point of view of ultrasound examination by:
  ✓ Determination of longitudinal and transversal ultrasound waves propagation;
  ✓ Attenuation coefficient determination;
  ✓ Material noise level metering;
  ✓ Inside discontinuities finding.

Ultrasound wave propagation speed, attenuation, material noise level, are determined in the same way as in case of calibration blocks.

According to the Management Quality System each reference block will have marked the followings:
  ✓ Conformity with the SR EN 1714 standard stipulations;
 ✓ Material quality;
  ✓ Manufacture series;
  ✓ Manufacturer trade.
And will be delivered together with:
  a. A quality certificate which certifies:
  ✓ Material quality;
  ✓ Chemical composition;
  ✓ Average value of transversal ultrasound wave speeds measured;
  ✓ Attenuation average value;
  ✓ Material noise level.
  b. Bulletin of metrology control with sizes of block and reference reflectors.

4. Manufacture, check and control technologies of calibration and reference blocks

They are based on the following two large groups of technologies:

a. Execution for each calibration and reference block (examples in figures no. 1 and 2);
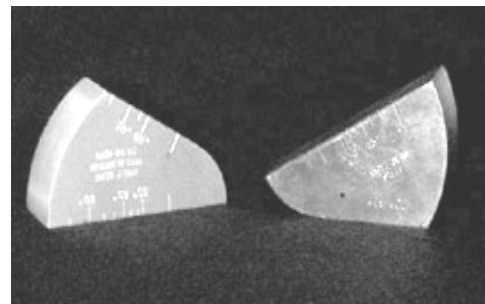
***Fig. 1** – Calibration block no. 2*

Fig. 2 – Reference block

b. Check and control commonly for all types, as it follows:

➢ **TV 01** – „Technology for receiving the by-products used for calibration and reference blocks manufacturing"

➢ **TV 02** – "Technology for check and control the material surface by visual and penetration liquid examinations".

➢ **TV 03** – „Technology for check and control of several material characteristics by ultrasound nondestructive examinations (propagation speed, attenuation, material noise, inside discontinuities) used to make the calibration and reference blocks".

➢ **TV 04** – „Technology for check and control of sizes (lengths and angles) used to make calibrating and reference blocks".

➢ **TV 05** – „Receiving technology and quality certificate issuing and marking the calibration and reference blocks".

References

[1].**Tovică M.,** *Metode de evaluare a componentelor structu-rilor metalice cu defecte, pe baza conceptelor mecanicii ruperilor.* Curs ISIM Timişoara, 2000 România,

[2]. **Stanciu Cr.,** *Studiu documentar şi de marketing privind blocurile de etalonare şi referinţă.* S.C. UZINSIDER Engineering Galaţi, 2003.

[3]. **Ciobanu E., Ciobanu M.,** *Certificarea produselor conform reglementărilor Uniunii Europene.* Revista Tribuna Calităţii nr. 4 ÷ 5, Anul IV, aprilie-mai 1999, pg.52 ÷ 62. ISSN 1224-3116

[4]. **Volker D., Platte M., Vogt M.,** *Controlul ultrasonic.* Principii şi aplicaţii industriale, Focşani, 1998,

[5]. **SR EN ISO 17025,**: *Cerinţe generale pentru competenţa laboratoarelor de încercare şi etalonare,* 2001

[6]. **Markucic D.,.Mudronja V., Sanjin M., Runje B.** *Quality Requirements for Ultrasonic Testing Calibration Blocks* NDT. Net-vol. 8 no. 3 pp 1 ÷ 8. , 2003

[7]. **Millea A.,** *Informaţie şi incertitudine în măsurători.* Editura Tehnică. Seria tehnică, 1981, Bucureşti.

[8]. **Bohăţiel T., Năstase E**., *Defectoscopie ultrasonică fizică şi tehnică,* Tehnică Bucureşti, 1980, România

SURFACE TENSION OF LIQUID COPPER IN DILUTE OXYGEN CONCENTRATIONS

Maria VLAD, Elisabeta VASILESCU

"Dunărea de Jos"University of Galati

e-mail: mvlad@ugal.ro

ABSTRACT

The studies of this paper regarding the influence of low oxygen contents on the liquid copper surface tension had as base „sessile drop" method and the determination of the oxygen content using calculation ratio where partial pressure of the oxygen is in equilibrium with the melt in a gaseous atmosphere. The surface tension of the liquid copper, with very low oxygen contents has been studied at various temperatures (1373, 1423, 1473, 1523 and 1573 K).

KEYWORDS**:** superficial tension, copper, oxygen content

1. Introduction

The „sessile drop" method makes the size analysis of a drop resting on a horizontal and flat support, figure.1. The drop is considered in equilibrium under the action of the capillary forces and its weight.
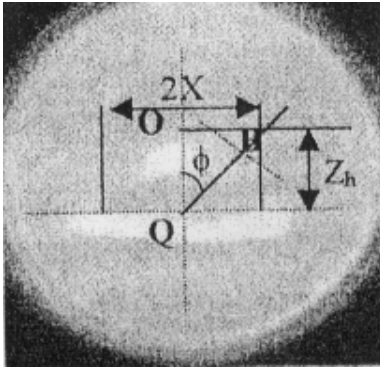
Fig. 1. *Geometry of a drop rested on an inactive support.*

The pressure, P, of the liquid in a point B is given by the relation:

$$P = \sigma\left(\frac{1}{R_1} - \frac{1}{R_2}\right) = \rho g z + c \qquad (1)$$

where: z – is the vertical distance of point B from the axis origin,

g – is gravity acceleration,

ρ - is density difference between liquid and environment,

R_1 and R_2 curvature radius of the point B considered by interface of a tow normal planes, c – is a constant.

If X is the abscissa of the point B considered at interface and φ - is the angle made by the normal to the surface in this point and by the vertical axis, one of the curvature is $R_1 = X/X\sin\varphi$, and the other one is $R_2 = R$.

Consequently:

$$\sigma\left(\frac{1}{R} + \frac{\sin\varphi}{X}\right) = \rho g z + c \qquad (2)$$

Studying the condition of the limit, y=0, $R_1 = R_2 = b$, where b is curvature radius at drop top, it is concluded c=2 σ/b. Relation. (2) may be as following:

$$\frac{b}{R} + \frac{b\sin\varphi}{X} = 2 + \frac{\rho g b^2}{\sigma}\cdot\frac{z}{b} = 2 + \beta\frac{z}{b} \quad (3)$$

The drop shape is depending on the parameter $\beta = \rho g b^2/\sigma = b^2/a^2$, where β is named shape factor and a^2 capillary constant. Using the numerical calculation proposed by Bashforth and Adams, the analyses of the drop profile allows determination of value a^2 and, consequently, of a superficial tension:

$$\sigma = \frac{b^2}{\beta} g\rho = z^2 g\rho \qquad (4)$$

Drop parameters required for surface tension determination are determined by taking a photo of the apparatus belonging to the outfit used for determination. Also, photos have access to the measurement of the joining angle θ of the liquid on the support. Generally, the measured parameters are

the equatorial diameter 2R, the distance z from drop top to equatorial plane, or the distance h from point O to point A. The precise position of this plane is not easy to be determined because it is not a symmetry plane.

2. Materials and equipment

The experimental determination was made at Miskolc University on an installation, schematically represented in figure.2.
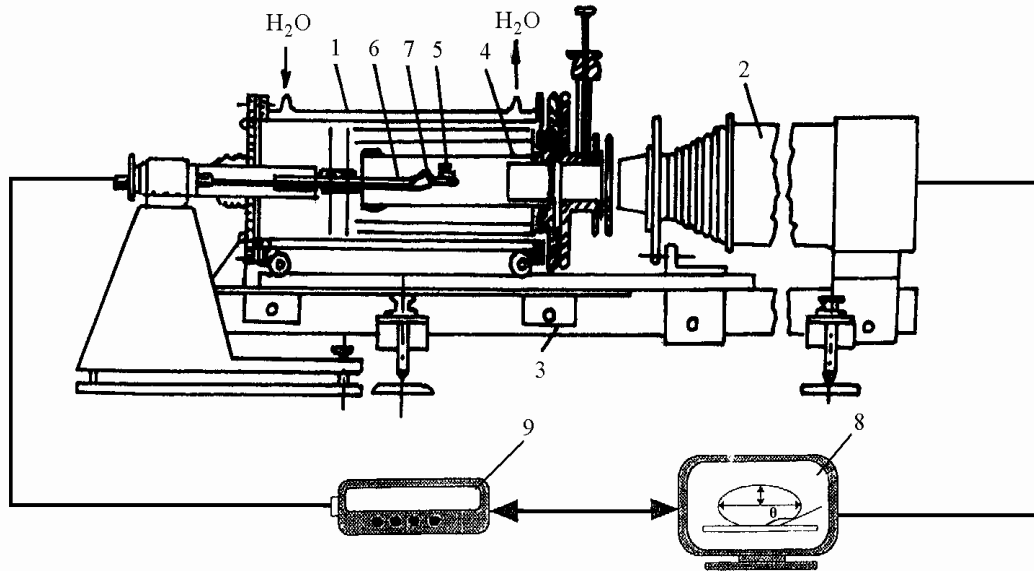
Fig. 2. *Schematic arrangement of the experimental apparatus.*

1. furnace cooler;
2. camera CCD and microscope objective
3. support
4. Al_2O_3 protective tube
5. alloy drop;
6. thermocouple
7. Al_2O_3 support
8. image of the metal drop
9. digital multimeter

Heating and test specimen melting were made by a horizontal electrical resistance furnace with a silicon carbide heating element.. In the furnace is a zone of uniform temperature along side of 4 cm where temperature variation is ± 1 K and a zone of 8 cm length where temperature variation is ± 5 K at 1723 K. Drop temperature was measured by a thermocouple Pt-PtRh 13 placed under the purity recrystallized Al_2O_3 disk, used as support of the drop. Disk surface was polished with corundum powder and well washed, in advance, in alcohol and acid solution, distilled water and acetone, and heat up in vacuum at about 1700 K afterwards. The photos of the molten hot drop were made by a 35 mm camera with fix focusing combined using 5 or 10 mm diameter steel balls.

3. Experimental procedure

The copper used as test specimen having 99,99% purity was vacuum remelted. To check the molten copper drop condition and measure surface tension in pure hydrogen atmosphere, when

$P_{O_2} < 10^{-20}$ atm. same photo have been taken. After introduction of $H_2 - CO_2$ mixture it was found that molten copper drop reached in equilibrium with this gas after about 2 hours from mixed gas admission. The measurements of the superficial tension were made after still maintaining the equilibrium state for another hour. The partial pressures of the oxygen in equilibrium with $H_2 - CO_2$ mixtures were determined at high temperature, considering the gaseous mixture as H_2, CO_2, H_2O and CO attending to the reaction:

$$H_2 + CO_2 = H_2O + CO \qquad (5)$$

The equilibrium constant K of the reaction (5) is given by the relation:

$$k = \frac{P_{H_2O} \cdot P_{CO}}{P_{H_2} \cdot P_{CO_2}} \qquad (6)$$

Between the partial pressures of the gases $H_2O(v)$, CO, H_2 and CO_2 the following relation could be written.

$$\frac{(P_{CO_2})_i}{(P_{H_2})_i} = \frac{P_{CO_2} + P_{CO}}{P_{H_2O} + P_{H_2}} \qquad (7)$$
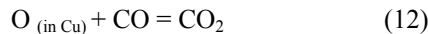
where coefficient „i" is referring to the initial gaseous mixture. Considering $P_{H_2O} = P_{CO}$ and replacing equation (6) into (7) results in:

$$\frac{(P_{CO_2})_i}{(P_{H_2})_i} = \frac{P_{CO_2}(1 + P_{CO_2}/P_{CO})}{P_{CO}(1/k + P_{CO_2}/P_{CO})} \qquad (8)$$

$$P_{O_2} = \frac{1}{4}k_1^2\left[\frac{(P_{CO_2})_i}{(P_{H_2})_i} - 1 + \sqrt{\left\{\frac{(P_{CO_2})_i}{(P_{H_2})_i} - 1\right\} + \frac{4(P_{CO_2})_i}{k(P_{H_2})_i}}\right]^2 \qquad (11)$$

As k and k_1 are known for a given temperature the equilibrium partial pressures of the mixture's oxygen has been calculated from the equation (11) for a given ratio $(P_{CO})_i$ / $(P_{H_2})_i$ of the initial mixture. Finding the partial pressure of the oxygen in gaseous phase by the above mentioned relations, the dissolved oxygen content in molten copper could be calculated supposing that CO-CO$_2$ mixture is in equilibrium with the melt.

The chemical reaction was considered:

$$O_{(in\ Cu)} + CO = CO_2 \qquad (12)$$

Considering the chemical reaction:

$$CO_2 = CO + ½ O_2 \qquad (9)$$

$$k_1 = \frac{P_{CO} \cdot P_{O_2}^{1/2}}{P_{CO_2}} \qquad (10)$$

So that the following expression is obtained from equation (8) and (10

$$k_2 = \frac{P_{CO_2}}{P_{CO} \cdot a_O} \qquad (13)$$

where a_O is the oxygen activity in the molten copper.

The temperature dependency of k_2 constant is given by Sake as following:

$$\log k_2 = \frac{10600}{T} - 3.82 \qquad (14)$$

Replacing equation (10) in equation (13) the oxygen activity in molten copper, a_O, was determined from relation:

$$a_O = \frac{1}{2k_2}\left[\frac{(P_{CO_2})_i}{(P_{H_2})_i} - 1 - \sqrt{\left\{\frac{(P_{CO_2})_i}{(P_{H_2})_i} - 1\right\}^2 + \frac{4(P_{CO_2})_i}{k(P_{H_2})_i}}\right] \qquad (15)$$

At very low concentration of oxygen $a_O = [\%O]$ so that [%O] could be calculated with equation (15).

4. Experimental results

The experimental results of the surface tension variation function of copper temperature at low quantities of oxygen are given in table 1.

The surface tension variation on liquid copper with 0.012% oxygen; versus temperature and $\log P_{O_2}$ is given in table 2.

Table 1. *The surface tension variation of copper with low oxygen contents at different temperatures*

Number	0,005 % oxygen		0,012 % oxygen		0,068 % oxygen	
	T[K]	σ [mN/m]	T[K]	σ [mN/m]	T[K]	σ [mN/m]
1	1373	1296	1373	1186	1373	915
2	1423	1293	1423	1194	1423	943
3	1473	1291	1473	1208	1473	965
4	1523	1290	1523	1216	1523	980
5	1573	1276	1573	1225	1573	996

Table 2. *The surface tension variation on liquid copper with 0.012% oxygen; versus temperature and* $\log P_{o_2}$

Number	1373 K		1473 K		1573 K	
	$\log P_{o_2}$ [atm]	σ [mN/m]	$\log P_{o_2}$ [atm]	σ [mN/m]	$\log P_{o_2}$ [atm]	σ [mN/m]
1	-11.52	1298	-11.21	1292	-11.02	1288
2	-10.05	1279	-9.93	1281	-9.90	1285
3	-8.82	1225	-8.73	1229	-8.75	1238
4	-8.20	1188	-8.11	1210	-8.10	1227
5	-7.60	1138	-7.10	1161	-7.20	1180
6	-6.52	917	-6.31	967	-6.45	998

Relation between the surface tension (σ) of liquid copper with 0.005% oxygen at different temperatures and $\log P_{o_2}$ is given in fig.3
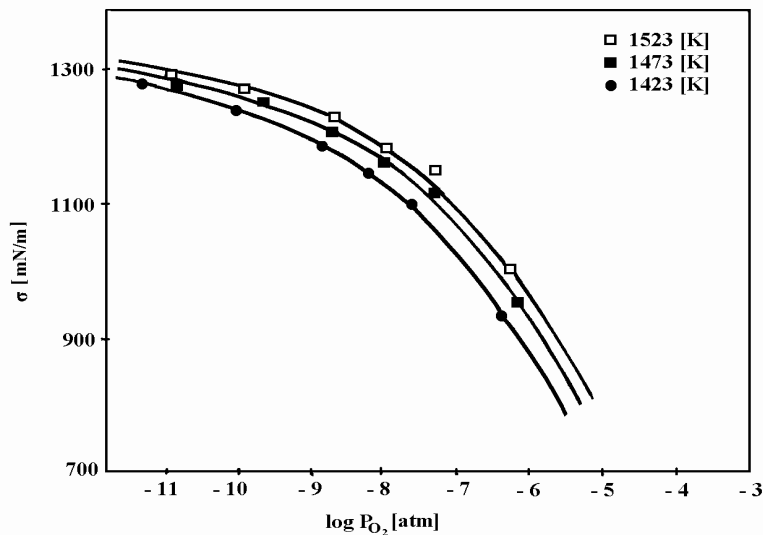
Fig. 3. *Relation between the surface tension (σ) of liquid copper with 0.068% oxygen at different temperatures and* $\log P_{o_2}$

5. Conclusions

1. The determination of the oxygen content was made by using calculation ratio where partial pressure of the oxygen is in equilibrium with the melt in a gaseous atmosphere.

2. The experimental results show that at 0.005% oxygen the influence of oxygen on surface tension of liquid copper is very small

3. For a little bit higher oxygen concentration in copper (0,012 % oxygen and 0,068 % oxygen) could be noted a light increase of the surface tension on temperature increase.

References

[1].**Taihei Matsumoto, Hidetoshi Fujii, Takaharu Ueda, Masayoshi Kamai and Kiyoshi Nogi**, *Measurement of surface tension of molten copper using the free-fall oscillating drop method,* Meas. Sci. Technol. 16**,** p**.** 432-437, 2005

[2]. **Zhangfu Yuan, Jianfeng Fan, Jing Li, Jiajun Ke and Kusuhiro Mukai,** *Surface tension of molten bismuth at different oxygen partial pressure with the sessile drop method,* Scandanavian Journal of Metallurgy Volume 33, p. 338 December 2004.

[3]. **P. Sahao, T. Debroy**, **and Mc.Nallan N.J.,** *Metal Transaction* B., vol.19B, 1988, p.483-490.

[4].**Keene B**.J - .*International MaterialsReviews*,vol.38,nr.4,199

[5]. **M.Vlad**, Thesis of doctor, *Researches on microalloying copper base alloys*, "Dunarea de Jos" University, Galati, 1994, Romania.

RESEARCHES CONCERNING PHASE TRANSITION OF ZIRCONIUM TITANATE PREPARED BY ELECTROLYTIC METHOD

Livia GHEORGHIES
"Dunarea de Jos" University of Galati
email: Livia.Gheorghies@ugal.ro

ABSTRACT

Powder zirconium titanate ceramics obtained by an electrolytic method has been investigated. Continuous phase transition were found to occur in powder zirconium titanate above and below a major discontinuity at $1120^oC\pm10^oC$. The phase transition is characterised by a decrease in the length of the longest unit-cell dimension, on conversion of the high-temperature form to the low-temperature structure. The unit-cell volume decreases continuously and linearly with decreasing temperature.

KEYWORDS: zirconium titanate, electrodeposition, phase transition, structure

1. Introduction

Zirconium titanate is a ceramic material that is used not only in the refractory industry but has application in electronic industry. Zirconium titanate is well known for the stability of some properties, namely those dielectrics, as well as for the small electric leakage. All these properties lead to its using in fabrication of condensers and resonant components at filters and oscillators with stable frequency in microwaves field.

Zirconium titanate is one of the most important ferroelectric materials used in manufacturing of ceramic transducers [4, 5]. Along with extension of using domain of zirconium titanate, the interest for preparation crystalline structure, phase transformation and for factors that influence the dielectric properties has been amplified.

Currently, is known that solid solution of $ZrTiO_4$-$Zr_5Ti_7O_{27}$, over temperature of 1200^oC, has an orthorhombic structure of α-PbO_2 type where zirconium and titanium atoms are random distributed into octahedral holes that are equivalents point of view of symmetry, such as presented in figure 1. Below 1200^oC, all compositions suffer a continuum phase transformation characterised by an increased arrangement of zirconium and titanium atoms.

For compositions that are similarly with $ZrTi_2O_6$ (e.g. $Zr_5Ti_7O_{24}$) ordinate structure has zirconium atoms segregated in each the third octahedral layer along of axis a, as in figure 1 (b) [1]. The passing from the form that is typical for the high temperature to the form that is specific at low temperature is characterised by a decreasing of the dimension of the higher elementary cell. The dimensions of the elemental cell are dependent of the thermal treatment history. In technical literature there are papers that present data concerning solid solutions of zirconium titanate obtained at high temperatures starting from titanium oxide and zirconium oxide.

2. Experimental

Present study has main aim the monitoring the structure of zirconium titanate at high and low temperature prepared by electrolytic method [3].
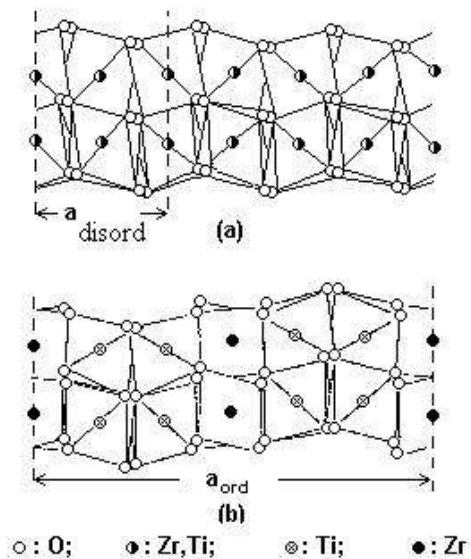

o : O;   ◐ : Zr,Ti;   ⊗ : Ti;   ● : Zr

Fig. 1. *Projection of zirconium titanate on (010) plane.*

As opposed to classical methods where temperatures around of 1500^oC are necessary, in this case zirconium titanate is obtained at temperature of 600^oC-800^oC. After thermal treatment accomplished in air, powder, initially being in amorphous state, becomes crystalline.

This aspect has been carried out by X-ray diffraction method on DRON-3 equipment in CuKα radiation with U=32kV and I= 22mA.

It is worthy of note that powder didn't contain one of individual components of zirconium or titanium oxides and the analysis performed with electronic probe sowed a ratio Zr/Ti in the 0,97-1,02 range.

Hereby, obtained powder has been subjected to certain thermal treatments into chamber of high temperature of type UDV-1800 that is an annex of X-ray diffractometer.

The temperature was measured by a Pt-PtRh (10%) thermocouple having an accuracy of $\pm 1^oC$ and electronic controlled.

The heating was done up to 1400^oC, monitoring the phase modification and evolution of lattice parameters by using a computerised technique on base of diffraction data [2].

3. Results and discussions

Different samples of zirconium titanate have been subjected to thermal treatment at various temperatures in range of 800^oC-1400^oC. The heating was performed with a rate of 1^oC/min.

Before recording the diffraction spectrum, the sample has kept a hour at treatment temperature. The experiments were performed in two manners.

A first mode consisted in monitoring of the same sample at diverse temperatures of thermal treatment, both heating and cooling.

The second mode consisted in heating of sample at each temperature of chosen thermal treatment, thus the X-ray diffraction spectrum was recorded.

The performed calculus didn't evinced significant differences in order to be taken in discussion.

In figure 2 the variation of lattice parameters versus thermal treatment temperature. The lattice parameter was estimated by measuring the angular position of X-ray diffraction lines appeared at high angles. In this way a good the accuracy of lattice parameter is obtained.

It was ascertain that the lattice parameter having the higher value, namely **c**, presents an accentuate variation in temperature range of 1100-1200^oC.

This result is in accordance with measurements of electric conductivity In range of temperatures corresponding to transition phase, that is approximate to 1200^oC, a significant variation of electric

conductivity was carried out that can be connected to a modification of the electric charge type.
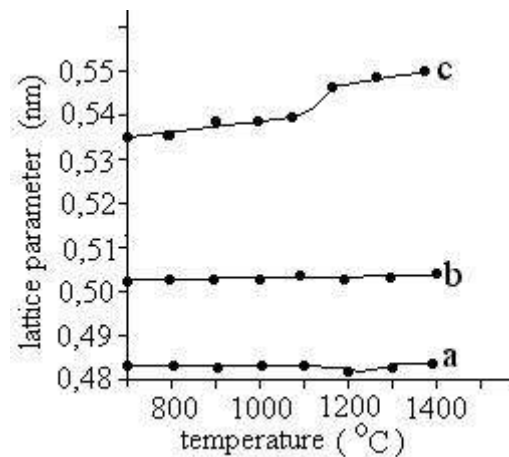
Fig. 2. *Variation of dimension of elemental cell on thermal treatment temperature.*

These results were interpreted as indicating a structural transition that occurs in this temperature range and that is accompanied of a deficiency of oxygen at high temperature and an excess of oxygen at low temperature [6].

Beside the accentuate variation of lattice parameter **c** which occurs at transition temperature between phase present at high temperature and phase from low temperature, a weak linear variation both above and bellow transition temperature.

The dimensions in direction of axis **a** and **b** remain unchanged after phase transition. In vicinity of transition temperature order-disorder a small variation of parameter **a** ascertained, but it can be considered as minor in regard to spread of experimental data. In studied temperature range, parameter **b** didn't present important changes.

The volume of elemental lattice presents a weak variation in regard to temperature. It continually and linearly decreases in proportion as thermal treatment temperature decreases both for phase from low temperature and the phase from high temperature.

The transition from the form that is present at high temperature to the form that is present at low temperature difficult occurs and demand a long time, it depending, probably, of cooling rate and thermal treatment temperature. Hereby, the cooling from 1400^oC at temperature around 700^oC having a rate of 1^oC/h is not accompanied of a complete transformation.

If the cooling occurs from temperature of 1200^oC at 700^oC, having the same rate, it is possible to obtain a complete passing at structure from low temperature. The difficult kinetic of transformation is an index of a structural changes that requests a

rearrangement on long distance of cations from lattice.

The continuously decreasing of volume of elemental lattice can correspond to a "modulation" of packing of anions as a response to ordering of cations. This fact can change the coordination of zirconium from six to seven or eight as is in other structures where zirconium is present.

The "modulation" of anions packing doesn't lead to a modification of crystal symmetry, fact that is proved by X-ray diffraction spectrum.

Continuously phase transition can be connected to continuously thermodynamic changes concerning to order-disorder characteristic of zirconium and titanium ions. The diffraction studies with neutron and electrons, as well as electronic microscopy can bring further information hereto.

4. Conclusions

1. Zirconium titanate powder prepared by electrolytic method has been subjected to thermal treatment and by XRD technique the lattice parameters were estimated at various temperatures.

2. During thermal treatment the lattice parameters **a,** and **b** remain unchanged, while the lattice parameter **c** presents an accentuate variation in temperature range of 1100-1200°C.

3. The changes of lattice parameter **c** can be connected with significant variation of electric conductivity, indicating a structural transition

accompanied of a deficiency of oxygen at high temperature.

4. At the same heating or cooling rate, the transition of lattice cell between the same two temperatures occur with different transformation kinetics due to further requested time for rearrangement on long distance of cations from lattice.

5. The continuously decreasing of volume of elemental lattice can correspond to a "modulation" of packing of anions as a response to ordering of cations.

References

[1]. **Christoffersen, R., P. K. Davies**, 1992, "*Structure of Commensurate and Incommensurate Ordere Phase in the System $ZrTiO_4$-$Zr_5Ti_7O_{24}$*", J. Am. Ceram. Soc. 75, 3**,** pp. 563-69.

[2]. **Grosse-Kunstleve, R. W., McCusker, L. B., Baerlocher, Ch.,** 1997, "*Powder Diffraction Data and Crystal Chemical Information Combined in an Automated. Structure Determination Procedure for Zeolites*" J. Appl. Cryst. 30, pp. 985-995

[3]. **Gheorghies, L**., 1998, "*Contribuţii la obţinerea şi studiul unor electrodepuneri ceramice cu proprietăţi superioare*", Teza de doctorat, Universitatea "Dunărea de Jos" din Galaţi.

[4]. **Moulson, A. J., Herbert, J. M.,** *Electroceramics*, 1990, Ed. Chapman & Hall, London, U. K.

[5]. **Negas, T., Yeager, G., Bell, S., Amren, R.,** 1990, "*Chemistry and Properties of Temperature Compensated Microwave Dielectrics*", pp. 21-38, Ed. P. K. Davies and R. S. Roth, Washington, DC,

[6]. **Wolfram, G., Gobel, E**., 1981, "*Existence Range, Structural and Dielectric Properties of $Zr_xTi_ySn_zO_4$ Ceramics (x+y+z=2)*", Mater. Res. Bull., 16, 11, 1455-63,.

FUEL ECONOMY AT THE HEAT TREATMENT FURNACES OF STEEL CAST PIECES

**Lilica IVANESCU, Alexandru IVANESCU,
Antoaneta ENE**

"Dunarea de Jos" University of Galati
e-mail: ivanescu.lilica@ugal.ro

ABSTRACT

The paper presents a study made at the annealing furnaces for homogenization of cast pieces regarding the replacement of marsh gas with blast furnace gas, in a proportion of 100%. In this way an important economy of marsh gas is achieved, representing a special interest because its international deficit and its putting up the price.

KEYWORDS : blast furnace gas, oxygen, fuel economy

1. Introduction

At present, in Mixed Foundry of Mittal Steel Iron and Steel Works at Galati, at the heat treatment furnaces of steel moulded pieces, the marsh gas is used as fuel [1-3] which is, as we know, an expensive and defficitary fuel. On the other hand in many foundries, as is the case of the above mentioned one, there are fuel wastes such as coke gas or furnace gas.

The paper presents a study made at the annealing furnaces of the steel moulded pieces homogenization regarding the replacement of marsh gas with furnace gas in a 100% proportion. Thus an important economy of march gas is obtained. The provision that has to be complied with is that the same amount of heat as in the case of the replaced marsh gas should be obtained in the working space of the furnace, in the different options of fuel utilization. In order to achieve that, in the case of the combustion of the blast furnace gas to a 100% degree, the using of oxygen-enriched air during combustion has to be done. In this paper the concentration of oxygen in the oxygen-enriched air is determined in the case of the hundred percent combustion of furnace gas.

2. Technical characteristics of the annealing furnaces of the steel moulded pieces homogenization

- The furnace capacity (pieces + supports), C=75t;
- The bedstone surface, S_V=32 m^2.
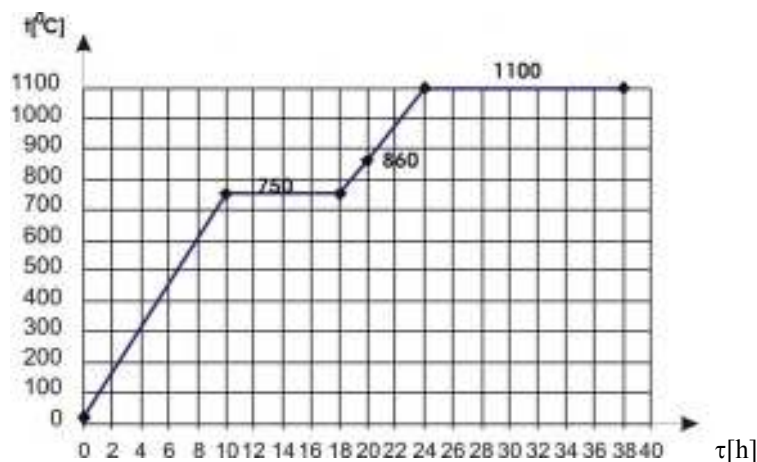- The maxim piece temperature, t_m=1100 ^{0}C;

***Fig.1.** The diagram of the steel moulded pieces heating in the homogenizing annealing furnaces*

- The furnace temperature (technological), $t_{tech}=t_m+(100-150)^0C$;
- The burning unit:
  12 burners x 50 Nm^3/h
  12 burners x 20 Nm^3/h
- Marsh gas consumption, D_{CH_4} =400 Nm^3/h;
- The cycle duration, τ_{cycle}=38h;
- The heating diagram (see fig.1).

3. The calculus of the fuel burning

The burning calculus is made in two varieties, namely marsh gas and furnace gas in a 100% proportion, respectively.

The calculus relations are the following [4]:
- the fuel chemical composition:

$CH_4+CO+H_2+CO_2+O_2+N_2+H_2O=100$ %
$[CH_4]+[CO]+[H_2]+[CO_2]+$
$+[O_2]+[N_2]+[H_2O]=1Nm^3$ (1)

- the inferior calorific power H_i, in [kJ/Nm^3 fuel]:

$$H^i = [CH_4] \cdot H_i^{CH4} + [CO] \cdot H_i^{CO} +$$
$$+[H_2] \cdot H_i^{H2}$$ (2)

where:
$[CH_4], [CO], [H_2]$- the quantities of the combustion elements, in [Nm^3/Nm^3 fuel];
$H_i^{CH4}, H_i^{CO}, H_i^{H2}$ = inferior calorific powers of the combustion elements, in [kJ/Nm^3];

$$H_i^{CH4} = 35500 \text{ kJ/Nm}^3$$
$$H_i^{CO} = 12740 \text{ kJ/Nm}^3$$
$$H_i^{H2} = 12765 \text{ kJ/Nm}^3$$

- the minimum amount of oxygen necessary for the combustion, O_2^{min}, in [Nm^{3}O$_2$/Nm^3 fuel]

$$O_2^{min} = 2[CH_4] + \frac{1}{2}[CO] + \frac{1}{2}[H_2] - [O_2]$$ (3)

-the theoretic air necessary for the combustion, L_0, in [Nm^{3}air/Nm^3 fuel]:

$$L_0 = \frac{100}{21} \cdot O_2^{min}$$ (4)

- the real air used for the combustion, L_r, in [Nm^{3}O$_2$/Nm^3 fuel]:

$$L_r = \lambda L_0$$

where:

λ – the coefficient of excess air; the adopted value: λ=1.05

-the quantity of the burned gases, V_{ga}, in [Nm ga/Nm^3 fuel]:

$$V_{ga} = V_{CO_2} + V_{H_2O_{vap}} + V_{N_2} + V_{O_2excess}$$ (5)

where:

$V_{CO_2} = [CO_2]+[CH_4]+[CO]$

$V_{H_2O_{vap}} = 2[CH_4]+[H_2]+[H_2O]$

$V_{N_2} = 0.79L_r+[N_2]$

$V_{O_2excess} = 0.21(L_r - L_0)$

-the participations of the component elements of the burned gases, r_i :

$$r_{CO_2} = \frac{V_{CO_2}}{V_{ga}}$$ (6)

$$r_{H_2O_{vap}} = \frac{V_{H_2O_{vap}}}{V_{ga}}$$

$$r_{N_2} = \frac{V_{N_2}}{V_{ga}}$$

$$r_{O_2excess} = \frac{V_{O_2excess}}{V_{ga}}$$

$$\sum_{i=1}^{4} r_i = 1$$

-the real burning temperature [4], t_r, [^{0}C]:

$$t_r = \eta_{pyr} \frac{0.98 \cdot H_i}{V_{ga} \cdot c_{ga}}$$ (7)

where:
η_{pyr} - the pyrometric efficiency; the adopted value η_{pyr} =0.7;
H^i – the inferior calorific power, [kJ/Nm^3 fuel];
V_{ga} – the volume of the burned gases, [Nm^3/Nm^3 fuel],
c_{ga} – the specific heat of the burned gases [kJ/Nm^{3}grd].

-the specific heat of the burned gases c_{ga}, [kj/Nm^{3}grd]:

$$c_{ga} = \sum_{i=1}^{4} c_i \cdot r_i$$ (8)

where:
c_i – the specific heats of the components of the burned gases, which are tabelled as a function of temperature. The adopted value for the temperature of

the burned gases is $t_r = 1000\ ^0C$ and $c_{ga}\ 1000\ ^0C$ can be calculated using the values:

$$c_{CO_2}\ 1000\ ^0C = 2.2035 \text{ kJ/Nm}^3\text{grd}$$

$$c_{H_2O_{vap}}\ 1000^0C = 1.7229 \text{ kJ/Nm}^3\text{grd}$$

$$c_{N_2}\ 1000^0C = 1.3917 \text{ kJ/Nm}^3\text{grd}$$

$$c_{O_2}\ 1000^0C = 1.4775 \text{ kJ/Nm}^3\text{grd}$$

It results:

3.1. The burning of the marsh gas

$$c_{ga}\ 1000^0C = 0.091 \cdot 2.2035 +$$
$$+ 0.182 \cdot 1.7229 + 0.717 \cdot 1.3917 +$$
$$+ 0.01 \cdot 1.4775$$

$$c_{ga}\ 1000^0C = 1.529\ \text{kJ/Nm}^3\text{grd}$$

$$t_r = \frac{0.7 \cdot 0.98 \cdot 35500}{11 \cdot 1.529} = 1447.9\ ^oC \cong 1448\ ^oC$$

$$\text{error} = \frac{t'_r - t_r}{t'_r} 100 =$$
$$= \frac{1448 - 1000}{1448} 100 = 30.9\% \gg 5\%$$

With the admitted error of 5%, $c_{ga}\ 1448^0C$ is calculated, by determining the specific heats of the components by interpolation, as a function of their values at the temperatures of 1400 ^0C and 1500 ^0C.

$$c_{CO_2}\ 1448^0C = 2.3136 + \frac{48 \cdot 0.0218}{100} = 2.324$$

$$c_{H_2O}\ 1448^0C = 1.828 + \frac{48 \cdot 0.0247}{100} = 1.8398$$

$$c_{N_2}\ 1448^0C = 1.4348 + \frac{48 \cdot 0.0092}{100} = 1.4392$$

$$c_{O_2}\ 1448^0C = 1.5203 + \frac{48 \cdot 0.0091}{100} = 1.5246$$

$$c_{ga}\ 1448^0C = 0.091 \cdot 2.324 + 0.182 \cdot 1.8398 +$$
$$+ 0.717 \cdot 1.4392 + 0.01 \cdot 1.5246$$

$$c_{ga}\ 1448^0C = 1.593 \text{ kJ/Nm}^3\text{grd}$$

$$t''_r = \frac{0.7 \cdot 0.98 \cdot 35500}{11 \cdot 1.593} = 1389.7 \cong 1390^0C$$

$$\text{error} = \frac{1390 - 1448}{1390} 100 = -4\% < -5\%$$

$$t_r^{CH_4} = 1390\ ^oC$$

3.2. The burning of the furnace gas

$$c_{ga}\ 1000^0C = 0.2571 \cdot 2.2035 + 0.056 \cdot 1.7229 +$$
$$+ 0.6824 \cdot 1.3917 + 0.0045 \cdot 1.4775 = 1.619$$

$$t'_r = \frac{0.7 \cdot 0.98 \cdot 3716}{1.581 \cdot 1.619} = 995.9 \cong 996^o C$$

$$\text{error} = \frac{996 - 1000}{996} 100 = -0.4\%$$

$$t_r^{GF} = 996^o C$$

The thermodynamic parameters at the burning with atmospheric air of the marsh gas or furnace gas respectively, and the chemical composition of the fuel are given in Tables 1 and 2.

The thermodynamic parameters at the burning with atmospheric air

Table 1

Fuel	The chemical composition of the fuel [%]								The calorific power, H_i [kJ/Nm³]	O_2^{min} [Nm³/ Nm³ fuel]
	CH_4	CO	H_2	CO_2	O_2	N_2	H_2O	Tot.		
Marsh gas	100	-	-	-	-	-	-	100	35500	2
Furnace gas	0.20	22.45	6.15	18.00	0.20	50.70	2.30	100	3716	0.145

Table 2

Fuel	L_0 [Nm^3/ Nm^3 fuel]	L_r [Nm^3/ Nm^{3}fuel]	V_{ga} [Nm^3/Nm^3 fuel]					Participations in the burned gases, r_i					Burning temp.
			V_{CO_2}	V_{H_2O}	V_{N_2}	V_{O_2ex}	Tot.	r_{CO_2}	r_{H_2O}	r_{N_2}	r_{O_2ex}	Tot.	
Marsh gas	9.52	9.996	1	2	7.89	0.1	11	0.091	0.182	0.717	0.01	1	1390
Funace gas	0.690	0.724	0.4065	0.0885	0.0789	0.0071	1.581	0.2571	0.0560	0.6824	0.0045	1	996

4. Study regarding the utilization of the furnace gas in a proportion of a hundred percent at burning

As it results from § 3.2. the burning temperature of the furnace gas with atmospheric air is 996 ^{0}C. The technological process of the homogenizing annealing furnace neccessitates an optimal temperature in the working space of 1200-1250 ^{0}C.

A method to increase the burning temperature is the utilization, at burning, of the oxygen enriched air.

The oxygen concentration in the enriched air (fig. 2) is calculated with the relation [5]:

$$x = \frac{\lambda\left\{\frac{1}{2}[CO]+\frac{1}{2}[H_2]+2[CH_4]-[O_2]\right\}}{\frac{\eta_{pyr}\cdot 0.98\cdot H_i}{t_f\cdot c_{ga}}-\frac{1}{2}[CO]-[CH_4]-[CO_2]-[H_2O]-[N_2]-\frac{1}{2}[H_2]-[O_2]} \quad (9)$$

considering $t_f = t_m+150=1250$ ^{0}C.

$c_{ga}{}^{1250^0C}$ is calculated as follows,

$$c_{ga}{}^{1250^0C} = \sum_{i=1}^{4} r_i \cdot c_i$$

using the values:

$$c_{CO_2}{}^{1250^0C} = 2.2768$$

$$c_{H_2Ovap}{}^{1250^0C} = 1.7898$$

$$c_{N_2}{}^{1250^0C} = 1.4197$$

$$c_{O_2}{}^{1250^0C} = 1.5055$$

$$c_{ga}{}^{1250^0C} = 0.2571\cdot 2.2768 + 0.056\cdot 1.7898 + 0.6824\cdot 1.4197 + 0.0045\cdot 1.5055 = 1.661$$

$$x = \frac{1.05\left(\frac{1}{2}0.2245+\frac{1}{2}0.0615+2\cdot 0.002-0.002\right)}{\frac{0.7\cdot 0.98\cdot 3716}{1250\cdot 1.661}-\frac{1}{2}0.2245-0.002-0.18-0.023-0.507-\frac{1}{2}0.0615-0.002}$$

$$x = \frac{1.050\cdot 0.145}{1.2277-0.857} = 0,41$$

For $t_f=t_m+100=1200$ ^{0}C

$$c_{CO_2}{}^{1200^0C} = 2.2638$$

$$c_{H_2Ovap}{}^{1200^0C} = 1.7769$$

$$c_{N_2}{}^{1200^0C} = 1.4143$$

$$c_{O_2}{}^{1200^0C} = 1.5005$$

$$c_{ga}{}^{1200^0C} = 0.2571\cdot 2.2638 + 0.056\cdot 1.7769 + 0.6824\cdot 1.4143 + 0.0045\cdot 1.5005 = 1.652$$

and

$$x = \frac{1.05\cdot 0.145}{1.285-0.857} = 0.355$$

For $t_m= 860$ ^{0}C , $t_f= 860+150=1010$ ^{0}C

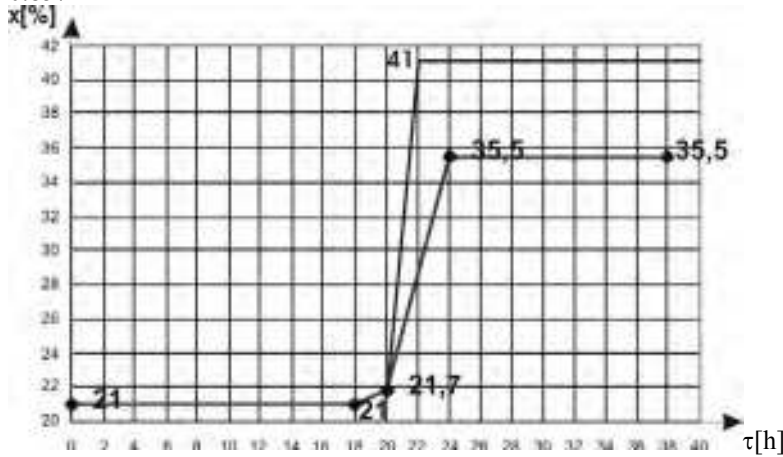$$x = \frac{1.05 \cdot 0.145}{1.558 - 0.857} = 0.217$$

Fig.2. *The oxygen concentration in the enriched air in the case of the furnace gas burning.*

5. Economic efficiency

The costs are the following:
   CH_4 = 189.18 USD/1000 Nm^3
   GF = 13.55 USD/1000 Nm^3
   Oxygen = 86.15 USD/1000 Nm^3
   Air = 7.68 USD/1000 Nm^3

5.1. The case of the marsh gas burning

Using the values of the average flowrates of marsh gas taken from Fig. 3, the costs are calculated as following:

a) during the period τ_1=(0-10) h
$$D_{CH_4} = 135 \text{ Nm}^3/\text{h}$$

$$D_{air} = L_r\, D_{CH_4}$$

$$D_{air} = 9.996 \cdot 135 = 1349.5 \text{ Nm}^3/\text{h}$$

$$C_1 = 135 \cdot \frac{189.18}{1000} + 1349.5 \frac{7.68}{1000} =$$
$$= 35.9 \text{ USD}/\text{h}$$

b) during the period τ_2=(10-14) h
$$D_{CH_4} = 245 \text{ Nm}^3/\text{h}$$

$$D_{air} = 9.996 \cdot 245 = 2449 \text{ Nm}^3/\text{h}$$

$$C_2 = 245 \cdot \frac{189.18}{1000} + 2449 \frac{7.68}{1000} = 65.15 \text{ USD}/\text{h}$$

c) during the period τ_3=(14-24) h
$$D_{CH_4} = 330 \text{ Nm}^3/\text{h}$$

$$D_{air} = 9.996 \cdot 330 = 3298.7 \text{ Nm}^3/\text{h}$$

$$C_3 = 330 \cdot \frac{189.18}{1000} + 3298.7 \frac{7.68}{1000} =$$
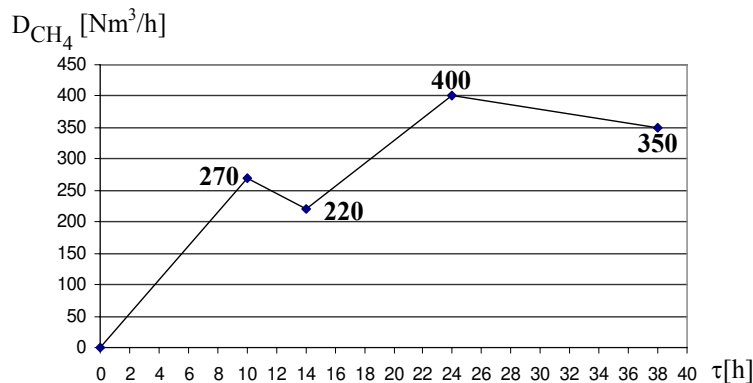$$= 87.76 \text{ USD}/\text{h}$$

Fig.3. *The variation of the marsh gas flowrate as a function of the treatment duration, in conformity with the exploitation data.*

d) during the period τ_4=(24-38) h
$$D_{CH_4} = 375 \text{ Nm}^3/\text{h}$$

$$D_{air} = 9.996 \cdot 375 = 3748.5 \text{ Nm}^3/\text{h}$$

$$C_4 = 375 \cdot \frac{189.18}{1000} + 3748.5 \frac{7.68}{1000} =$$
$$= 99.72 \text{ USD/h}$$

$$C_{CH_4} = \sum_{i=1}^{4} C_i \tau_i$$

The total cost is:

$$C_{CH_4} = 35.9 \cdot 10 + 65.15 \cdot 4 + 87.76 \cdot 10 + 99.72 \cdot 14 =$$
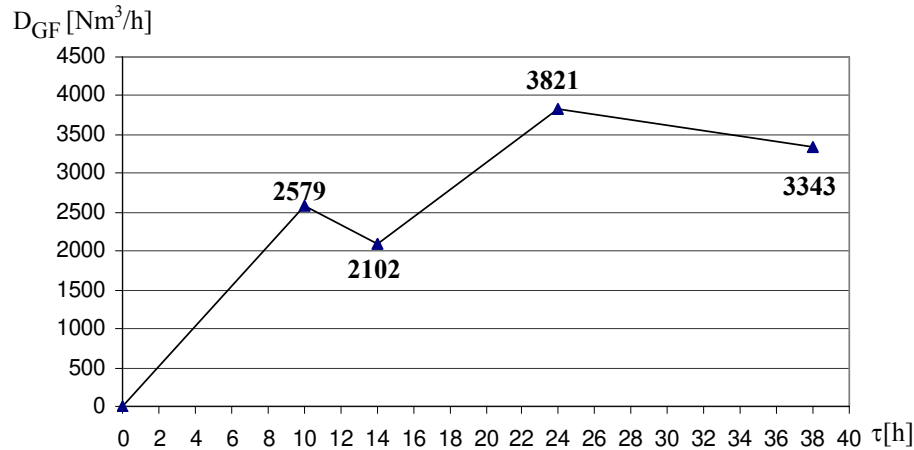$$= 2893.28 \text{ USD/cycle}$$

Fig.4. The variation of the furnace gas flowrate as a function of the treatment duration, determined from the calculations.

5.2. The case of the furnace gas burning

The values of the furnace gas flowrates in Fig. 4 have been calculated with the relation [6]:

$$D_{GF} = D_{CH_4} \frac{H_i^{CH_4}}{H_i^{GF}} \quad (10)$$

where:
D_{GF}, D_{CH_4} - the flowrates of the marsh gas and the furnace gas, respectively, in [Nm³/h];
$H_i^{CH_4}, H_i^{GF}$ -the calorific powers, [kJ/Nm³].

a) For $\tau_1 = 18h$ burning of the furnace gas with atmospheric air, the average flowrate of furnace gas, calculated in conformity with Fig. 4, is:

$$D_{GF} = 1780 \frac{Nm^3}{h}$$

and using the value
$$L_r = 0.724 \text{ Nm}^3 \text{air/Nm}^3 \text{GF}$$
the cost is:

$$C_1 = \left(1780 \frac{13.55}{1000} + 0.724 \cdot 1780 \frac{7.68}{1000}\right) 18 =$$
$$= 612.16 \text{ USD}$$

b) In the case of the furnace gas burning with oxygen enriched air:
 - the oxygen enriched air L'_r,[Nm³/Nm³ fuel] is:

$$L_r' = \frac{100}{x} O_2 \text{min} \quad (11)$$

where x is oxygen concentration [%];
 - the flowrate of the oxygen enriched air, D'_{air}, in [Nm³/Nm³ fuel] is [6]:
$$D'_{air} = D_{GF} L'_r \quad (12)$$

$$\begin{cases} D'_{air} = D_{O_2} + D_{air} \\ x = \dfrac{D_{O_2} + 0.21 \cdot D_{air}}{D_{O_2} + D_{air}} \end{cases} \quad (13)$$

It results:
$$\begin{cases} D_{air} = \dfrac{D'_{air}(1-x)}{0.79} \\ D_{O_2} = \left(\dfrac{x - 0.21}{0.79}\right) D'_{air} \end{cases} \quad (14)$$

• For the range $\tau_2 = (18-24)h$, it is considering an average oxygen concentration in air x=30%,
and an average value for the furnace gas flowrate of

$$D_{GF} = 3305.3 \text{ Nm}^3 / h$$

taken from Fig. 4, resulting:

$$L'_r = \frac{100}{30} 0.145 = 0.483 \frac{Nm^3}{Nm^3 \text{ fuel}}$$

$$D'_{air} = 3305.3 \cdot 0.483 = 1596.5 \text{ Nm}^3 / h$$

$$D_{air} = \frac{1596.5(1-0.3)}{0.79} = 1414.6 \, Nm^3 / h$$

$$D_{O_2} = \frac{0.3-0.21}{0.79} \cdot 1596.5 = 181.88 \frac{Nm^3}{h}$$

• For the range τ_3 = (24-38)h, it is considering an average oxygen concentration in air x= 37%, and an average value for the furnace gas flowrate of

$$D_{GF} = 3582 \, Nm^3 / h$$

taken from Fig. 4, resulting:

$$L'_r = \frac{100}{37} 0.145 = 0.392 \, Nm^3 / Nm^3 \text{ fuel}$$

$$D'_{air} = 3582 \cdot 0.392 = 1404.1 \, Nm^3 / h$$

$$D_{air} = \frac{1404.1(1-0.37)}{0.79} = 1119.7 \, Nm^3 / h$$

$$D_{O_2} = \frac{0.37-0.21}{0.79} 1119.7 = 226.7 \, Nm^3 / h$$

$$C_3 = \left(3582\frac{13.55}{1000} + 1119.7\frac{7.68}{1000} + 226.7\frac{86.15}{1000}\right)14$$

$$C_3 = 1073.3 \text{ USD}$$

$$C_{GF} = C_1 + C_2 + C_3 = 2113.36 \text{ USD/cycle}$$

$$\boxed{\begin{array}{l} \text{Economy} = C_{CH_4} - C_{GF} = \\ = 779.92 \text{ USD / cycle} \end{array}}$$

6. Conclusion

In the case of burning of the furnace gas with atmospheric air, a burning temperature of 996 ^{0}C has resulted. This burning temperature assures the heating of the pieces from the homogenizing annealing furnace in the first period of the 18 hours cycle. Forward, in order to increase the burning temperature .

$$C_2 = \left(3305.3\frac{13.55}{1000} + 1414.6 \cdot \frac{7.68}{1000} + 181.88\frac{86.15}{1000}\right)6$$

$$C_2 = 427.9 \text{ USD}$$

of the furnace gas, oxygen enriched air is used, reaching an average oxygen concentration in air of approx. 37%.

Calculating the costs for the two varieties, first burning of the furnace gas with atmospherican oxigen enriched air and second burning of the marsh gas with atmospheric air, respectively, a smaller cost has resulted in the case of burning the furnace gas than in the case of the marsh gas, the economy being of 779.92 USD/cycle.

The economy of marsh gas, achieved by the utilization of the furnace gas, presents a special interest because of the deficit of the marsh gas on the global market and its putting up the price.

References

[1]. **Vlădea I**., *Tratat de termodinamică tehnică şi transmitere a căldurii*, Editura Didactică şi Pedagogică, Bucureşti, 1974.

[2]. **Popa B**., *Transferul de căldură în procesele industriale*, Editura Dacia, Cluj, 1975.

[3]. **Brunklaus J**., *Cuptoare industriale*, Editura Tehnică, Bucureşti, 1977.

[4]. **Ivanescu L**., *Raţionalizarea consumului de combustibil la agregatele termice metalurgice*, Editura Fundaţiei Universitare "Dunarea de Jos", Galaţi, 2002.

[5]. **Ivanescu, L., Ivanescu, A., Cananau, N., Neacsu. M,** *Procedeu de ardere a combustibililor cu puteri calorice mici,* Brevet inventie Nr.a 200300313, Oficiul de stat pentru inventii şi mărci, Bucureşti, 2005.

[6]. **Ivanescu, L., Ivanescu, A., Cananau, N.**, *Cercetari privind utilizarea gazului de furnal în proporţie de sută la sută*, Contract cercetare Nr. 328, Galaţi, 2003.

PREDICTION OF WORK PARAMETERS IN A FIVE STAND COLD MILL

Stefan DRAGOMIR, Marian BORDEI,
Beatrice TUDOR

"Dunarea de Jos"University of Galati
e-mail: doromir@email.ro

ABSTRACT

The accurate prediction of work parameters is essential for a quality product. A mathematical model is used for parameters calculus. It is important to directly predict the roll force and the other parameters and to compute a corrective coefficient. Combining the network of work parameters and the mathematical model grove up the possibility to obtain parameter who give a new quality for laminates strip.

KEYWORDS: *cold rolling mill, stand, work parameters.*

1. Introduction

A rolling mill process for sheet processed consists in five stands where the force and the thickness tension between each stands is measured.

The roll gap is the distance between two working rolls, most important variable to affect the actual output thickness of the strip. The set parameter values are dynamically adjusted as the strip thickness and tension are measured during milling. After milling finishes, certain parameter adjustments are made in post calculation.

The initial setting produced by the mathematical model give errors that can usually be compensated by the real – time controller, but large errors lead to quality decline and cost increase.

The installed system produces the initial settings on the tension roll and the force prediction values with the settings from the mathematical model. The human operator is monitoring and comparing both settings.

Using a mathematical model, the mill settings are determined before a strip enters in the mill, like the work load, the roll gap for each stand is calculated, the speed in each stand (from the first stand to the four stand).

It is known to be a function of many variables, with an exception of the roll force. It is essential to predict the roll force. In most steel works, it is calculated using mathematical formula based on the metallurgical and mechanical knowledge:

$$F_m = f(H_i, H_o, T_b, R_{p\,0,2}, \mu, v_e, n_r) \qquad (1)$$

where F_m - the roll force produced by the mathematical model.

Those factors which affect the roll force include the incoming and target thickness (H_i and H_o), backward and forward tension (T_b and T_f), deformation resistance ($R_{p\,0,2}$), friction coefficient (μ), and other constants. The first four factors (thickness and tension) are constant and impose.

The rolling stands press a strip of steel using upper/lower rolls to a desired thickness. The gap between upper/ lower rolls determines how much pressure or force is applied. Thickness and tension is measured while the strip is processed, and then for real – time control like in the figure 1.

The mathematical model does not take all the factors into account. The friction coefficient is known to be affected by working roll parameters such as the rolling speed, the roll surface, the oil used, etc. [1]. However, the mathematical model employs only the rolling speed in calculating the friction coefficient. The mathematical model's prediction values (F_m), against the target values (F) are selected in the time of coil processed. The parameters predictions involve many other factors whose exact relations are not well understood and the mathematical model is far from perfect.

Recent studies [1] about the roll force tension and coil width prediction were made in two directions, first in improving the mathematical model and second in employing the network of parameters.
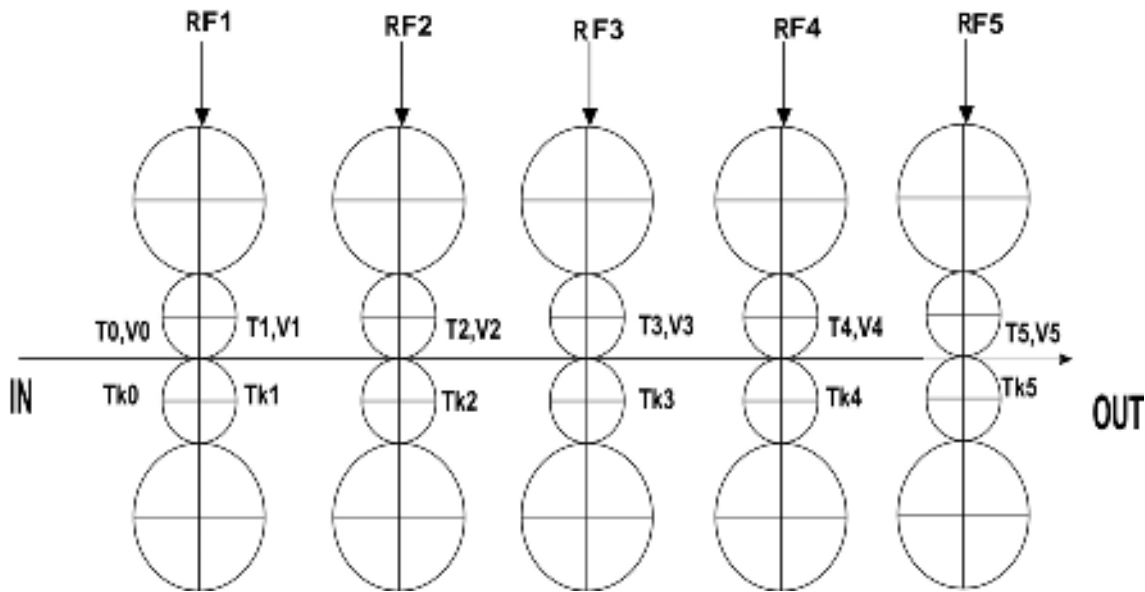
Fig.1. *Control of cold rolling mill process, with presetting in precalculation, which is related to thickness control.*

The networks of work parameters were used to calculate the roll force with the improved prediction accuracy in cold rolling process.

Many factors not considered in the mathematical model can be incorporated in networks of work parameters.

It can predict the tension, coil with roll force or produce a corrective coefficient to be multiplied to the prediction of the mathematical model.

2. Prediction by neural networks

The selected input variables are shown in the figure no.1. The first six came from the mathematical model. The roll force values were obtained from measurement.
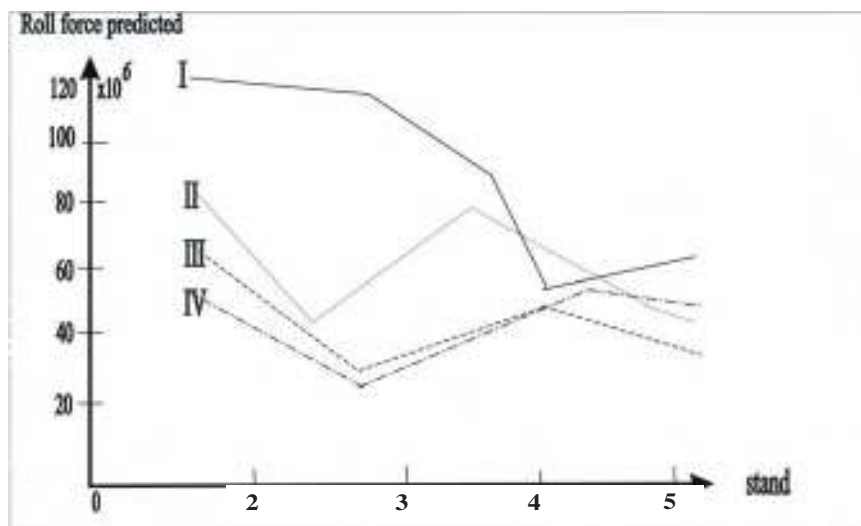

Fig.2. *The predicted values of roll force.*

This model is the mathematical model's predictions to the target values for the training data set with a constant scaling factor and a mathematical model's predictions.

The model of roll force prediction are given in figure no.2. The only exception was stand no.5, where the mathematical model is exactly.

The networks of work parameters, the multilayer perceptions, are unpredictable behavior in a novel environment. Improvement in average performance is not sufficient enough to convince a factory manager who is usually willing to keep a more reliable even if less accurate, old model.

When the single networks of work parameters were tested they reduced the errors on average by 60%.. A large error in roll force prediction causes a large error in roll gap which in turn could lead to the coil rupture. A single incident of operation interruption could wipe out the advantages that model. The average prediction for coil tension is shown in figure 3.
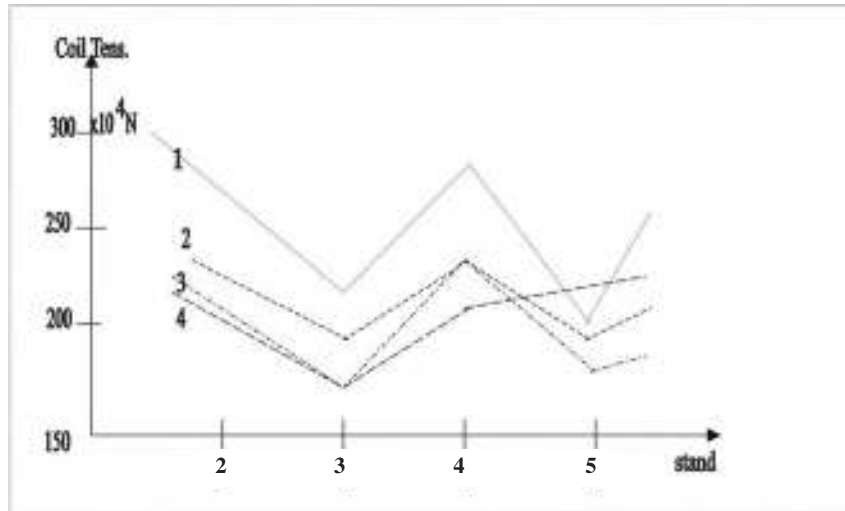
Fig. 3. *Average prediction of coil tension*
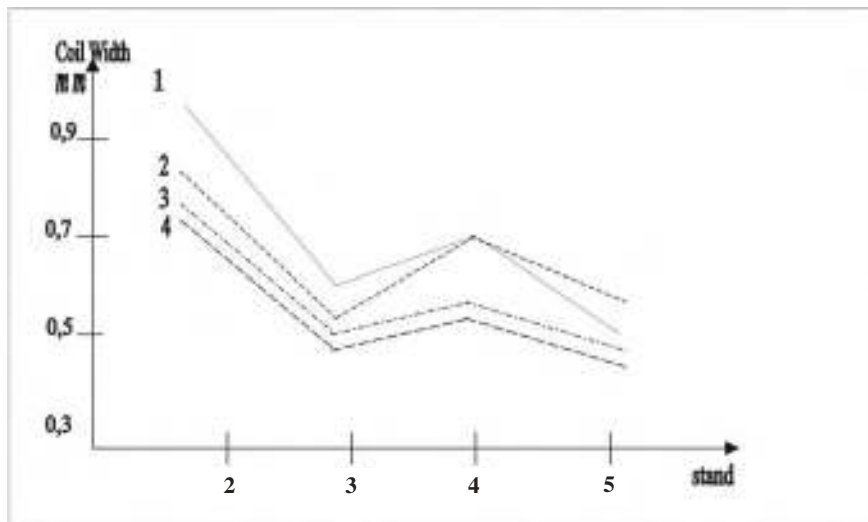
Fig.4. *Average prediction of coil width*

Reliability breakdown seems to result from the following causes: first, the distribution of the training patterns. I tried to collect as many coil data as possible, the twelve months worth of data my not be sufficient, given that many of which were discarded due to noise. It is difficult to even test if the training data have the same distribution as future data.

Transmission error is introduced when a large amount of data is passed from one computer to another. It appears in the form of irregular characters, missing values, or nonsense values such as zero temperature or zero roll force. The data with this type of noise are relatively easy to identify.

However, sensor noise is difficult to detect because it is not clear what the "correct" value range

is for some variables. The average prediction for coil width is shown in figure no. 4.

One can improve the network reliability by estimating the network's error and ignoring the network output when it is to large [2]. Given the same input variables. The network of parameters could not correctly estimate the prediction error.

Another approach is to detect the novelty of a test pattern's input. If it is novel, the reasoning goes, the network is not likely to make a reliable prediction. We analyzed the correlation with the prediction error in order to identify the default domain. If a new coil's input came from the aberrant domain, the mathematical model was instead used for prediction.

3. Conclusions

Using the roll force –prediction models we can show that the prediction errors of the currently used mathematical model reduced by 30-50%. The substitutive model directly predicts the roll force, while the corrective model produces a correct coefficient, which is then multiplied to the mathematical models prediction. Additional variables which were not used in the mathematical model were found to be necessary for the substitutive model only. The networks of parameters can be easily retrained if necessary. The retraining period does not have to be fixed such as monthly or yearly .It will be more proper to determine it dynamically by monitoring the trend of prediction error.

The network of parameters are planned to be used in daily operation. One difficulty is to estimate the financially savings resulting from the improved quality.

The using of network of work parameters have a potential to improve the accuracy of dimensions and too the quality of laminated strip.

References

[1]. **Sungzoon Cho, Yongjung Cho, Sungchul Yoon**, "*Reliable Roll Force Prediction in Cold Mill Using Multiple Neural Network*" IEE TRANSACTIONS ON NEURAL NETWORK, Vol 8,Nr 4 1977.

[2]. **C. Bishop**, "*Neural Networks for Pattern Recognition*". Oxford,U.K:Oxford Univ. Press. 1995.

[3]. **D.Cohn, L. Atlas, R. Ladner,** "*Improving generalization with active learning*", Machine Learning,vol.15 no.2, pp.201-221,1994.

[4]. Pohang Iron and Steel Company Tech.Rep.2nd Cold Mill Contr. Equipment (PCM part), POSCO, Korea, 1989.

[5]. **W. Lee**, "*Improvement of set-up model for tandem cold rolling mill*", Tech. Rep. POSCO Res.Inst.Sci.Technol., 1994.

[6]. **N. Pican.F., Alexandre and P. Bresson**, "*Artificial neural networks for the presetting of a steel temper mill*", IEEE Expert,vol.11,no1.pp.22-27.1996.

[7]. **N. Portman**. "*Aplication of neural nerworks in rolling mill automation*", Iron and Steel Eng.,vol.72 ,no.2, pp.33-36.1995.

[8]. **B. Rosen**, "*Ensemble learning using decorrelated neural networks*", Connections Sci.,vol.8,pp.373-384,1996.

THIN METALLIC SUPERFICIAL LAYERS WITH SPECIAL PROPERTIES DEPOSED ON STEELS BY ELECTRIC DISCHARGE IN IMPULSE

**Sorinel TANASUCA, Ioan ALEXANDRU,
Sorin Iacob STRUGARU, Adrian ALEXANDRU**
"Gh. Asachi" Tehnical University Iasi
e-mail: axa72us@yahoo.com

ABSTRACT

The surface engineering, as interdisciplinary technical science is a relative new concept which appeared in high developed countries as a result of the processing of the metallic materials with distinct properties and as a result of spectacular development of the thermal treatments.

The obtaining of the thin layers by electric spark presents some advantages as: high adherence of the layers, permits deposition of all materials which have electrical conductivity, but there are some disadvantages as: residual stress in layer and large roughness.

KEYWORDS: thin layer, electric discharge, impulse, properties

1. Introduction

The surface engineering, as interdisciplinary technical science is a relative new concept which appeared in high developed countries as a result of the processing of the metallic materials with distinct properties and as a result of spectacular development of the thermal treatments.

According by David Melford, "Surface Engineering" consists in essence in designing of surface and sublayer between, as a system, for conferring performances neither one not having selected separately. So, the surface engineering is not a simple superficial treatment technology, but is about designing of the system basic material – superficial layer thus it too responsible at it role at rational use of materials and at accessible cost prices.

In figure 1 are presented the characteristic areas, the proprieties and some of the criterions in consideration at designing of a system basic materials – superficial layer.
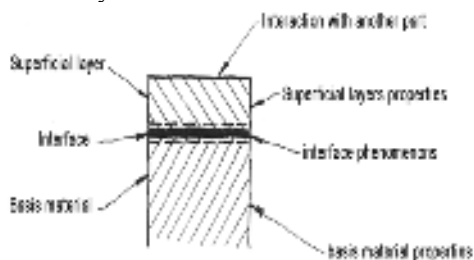

Fig. 1. *Characteristically areas and proprieties.*

The obtaining of the thin layers by electric spark presents some advantages as:

high adherence of the layers, permits deposition of all materials which have electrical conductivity, but there are some disadvantages as: residual stress in layer and large roughness.

The deposition and alloying by electric spark (DAES) uses inverse polarity (the part = cathode, the electrode = anode). In this case the deposition takes place in air or another gas, the electrode making a vibrating movement with or without a rotation.
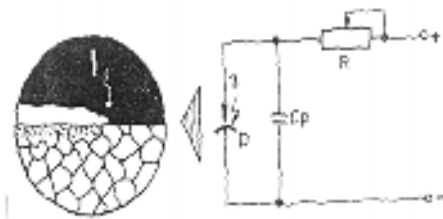

Fig. 2. *Superficial hardening by electric spark. a – the process; b – the electrical scheme.*

The deposition process begins when the electrode is near the part at a critical distance ($\cong 10$ μm) when takes place the electrical discharge in impulse (the spark) which ends at the contact of the electrodes.

Because of high energy, on the surface of electrodes appears craters of electric erosion by melting and vaporisation. The obtained material, under the influence of hydrodynamic pressure and hydrodynamic force from the channel of discharge is deposed on the part in small quantity $(2–3)\cdot 10^{-6}$g.

The discharge energy takes values between 8 … 18 Joule at 15 … 220 V, and the intensity of medium current may be 0,2 … 80 A.

Decreasing the energy of discharge has as result smaller thickness of deposed layers, smaller roughness and the deposed layer is more dense with more clean surface.

The process takes place with a electrode which vibrates at a 50 … 400 Hz frequency. The vapor pressure from interelectrodic space is very big (10^8 Pa).

The characteristic feature of this process is the polar transfer of the material from electrode or from interelectrode space is limitated by the parameters of work system (the discharge energy) and by the nature of the material from part and electrode.

2. Research and results

The research work consist in deposition of wolfram on a steel OLC55 – STAS 880-88 normalised (850^0C/air) and quenched at 840^0C/oil tempered at 600^0C/air with work surface grinded at Ra = 5 … 10μm.

The chemical composition of the steel is: 0,57%C; 0,74% Mn; 0,23% Si; 0,022% P; 0,025% S; 0,24% Cr.

The deposition scheme of thin layers is presented in figure 3.
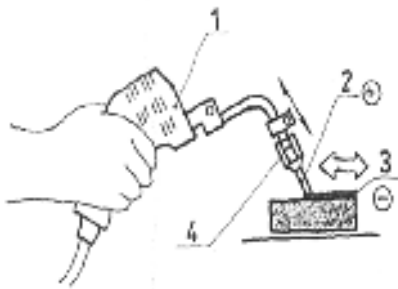
Fig. 3. *The device for deposition of thin layers; 1 – vibrator; 2 – electrode; 3 – deposed layer on the part; 4 – device for electrode fixing.*

Work parameters at the deposition of the thin layers using on original device for electrical discharge in impulse MAX 101 where:

- the angle of electrode 70^0
- the energy of discharge in impulse 0,3 J
- tension: 220 V
- current intensity: 1,2 A
- frequency of vibration of electrode: 100 Hz
- productivity: 2 cm²/min
- thickness of deposed layers 0,022 … 0,03 mm
- thickness of the electrodes: 2,2 mm

The sample were in slide shape with dimensions: 53x10x1 mm for determination of weight and arrow in time of deposition and cylindrical shape (φ 8x60 mm) for determination of microhardness, abrasive wear resistance and structure.

On the slide samples were made roughness measurements and carrying of surface on thin layers deposed with W electrode.

By successively deposition on slide samples of more layers of W with different specific time results that the weight of samples increase till third deposition (M_1, M_2, M_3), after that, at fourth deposition, the weight of the samples decrease (M_4) as is presented in table 1 and figure 4. the bending arrow of slide sample increases after all four depositions (a_a, a_2, a_3) and decreases after a determination by vibrating electrode without electrical discharge in impulse (table 2; figure 5).
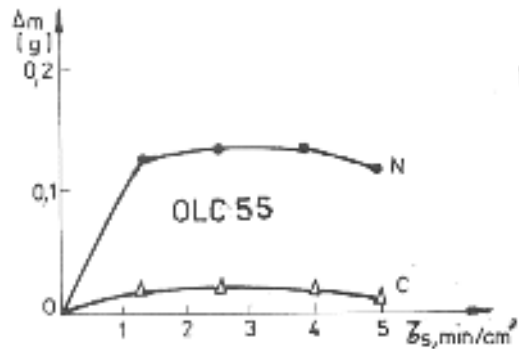
Fig. 4. *the variation of weight in specific time of deposition on OLC 55 steel.*
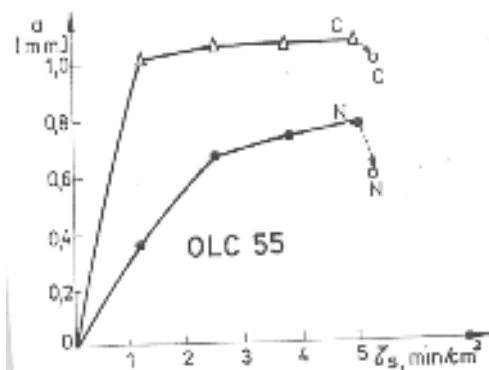
Fig. 5. *The variation of the bending arrow on OLC 55 steel.*

From table 1 results that the bigger weight (ΔM_1) is obtained at the deposition of the first layers, at other layers deposed, the weight is smaller and after the fourth deposition the weight decreases.

So, for deposed layers with a certain weight are necessary one or two deposition. By increasing of the specific deposition time, or of the number of depositions with out the layer deposed before is

pulverisated and the weight and the final thickness of layer decrease.

The bending arrow (a) is maximum at the first deposition (a_1) and increases at the second deposition (a_2) then at the next depositions the increasing is smaller.

By detention with vibrating electrode without electric spark, the bending arrow decrease.

The deposed weight on steel with the initial state normalised and detensionated is aprox. 10 time bigger at the first deposition ($\tau_s = 1,25$ min/cm^2) in comparison with weight deposed on the some steel hardened and detensionated; at the second and third depositions ($\tau_s = 2,5; 3,75$ min/cm^2) the deposed weight is small and the difference between the normalised state and the hardened state are of 2 … 3 time bigger at each deposition.

Taking together the weight contribution and the bending arrow obtained after each deposition, results that at the second, third and fourth depositions, however that the weight contribution is not significant, or even negative, the arrow increase, so appears internal stress.

The final circles from figure 6 are the smaller values of the arrow after detention by vibrating with the electrode without electric spark.

Results that at the deposition and alloying by electric spark (DAES) in terms of this research, the specific time of deposition must be under 2 min./cm^2 for obtaining of a weight contribution (thickness of deposed layer) and minimal stress. At the finish of the deposition if is make a detensionation by vibrating electrode, the stretched stress from layer decreases, removing the danger of fissure of the deposed layer.

From the analysis of the data of Table 2 results:

– the microhardness of the deposited layer does not depend on the initial status of the steel OLC 55;
– the microhardness of the sublayer has a greater value for the improved steel OLC 55 (c) than in a normalised status;
– the deposition of W through electric spark on the normalised steel OLC 55 produces a microalloy of the sublayer, implicitly a substantial growth of the microhardness, while the deposition in the some hardened

steel produces a recovery of the sublayer roughness and portance of the surface resulted after the deposition of W with average values: they can be improved only through subsequent remaking (treatments into electrolytic plasma, extra-finishing etc.);

The microstructural analysis of the layer of W deposited on the steel OLC 55 into the 2 sets of thermal treatment (normalization and improvement) effectuated on an optic microscope (Neophot 21) at 100:1 parts into evidence a white, dense layer of big thickness deposited on the hardened steel and a white and less dense and thick layer deposited on the normalized steel. Figure 6, a.b.

a

b.

Fig. 6. *Steel OLC 55 a white layer deposited with W. a) improved status; b) nominalized status*.

Table 1

Sample	St.in	Mo	M1	M2	M3	M4	ΔM1	ΔM2	ΔM3	M4Δ	ΣΔMi
OLC55	N	4,1541	4,2804	4,2841	4,2848	4,2775	0,1252	0,0037	0,0007	- 0,0073	0,1223
	C	4,3218	4,3319	4,3401	4,3409	4,3381	0,0101	0,0082	0,0008	- 0,0028	0,0163
42MoCr11	N	4,2080	4,3405	4,3430	4,3439	4,3405	0,1325	0,0025	0,0009	- 0,0034	0,1325
	C	4,3511	4,3654	4,3718	4,3791	4,3702	0,0143	0,0064	0,0073	-0089	0,0189

Table 2

Sample	St.in	a_o	a_1	a_2	a_3	a_4	a_5	Δa_1	Δa_2	Δa_3	Δa_4	Δa_5
OLC55	N	0	0,35	0,66	0,71	0,76	0,59	0,35	0,31	0,05	0,05	-0,17
	C	0	1,01	1,24	1,25	1,28	1,08	1,01	0,23	0,01	0,03	-0,2
42MoCr11	N	0	0,43	0,57	0,67	0,71	0,47	0,43	0,14	0,10	0,04	-0,24
	C	0	0,20	0,40	0,52	0,68	0,24	0,2	0,2	0,12	0,16	-0,44

3. Conclusions

The thin layer of W deposited on the supports of non-allied steel assures the resistance to corrosion to a great hardness, the resistance to wearing not and to the refraction of the pieces. The deposition of this layers of W on steel supports through electric discharge in impulse (the electric spark is an efficient method of obtaining pieces with special properties on the surface).

References

[1]. Alexandru Adrian. *Contribuţii privind alierea şi depunerea superficialăprin scânteie electricăşi influenţa tratamentelor termice asupra caracteristicilor straturilor obţinute ale materialelor metalice*. Teză de doctorat, Iaşi, 2002.

[2]. Abramciuc Alexandru. *Application electrospark alloying in production of electric contact. In Bul. I.P. Iaşi*, 2000.

[3]. Alexandru Adrian, ş.a. *Films metalic materials and biomaterials*. In Bul. I.P.Iaşi, Tom XLV, fasc. 1-2, 1999.

THE CORRELATION BETWEEN MECHANICAL CHARACTERISTICS AND TECHNOLOGICAL PARAMETERS IN HEAT TREATMENTS APPLIED TO MOULDING ALUMINIUM LIKE ATSi5Cu1

Carmen NEJNERU, Dan-Gelu GĂLUŞCĂ, Roxana-Gabriela CARABET, Dragos ACHIŢEI, Nicanor CIMPOEŞU

"Gh. Asachi" Technical University of Iasi

ABSTRACT

The paper contains an experimental study of colligating the technological parameters of the artificial aging operation namely time and soaking temperature with hardness and mechanical strength properties gained after the treatment. The tests were made on a moulding aluminum alloy like ATSi5Cu1 by using moulded test bars in metallic shell. There were realized metallographic photographs and strength tests.

KEYWORDS: aging, aluminum alloy, solution quenching, strength tests

1. Introduction

Solution heat treatment is used to alloys that present a solubility variation in solid state and have a biphasic structure before treated α + precipitate (biphasic structures are fragile, they don't plastically deform). The treatment consists in total or partial dissolve of the precipitate followed by a blast cooling to maintain the monophasic structure that gives the material a better workability through plastic proceedings.

Partial solution quenching apply to the alloys that have secondary precipitates and primary precipitates; through dissolving the secondary ones the solution heat-treated material become softer and easier to machine.

Aluminum alloys that accept solution heat treatment is grouped in two categories:

I – alloy without eutectic, deformable

II – alloy with eutectic, alloy for pieces casting

The main structural characteristic of aluminum alloys is the presence of some complex eutectics within a matrix of α solid solution based on aluminum.

By choosing the heat temperature in solution quenching, it must be assure on one hand a certain solid solution enriching with alloying elements so that through blast cooling the material reach a supersaturated degree and on the other hand to prevent melting the complex eutectics that brings to oxidations and the continuity loss of the metallic material. The structure and the chemical composition of complex eutectics are determined by the chemical composition of liquid alloys and by piece casting conditions, solidification and cooling that are influenced by its geometry and formation technology.

The objectives of applying ageing treatment to aluminum alloys establish and realize according to the obtain pattern of those products: plastic deformation or casting.

Die casting pieces or in moulding sand pieces have after cooling a structure made from solid solution with a certain supersaturated degree because of the fact that cooling speed after solidification is big for preventing the separation of secondary phases in equilibrium proportion. The possibility to adjust the values of mechanical characteristics through choosing the correct temperature and heating time is determined by the kinetics of transformation processes of the supersaturated solid solutions in cast alloys and solution heat-treated. The structures of aluminum alloys cast and heat-treated pieces are stable in heating. This happens because these alloys have a considerable eutectic proportion that links a part of the alloying elements and they form from hard soluble phases heating in solution heat treatment. In cast, structures the secondary phases have big dimensions and are uniformly distributed then in cold reduction and warm plastic deformation structures. That is why the temperature and heating period in solution quenching is higher and the temperature and heating period in ageing treatment is higher. In solution treatment, it is desired the dissolving of a bigger part of secondary phases and in ageing treatment, it is desired the precipitation of secondary phases from solid solution.

If we raise the heat temperature to the superior limit and increase the maintain period to this

temperature the transformation processes of the solution treatment structure develop entirely by accomplishing a complete supersaturated solid solution and raises through coalescence the precipitated crystals of hardened phases. These transformations determine a drop of the mechanical characteristics values, a raise of the plasticity values and a dimensional stability of the pieces.

2. The purpose of the paper

As it was presented in specialty literature, there are no data to specify the technological parameters (temperature, time) to which the artificial ageing heat treatment must be done for the ATSi5Cu1 alloy cast pieces so that the alloy could gain hardness and mechanical resistance properties to the exploitation demands. Therefore, it is imperious to find a compromise solution, to determine a heating

temperature and a maintain time so that the mechanic resistance and the hardness to have optimum values.

3. Experimental results

Some standard traction specimens were used and the solution heat treatments was made by heating at 550°C, maintain for 8 hours and water cooling and at the ageing treatment the temperature and maintain times varied into a certain interval. For the experiment it was used an cast aluminum alloy ATSi5Cu1 with the following chemical composition Al 92,2%, Cu 1,1%, Fe 0,6%, the rest being neglecting elements. There were made determinations of mechanical resistance and hardness on cast specimens from ATSi5Cu1 in different temperatures and maintain time, T = 140-260°C and t = 5÷11 h.

The experimental data were put into table 1.

Table 1. The experimental data

| t [h]	T = 140 [ºC]		T = 200 [ºC]		T = 260 [ºC]	
	HB_{mediu}	R_m [daN/mm²]	HB_{mediu}	R_m [daN/mm²]	HB_{mediu}	R_m [daN/mm²]
5	87,6	21,3	104,06	20,78	76,8	18,5
5,5	91,3	24,6	106,1	21,3	82,9	19,6
6	96,5	25,72	107,7	24,2	83,6	20,43
6,5	98,7	25,98	108,1	23,8	87,8	21,8
7	101,2	26,45	110,2	24,9	91,8	23,4
7,5	103,9	26,73	113,4	25,5	96,3	24,6
8	106,1	27,8	115,5	25,21	100,1	25,5
8,5	103,8	27,02	114,9	25,9	95,5	24,6
9	102,2	25,6	113,2	25,85	90,1	23,1
9,5	100,1	24,7	112,8	25,8	85,6	22,8
10	99,5	23,45	110,2	26	80,16	22,27
10,5	99,3	22,9	109,2	25,8	78,2	21,8
11	98,6	21,54	107	25,81	75,3	19,9
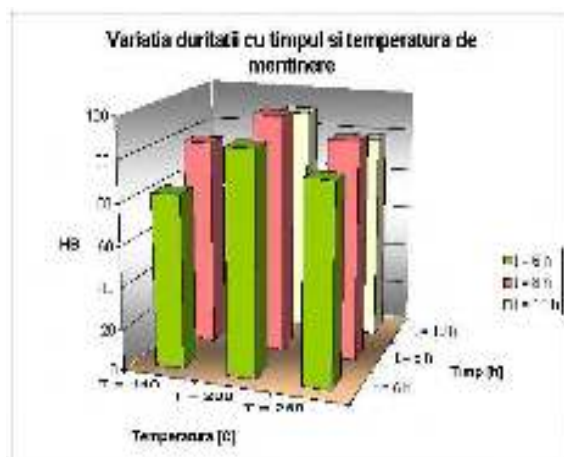
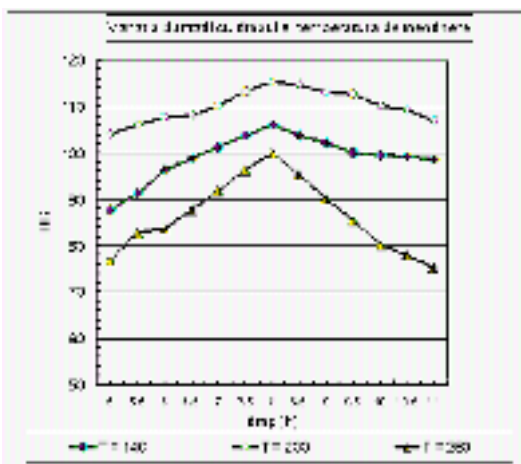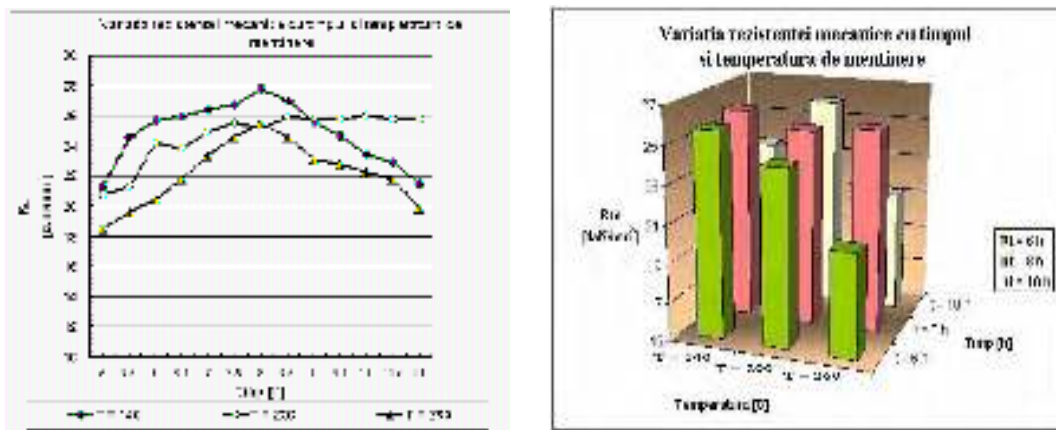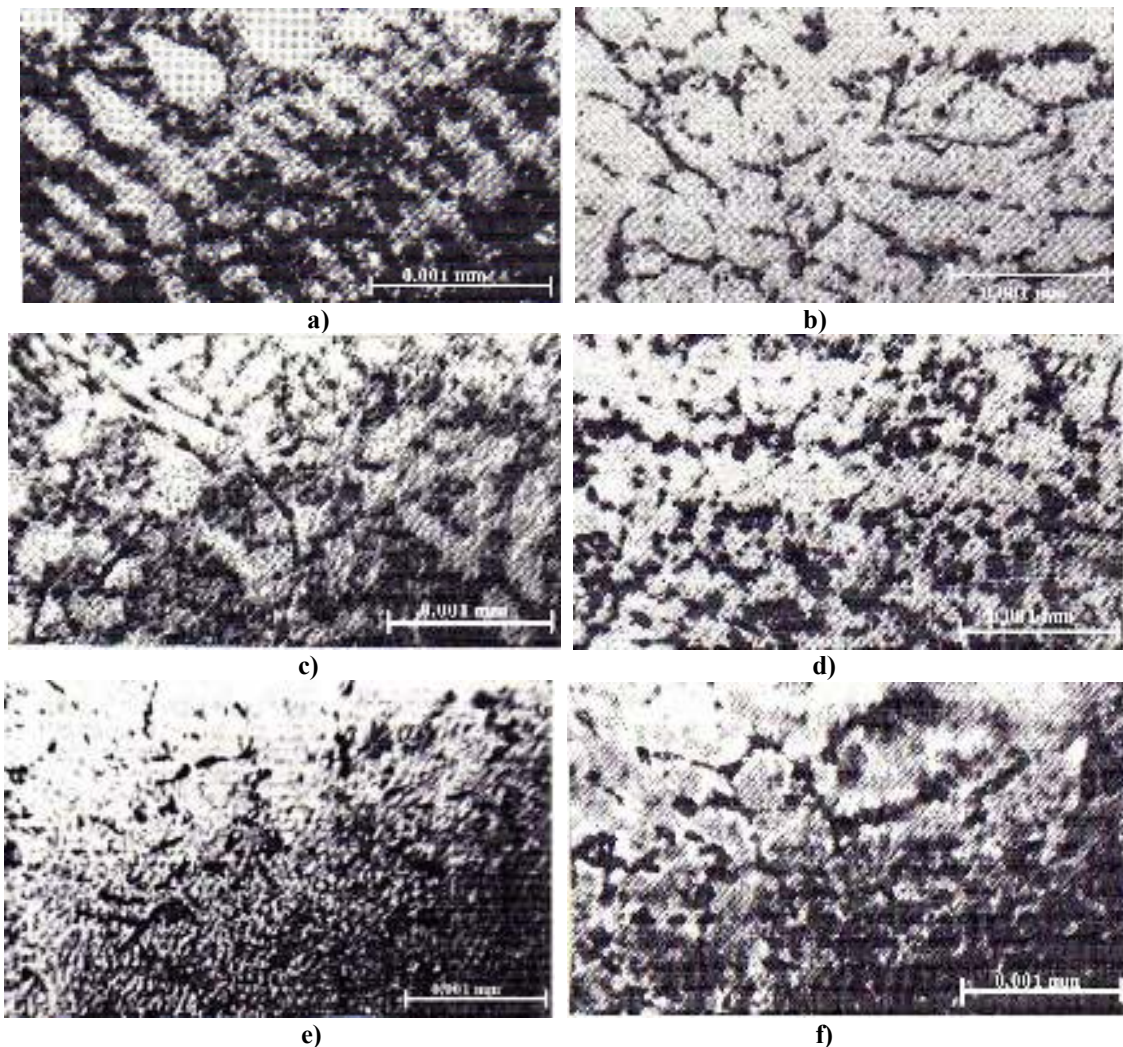*Fig. 1. Variation of Vickens hardness with maintain time, when temperature is constant*
$T_1 = 140$ °C, $T_2 = 200$ °C şi $T_3 = 260$ °C.
Maximum hardness appears in 200°C for a 8 hours maintain time.

Fig. 2. *Variation of ultimate strength with maintain time when temperature is constant*
$T_1 = 140°C$, $T_2 = 200°C$ și $T_3 = 260°C$.
Maximum ultimate strength appears for 6 and 8 hours maintain time and 200°C.

Fig. 3. *The microstructure of the specimens after solution quenching and artificial ageing.*
Obtained microstructures after 20% NaOH attack of ATSi5Cu1 aluminum alloy
a) cast test; b) solution treated test at 550°C, maintained for 8 hours and water cooled at 60°C;
c) solution treated and aged test at 140°C and maintained for 6 hours; d) solution treated and aged
test at 200°C and maintained for 5 hours; e) solution treated and aged test at 260°C and maintained
for 6 hours; f) solution treated and aged test at 200°C and maintained for 11 hours.

Studying the microstructures from figure 3, we notice a white structure of the solid solution and black colored eutectic. In a) we notice the denditric form of the cast structure; in b) the black colored eutectic is scattered at the grains boundaries of white solution; in c), d), e) and f) we notice an uniform distribution of the eutectic, acicular form, and it differs only straggling degree depending on temperature and maintain time. If the temperature and maintain time are bigger the eutectic distribution is smaller and more uniform.

4. Conclusions

1. We notice by studying the graphics that depending on the realized experiments we have a maximum for hardness in all three temperatures (140, 200, 260) and for 8 hours maintain time.

2. We notice from maintain temperatures point of view that maximum hardness is riched to 200°C maintain temperature.

3. We notice that from mechanical resistance point of view the maximum riches at 140°C and 8 hours maintain time.

References

[1]. **Carţiş Ioan** – *Tratamente termice*, Editura Facla, Timişoare, 1982.
[2]. **Suzana Gâdea, Maria Petrescu** – *Metalurgie fizică şi studiul metalelor*, Editura didactică şi pedagogică, vol. III, 1983.

INFLUENCE OF STEEL MODIFICATION ALLIED WITH 4-7%Si ON MACROSTRUCTURE

Clara CONSTANTINESCU

Valahia University of Targoviste

e-mail: clara@valahia.ro

ABSTRACT

The goal of this paper is to test the effect of odification process of liquid steel with 4-7% silicon content, in the course of pouring out from steel-smelting furnace into ladlet, on macrostructure. The research settled down that the mofification has a strong influence fulfilling a stressed refining of macrostructure.

KEYWORDS: modification, silicon steel, macrostructure

1. Introduction

The coarse grain of metallic materials means a negative factor for whole technological process of obtaining of finished products, this influencing both casting and semi-finished working. Actually, the favourable structure is the fineness structure with homogeneous distribution of all phases. The obligation,of the foundry departments consist in to obtain fineness pieces providing for made good technological properties and strength features associated to plasticity features. But, as industry, specially, at the solidifying of large weight metals, practically, never an ideal structure is obtained.

Relative to steels, naturally, without other technological interventions, the solidifying develops that a coarse, dendritic, heterogeneous structure being obtained. The phenomenon is amplified on high silicon content steels. The research done on the world plane carry on the silicon steel allied with 6.5% classically elaborated and cast is characterized by a very powerful transcrystallization, the area of columnar grains occupying complete section of cake ingot. These steels are characterized by a marked brittleness and cannot be rewardingly plastic deformed.

The operated tests consisted in the change of this natural trend of solidifying by adding of exogen crystal nuclei, phenomenon being as modification.

2. Experimental tests

The tests have been made in laboratory. Steels manufacture has been made in induction acid furnace of 50 kg capacity, metallic charge being consisted in silicon-steel sheet with the following chemical composition: 0.01 %C; 1.98%Si; 0.18%Mn; 0.045%P; 0.010%S; 0.01%Cr; 0.04%Ni; 0.03%Mo;

0.13%W; 0.01%V; 0.29%Al; 0.01%Ti; 0.05%Cu; 0.03%Ni. Alloying has been fulfilled by means of FeSi. After melting, steel has been poured out in a redness ladlet. During the pouring out from furnace into ladlet, into the stream of liquid metal an inoculant in proportion of 2% from liquid mass.

As inoculant, preheated,clean, metallic spherical bits, shots, respectively, oxides traceless with the diameter of 1-2mm. The shots characteristics are according to STAS 7482-86. Melting has been made into diameter bars of 50 mm and 80 mm, with and without modification. Chemical composition are listed in Table 1.

Table 1. Chemical composition of cast steels

Chemical composition, %	Nr. of charge/ Nr. of sample			
	1 / 1	1 / 1m	2 / 2	2 / 2m
C	0,11	0,11	0,12	0,12
Mn	1,27	1,27	1,35	1,35
Si	4,48	4,48	7,01	7,01
S	0,01	0,01	0,01	0,01
P	0,07	0,07	0,07	0,07
Cr	0,05	0,05	0,05	0,05
Ni	0,04	0,04	0,04	0,04
Cu	0,05	0,05	0,05	0,05
Mo	0,03	0,03	0,03	0,03
Al	0,32	0,32	0,26	0,26

The following samples have been taken:

* from charge 1

- sample 1(from unmodified steel)- Φ80*70

- sample 1 m (from modified steel)- Φ80*70

* from charge 2

- sample 2 (from unmodified steel) – Φ50*70

- sample 2 m (from unmodified steel) - Φ50*70

The obtained samples have been processed to study their macrostructure. Their process has consisted in:
- restriking
- polishing
- HCl solution pickling at 800C, from 20..30min;
- introducing into ammonium persulphate (10%), for5 min;
- cold washing;
- air jet drying.

3. Obtained results

The inoculant influence of liquid steel on macrostructure is powerful. In the case of unmodified steel the macrostructure consists in globular and columnar grains areas (fig.1 and fig. 2): cracks are performed.

Fig.1. *Unmodified steel macrostructure with 4%Si. Columnar crystals area is highlighted*

Fig.2. *Unmodified steel macrostructure with 7.07%Si. Columnar crystals area is seen. Also, cracks are observed.*

Modified structure steel consists in very high fine globular grains area and very high fine equiaxed presents in all sample section. It is highlighted that the columnar crystals completely came out (fig. 3 and fig. 4).

Fig.3. *Modified steel macrostructure with 4.48%Si. Columnar crystals are not found*

Fig.4*. Modified steel macrostructure with 7.07 %Si. It is noticed that the columnar crystals and cracks are not seen.*

4.Conclusions

The paper followed avoiding transcrystallization of steel cake ingot with high content of silicon. To achieve this goal by made modification tests, the obtaining of semi-finished product improved as structural as structural form. By introducing of exogenous crystal nuclei carried out the columnar dimension reduction crystals, which stimulates the marked reduction hypothesis of brittleness and plasticity improvement.

References

[1]. M. V.Maltev – *Modificarea structurii metalelor şi aliajelor,*, Ed. Tehnică, Bucureşti, 1966;
[2]. *Metaux - Corrosion - Industries*, Revue mensuelle, Nr.393, 1958 ;
[3]. Traian Dumitrescu s.a. Research regarding the modification process of steels, Anais do 8° Encontro Nacional do Sociedade Portuguesa de Materiais Procedings of the 8* National, 1997.
[4]. H. Shimonaka, Y.Ito, K.Matsumura, B.Fukuda - *Recent Development Non-Oriented Fe-Si Sheets*, Magn.Mat.26, 1-3, 97, 1982
[5]. W.Kappel, E.Cristescu, A.Pascale – *Studiu cu privire la aliajele Fe-Si. Caracteristici şi utilizări.*, ICPE, 1997.

SELECTIVE ORGANIC REACTIVE FOR DETERMINATION OF SEVERAL HEAVY METALS FROM DIFFERENT MATERIALS

Olga MITOŞERIU[1], Dan T. LEVCOVICI[2],
Gabriela FILIP[2]

[1] „Dunărea de Jos" University of Galati
[2] S.C.Uzinsider Engineering S.A. Galati
e-mail: olga.mitoseriu@ugal.ro

ABSTRACT

The research regarding the synthesis and characterization of tiobis-β-naphthol have established that it can be used as an efficient analytical reactive for separating through extraction the heavy metals in watery environments.

These studies have been presented in the CALIST program.

KEYWORD: organic reagents, heavy metals, residual waters

1. General

The practical and theoretical interest attached to the organic reactants is reflected by the large number of researchers which have focused their attention to this field and also by the significant contribution of this class of compounds to the development of the analytical chemistry. Due to the importance and advantages of the organic reactants, the studies carried out in this paper have been oriented so as to extend their scope of application.

The synthesis and critical approach of the literature to the chemistry of tiobis-β-naphthol and its derivatives have highlighted the theoretical and practical importance of the tiobisphenol due to their reactivity and possibilities of use in various fields especially as analytical reactant. In spite of this, only one application of tiobisphenol is known, namely reactant to gravimetrically determine the copper.

Tiobisphenol are organic combinations having the general formula R_2S, hypothetically generated from sulphide hydrogen by substituting the hydrogen atoms with phenol radicals. When $R = - C_{10}H_6 - OH$, tiobisphenol is formed.

The researches carried out under the CALIST program have significantly contributed to both the synthesis and characterization of tiobis-β-naphthol so as to make it usable as analytical reactant. Thus, the items below have been approached :

 ➤ synthesis and purification of the reactant;
 ➤ the study of the electronic spectra UV-VIS and IR
 ➤ solubility in different solvents
 ➤ the dissociation constant , identification reactions and reactivity with respect to some metal ions

The researchers have shown that the tiobis-β-naphthol can be used as efficient reactive in the extraction of some heavy metals from watery environment .

2. Synthesis of tiobis- β -naphthol

In order to obtain the tiobis-β-naphthol through a fast synthesis and from available substances a comparative study of the various preparation methods described by the literature has been carried out. To prepare the reactant, Tassinari's method has been chosen as amended by Kulkarni and Jadhov: sulphuration of the β-naphthol with sulphide dichloride as using as solvent the ethyl anhidru ether, a method which has been completed by the authors

Purity was found by melting point determination and elementary chemical analysis performance. Carbon and hydrogen were determined by gravimetric method using instruments for elementary analysis made by Knobloch.

The sulphide has been determined by desaggregation of the tiobis-β-naphthol in a nickel crucible with a mixture of anhidru sodium carbonate and sodium peroxide; from the melt dissolved into distilled water and further acidulated by HCl and barium sulphide has been precipitated to be subsequently filtered, dried, calcinated and weighted.

The elementary analysis of the tiobis-β-naphthol, with the chemical formula
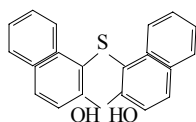
is given in Table 1.

The melting point is 216 ºC and the color is white.

Table 1

Chemical analysis, %	C	H	S
Calculated	75,45	4,40	10,07
Found	75,21	4,22	10,00

In order to highlight the spectral properties and make clear the reactivity if the tiobis-β-naphthol under different conditions, the synthesis of dehidrotiobis-β-naphthol and the tiobis-β-naphthol isomer has been performed with the melting point of 156ºC (isosulphide).The clarifications were necessary in order to use the tiobis-β-naphthol as analytical reactant

3. Electronic UV-VIS spectra

In order to characterize the initial reactants , to clarify the development of the used reactions and to subsequently compare the newly sintered substances, the UV-VIS spectra were recorded. To identify the UV absorbtion bands, the specific absorbtions of the β-naphthol, taken as reference term, were taken into account acc to fig.1.

In Table 2 the position and intensity of the absorbtion bands peaks characteristic to the studied compounds.
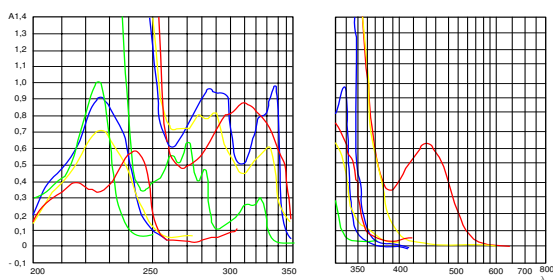
Fig. 1. *Electronic absorbtion spectra UV-VIS*
— tiobis-β-naphthol   — isosulphide
— β-naphthol   — dehydrosulphide

The UV VIS absorbtion spectra of the tiobis-β-naphthol, represented by chemical formula

$$S \diagdown \begin{matrix} C_{10}H_6\text{-OH} \\ C_{10}H_6\text{-OH} \end{matrix} \quad \text{and of isomeride or} \quad O \diagdown \begin{matrix} C_{10}H_6\text{-SH} \\ C_{10}H_6\text{-OH} \end{matrix}$$
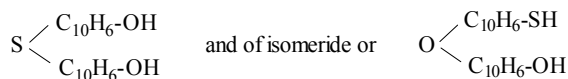
is similar to the β-naphthol absorbtion spectrum.

Table 2. *Position and intensity of the peaks of the absorbtion bands*

band \ compound		β-naphthol	isosulphide	tiobis-β-naphthol	dehydrosulphide
E	λ max [nm]	225	225	225	216
	ω [l·mol^{-1}·cm^{-1}]	100000	71000	91000	38500
K	λ max [nm]	-	-	-	242
	ω [l·mol^{-1}·cm^{-1}]	-	-	-	59000
B	λ max [nm]	272	278	284	312
	Δ λ	-	6	10	40
	ω [l·mol^{-1}·cm^{-1}]	6440	8180	9700	8800
R	λ max [nm]	328	333	336	444
	Δ λ	-	6	9	117
	ω [l·mol^{-1}·cm^{-1}]	3000	6200	9900	636

With all three substances the three types of bands characteristics to the substituted aromatic compounds are to be found. The peaks of the absorbtion bands E, due to the transitions, $\pi \to \pi*$ are located at 225 nm. Since transition is high, the band is of high intensity, decreasing from β-naphthol to isosulphide.

The bands of type benzenoidic – B, datorate tot unor tranziţii $\pi \to \pi*$, specific to the aromatic nucleus, have the peaks situated within the range 272 – 282 nm. They are of low intensity and therefore they are forbidden. Since on the aromatic nuclei of the naphtaline auxochrome groups +E, having non participating electron pairs (-S, -OH, -O-, -SH) are inserted, possible transitions $n \to \pi*$ occur which

form radical bands R with absorbtion peaks within the range 327–336 nm. Representing auxochrome groups +E, they are capable of interacting by conjugation p $\rightarrow$ π with the electrons π of the aromatic nuclei. Thus, the sulphide of the β-naphthol causes a batochrome displacement to the maximum of the bands B and R, simultaneously with a general effect of hyper-chrome. The fine structure of the bands almost disappears. The batochrome activity of the substituting element is even more obvious when the hetero-atom is less electronegative, which means it has more flexible non-participating electrons. The batochrome influence increases from iso-sulphide to di-β-naphthol, the bridging hetero-atom playing an important role. The dehydrosulphide features a characteristic electronic absorbtion spectrum. When λ = 242 nm, the absorbtion peak belonging to the conjugated band occurs-K of high intensity, accounted for by the existence of an unsaturated group which can be conjugated with the electrons π of the aromatic nucleus; ea se datorează unor tranziţii π $\rightarrow$ π*. The radical band, because of the transition n $\rightarrow$ π* of the quinone group $\diagup$C$=$O, appears displaced to the visible area, featuring an absorbtion peak of λ = 444 nm.

4. The IR spectra

The IR spectra for tiobis-β-naphthol were studied to examine their molecular structure and also to serve as reference for the comparison with other IR spectra of the derivative compounds and isolated in solid state. Thus information could be gathered with respect to the nature of their chemical bonds. The IR spectra fall within the range 400– 4000 cm⁻¹, in solid state with substances included into the potassium bromide on a Spectrometer Specord.

The IR absorbtion spectra are interpreted according to the literature, the specific bands being allocated according to the structure β-naphthol, tiobis-β-naphthol, dehydrosulphide and isosulphide (fig 2,3).

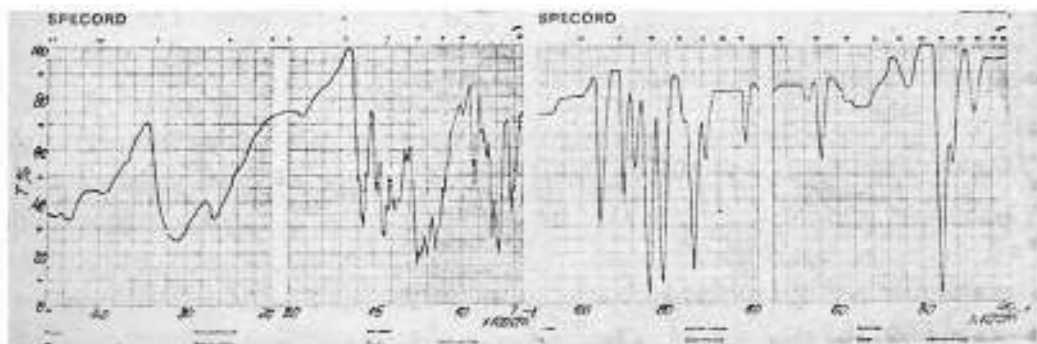*Fig. 2.* IR spectrum of β-naphthol.

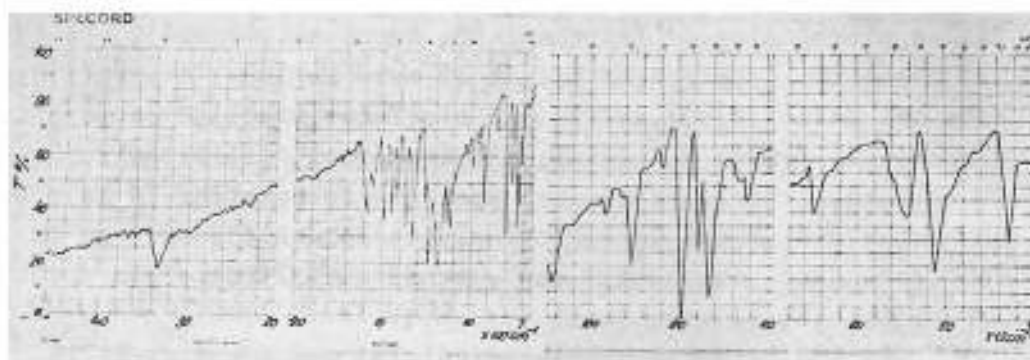*Fig. 3.* IR spectrum of tiobis-β-naphthol.

The valence vibration frequency of the hydroxyl group (ν OH) looks like a well defined band with λ = 3365 cm⁻¹, for tiobis-β-naphthol and λ = 3240 cm⁻¹ for isosulphide; since the dehydrosulphide has no OH groups, it has no absorbtion either in the range 3000 – 3600 cm⁻¹. The tiobis-β-naphthol and its isomer, by position α containing electron donor atoms able to form hydrogen bonds with the hydroxyl group from position β has, in addition to the free ν OH bands corresponding to the associated hydroxyl of lower frequency (λ = 3330 cm⁻¹ and λ = 3230 cm⁻¹ respectively). In the range 1000 – 1250 cm⁻¹ an intense valence vibration ν C-OH occurs, situated at

λ=1190 cm^{-1} for tiobis-β-naphthol and λ=1195 cm^{-1} for isosulphide.

The bands of the C-S bond are presented in the area 600 – 700 cm^{-1} range, of low intensity. Since with the aromatic compounds, due to the Ch deformation vibration outside the aromatic ring, identification becomes more and more difficult, allocation taking into account the absorbtions for the β-naphthol, tiobis-β-naphthol, dehydrosulphide and isosulphide.

Thus in the IR spectrum a band of λ = 650 cm^{-1} peak becomes obvious with the tiobis-β-naphthol and with the dehydrosulphide with λ = 652 cm^{-1}, bands which are absent in the spectrum of the β-naphthol and isosulphide.

For the isomer of the tiobis-β-naphthol an absorbtion band was identified at λ = 2500 cm^{-1} featuring a much lower intensity than that of the –OH group which is characteristic to the valence vibration ν S-H.

With iso- and dehydrosulphide, there appear the vibrations specific to the absorbtions ν_{C-O-C} assimilated with λ = 1240 cm^{-1} and λ = 1220 cm^{-1} respectively and absorbtions ν_{C-O-C} simmilar with λ = 1060 cm^{-1} and λ = 1020 cm^{-1} (less intense than the first).

The appearance of the carbonyl group with the oxidation compound of the tiobis-β-naphthol is accounted for by the presence in the IR spectrum of a band which is intense at λ = 1650 cm^{-1}, allocated to the valence vibration $\nu_{C=O}$.

The study of the UV-VIS and IR spectra carried out for the first time on the tiobis-β-naphthol of the oxidation product-dehydrotiobis-β-naphthol and its isomer – isosulphide - have enabled the identification of the functional groups, in compliance with the structure proposed for these compounds.

5. Solubility of the tiobis-β-naphthol

The literature only provides qualitative indications on the solubility of the tiobis-β-naphthol in some usual solvents. To determine different possibilities of using this substance in the analytical chemistry, its solubility was determined in a number of 27 solvents of different types. Determinations were made at 22ºC ± 1ºC. By using the solvent classification system acc to the donor-acceptor properties, we get the data in table 3.

The tiobis-β-naphthol is slightly soluble in protophiles and amphiprotos, such as cetones and esthers ; it is very little soluble in alcohols, ether or glacial acetic acid. The lowest solubility is to be found with the aprotic solvents. It is insoluble in formic acid and ordinary gasoline.

At the same time, solvents do influence the electronic spectra.

Table 3.

Solvent	Solubility (g/l)
A. Protolitici	
a. Protofili	
Dimethyl formamide	293,7
1-4 Dioxan	192,0
b. Amfiprotici	
- Ketone	
Acetone	97,5
Metiletilcetonă	98,0
Metil-npropilcetonă	71,9
Acetil-acetonă	48,0
- Esters	
Acetat de etil	98,3
Acetat de n-butil	22,4
- Alcooli	
Methanol	9,0
Ethanol	8,0
N-propane	9,8
N-butane	5,3
Izobutanol	7,1
- Nitroderivați	
Nitrometan	1,3
Nitrobenzen	14,4
- Eteri	
Ether ethylic	9,5
c. Protogeni	
Acid formic	-
Acetic acid	5,4
B. Aprotici	
Phenyl methane	5,5
Chloroform	5,9
O-xylene	1,9
Carbon dusulphide	1,2
Benzene	1,1
Ligroină	0,7
Eter de petrol	0,4
Tetraclorură de carbon	0,5
Gas	-

Thus both the position and shape of the absorbtion peaks along with the UV-VIS spectra band intensity are influenced by the solvent polarity. The positions of the absorbtion band peaks recorded for tiobis-β-naphthol in three solvents of different polarities are given in table 4.

Table 4. *Influence of solvents on the absorbtion band peaks of the tiobis-β-naphthol*

Solvent	Dielectric constant	transition	
		$\pi \rightarrow \pi^*$ λ max	$n \rightarrow \pi^*$ λ max
n-heptan		281,7	333,3
Ethylic alcohol	24,3	283,6	336,0
Methylic alcohol	32,6	285,6	338,0

Under the solvent action, a positive solvent – chromatic effect is visible with both types of transition; the batochrome displacement, with an increased solvent polarity, is low. Usually, the absorbtion band corresponding to the transitions of type $\pi \rightarrow \pi^*$ move batochromaly when the solvent polarity increases; the exciting state is more polar than the fundamental state as its is strongly stabilized by a polar solvent (the energy required for the electronic transition decreases).

The hydrogen bonds between the solute and the solvent also affect the shape of the electronic spectra. The protic solvents easily form hydrogen bonds with the atoms containing non-participating electrons. That is why the bands corresponding to transitions $n \rightarrow \pi^*$ are affected by the protic solvents. The formation of hydrogen bonds causes the absorbtion bands to move batochromaly to the molecules where the dipole moment of the excitation state is higher than the dipole moment of the fundamental state.

6. Determining of tiobis-β-naphthol dissociation constant

It is important to know the value of the analytical reactant dissociation constant in order to better understand the structure of the organic molecule and be able to predict their chemical behavior for analysis purpose .

In order to determine the dissociation constant the spectro-photometric method was used .

The tiobis-β-naphthol dissociation could be represented as follows:
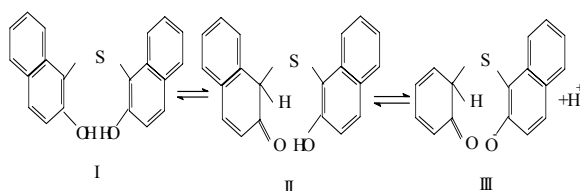
Structure III , proposed for the dissociated form of the tiobis-β-naphthol is accounted for by the aspect of the absorbtion spectrum in UV-VIS (Fig. 4) From the spectrum it is visible the existence of an absorbtion peak, at $\lambda = 244$ nm, which might be assigned to a band K (transition $\rightarrow \pi^*$), which is further due to a unsaturated group conjugated with the electrons π of the aromatic nucleus. With the dehydro-di-β-naphthol monosulfura (Fig.1), band K features an absorbtion peak at $\lambda = 242$ nm. The radical band R looks a little displaced for tiobis-β-naphthol at pH = 13 toward higher wave lengths, $\lambda_{max} = 362$ nm. Therefore, to determine the acid dissociation constant the simplified Comar method can be used . For the measurement purpose, those wave lengths have been chosen where only the reactive dissociated form is absorbing. From fig 4 it

can be seen then , from $\lambda = 370$ nm, the tiobis-β-naphthol dissolved into etilic or metilic alcohol, at pH<7 features no absorbtion.
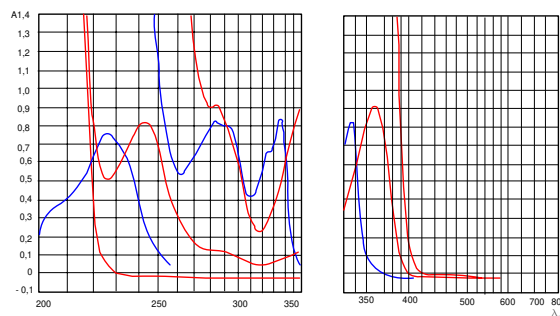
Fig. 4. *Electronic absorbtion spectra UV-VIS at tiobis-β-naphthol*
— etilic alcohol solvent
— pH=13

The reactant, dissolved into a NaCl solution, with pH=13 at the same concentration features absorbtion at $\lambda = 420$ nm. From the above reasons, measurements shave been carried out at $\lambda_1 = 400$ nm and respectively $\lambda_2 = 410$nm. A number of solutions of constant reactant concentration have been prepared, equal to 10^{-3} mol/l and different values of the pH; the absorbances at the chosen wave lengths have been measured. Assuming that the reactant dissociates with a monobase acid, acc to the scheme $HR = H^+ + R^-$, then its dissociation constant shall take the values :

$$K_{HR} = \frac{[H^+] \cdot x}{c - x} \qquad (1)$$

Where:
   [H] = concentration of the hydrogen ions;
   x - balance concentration of the reactant dissociation;
   c - total concentration of the reactant.

Acc. to the light absorbtion law, the sum of the reactant dissociated and non-dissociated absorbances is:

$$A = \varepsilon_{HR} \cdot 1 \, (c - x) + \varepsilon_{R^-} \cdot 1 \cdot x \qquad (2)$$

Where:
   ε_{HR} și ε_{R^-} – molar coefficients of HR and R$^-$ absorbtion respectively
   1 – making.

For the particular case of (2), for $\varepsilon_{HR} = 0$, we get:

$$x = \frac{A}{\varepsilon_{R^-} \cdot 1} \qquad (3)$$

By introducing x in the dissociation constant equation, we get a two-unknown value relation K_{HR} and ε_R^-:

$$K_{HR} = \frac{[H^+] \dfrac{A}{\varepsilon_R^- \cdot 1}}{c - \dfrac{A}{\varepsilon_R^- \cdot 1}} \qquad (4)$$

Solving this equation by means of two series of measurements, we shall have:

$$K_{HR} = \frac{A^i [H]^i - A^K [H]^K}{A^K - A^i} \qquad (5)$$

$$\varepsilon_R^- = \frac{A^i A^K ([H]^i - [H]^K)}{c \, 1 \, (A^i [H]^i - A^K [H]^K)}$$

(6)

As presented in Table 5, $pK_{HR} = 10,25$, complies satisfactorily with $pK_{HR} = 10,12$ determined potentiometrically.

Table 5. *Results obtained from the spectro-photometric measurement of the dissociation constant*

pH	H$^+$	A$_{400}$	A$_{410}$	K$_{HR}$ 400 nm	K$_{HR}$ 410 nm
10,92	$1,20 \cdot 10^{-11}$	0,840	0,292	$5,12 \cdot 10^{-11}$	$4,10 \cdot 10^{-11}$
10,80	$1,59 \cdot 10^{-11}$	0,800	0,272		
10,90	$1,26 \cdot 10^{-11}$	0,830		$7,53 \cdot 10^{-11}$	
10,80	$1,59 \cdot 10^{-11}$	0,800			
Average K$_{HR}$= $5,58 \cdot 10^{-11}$ pH$_{HR}$=10,25					

As a conclusion, the tiobis-β-naphthol is a low mono-base acid with the acid dissociation constant of $K_{HR} = 6,59 \cdot 10^{-11}$ and $pK_{HR}=10,18$.

7. Identification of tiobis-β-naphthol

The use of tiobis-β-naphthol in various domains asks for new determination and identification methods Thus the original oxidation method is proposed for the purpose of this study

The oxidation reaction of the dehydro-di-β-naphthol is characteristic for the tiobis-β-naphthol and makes use of the ferric nitrogen as oxidant.

The reaction takes place as follows: the tiobis-β-naphthol dissolved into etilic alcohol is treated with a concentrated ferric nitrogen solution. Initially a blue compound is obtained which turns into red upon heating, colors characteristic for the complex combinations with charge transfer, made up of tiobis-β-naphthol and ion Fe (III) acc to the ratio

Fe: HR=1:2 and Fe: HR=1:3 respectively. Upon boiling, the redox process is completed resulting in red – orange abundant precipitate. The isolated precipitated flushed in much water and purified by glacial acetic acid results in a fine crystalline light-red powder which does not contain any Fe, and having the 159°C.

The elementary and spectral analysis in the range UV-VIS indicates that dehydrosulphide has been obtained:

$$Fe^{3+} + 2C_{20}H_{14}O_2S \xrightarrow[-2H^+]{} Fe(C_{20}H_{13}O_2S)_2^+ \quad albastru$$

$$Fe(C_{20}H_{13}O_2S)_2^+ + C_{20}H_{14}O_2S \xrightarrow[-H^+]{} Fe(C_{20}H_{13}O_2S)_3 \quad rosu - caramiziu$$

$$Fe(C_{20}H_{13}O_2S)_3 \xrightarrow[-3H]{t^0 C} 3C_{20}H_{12}O_2S + Fe^{2+} \quad precipitat \; rosu - caramiziu$$
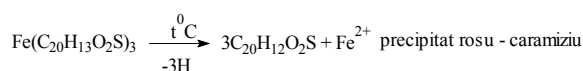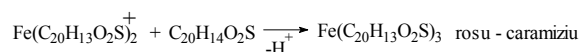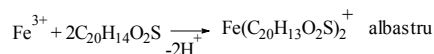
8. Conclusions

▪ The synthesis of the new reactant (tiobis-β-naphthol) as well as the latest researches on solubility , the dissociation constant, the original identification method and the UV- VIS and IR studies bring about important contributions to the tiobis-β-naphthol structure.

▪ The tiobis-β-naphthol having groups of (-S-) and (-OH-) situated in suitable positions features high reactivity being able to form a donor-acceptor bond with some metals.

▪ The tiobis-β-naphthol may be used for selective determination of several metals like: Cu^{2+}; Hg^{2+}; Mn^{2+}; Pb^{2+} etc. from different materials as: ore, rocks, used water etc.

References

[1]. **Mitoşeriu O.,** 1980, „Teză doctorat" Institutul Politehnic Iaşi.
[2]. **Perrin D.**, 1967, "Org. anal. Reaghentî, Izd. Mir", Moskva.
[3]. **Popa G., Moldovanu S.,** 1976, „Reactivi organici în chimia analitică." Editura Academiei, Bucureşti.
[4]. **Kulkarni V.G.,** 1956, - J. Indian Chem. Soc. 33, 738
[5]. **Tassinari G.,** 1889 – Gezz. Chim. Ital. 19, 349
[6]. **Popa G., Paralescu A.I.,** 1977 "Chimia analitică" Ed. Didactică şi Pedagogică, Bucureşti
[7]. **Neniţescu D.C.,** 1968 "Chimie organică" Ed. Didactică şi Pedagogică, Bucureşti
[8]. **Kaziţina A.L., Kupletscaia B.N.** 1971 "Primenenie If, Ir, I Yamrspectroscopii v organiceskoi himii, Izd. vîşaia şcola, Moskva
[9]. **Avram M., Mateescu G.D.** 1966 „Spectroscopia în infraroşu. Aplicaţii în chimia organică" Ed. Tehnică, Bucureşti
[10]. **Răileanu M.** 1976 „Rolul solvenţilor în reacţiile compuşilor organici" Editura Scrisul Românesc, Craiova, pag. 91-116
[11]. **Kreşkov P.A., Bâcona L.N., Kazarian A.N.** 1969 „Titrarea în mediu neapos" Ed. Tehnică, Bucureşti, pag. 41,69
[12]. **Luca C., Enea O.** 1971 „Determinarea constantelor analitice. Metode electrometrice şi optice" Editura Didactică şi Pedagogică, Bucureşti.
[13]. **Liteanu C.** 1963 - Studii şi cercetări. Chimie, Cluj, 1, 181.

EXPERIMENTAL RESULTS AT MODELLING OF THE FLOW AND DEFORMATION FIELDS AT THE PROFILES ROLLING

Nicolae CANANAU, Ionel PETREA,
Gheorghe COROBETE
"Dunarea de Jos" University of Galati
e-mail: **cananau.nicolae.ugal.ro**

ABSTRACT

This paper presents the results for modeling of the rolling process based at the deformable continuous medium mechanics, the theory of field lines. The rolling of the profiles and plates may be evaluated as the plane strain state process. Using the equations of the continuous medium and the initial conditions and the limits conditions we solved the speed field, the strain rate field, the strain field. Applying an adequate computation program we obtained the values of the field factors of modeling process. The results are showed into this paper.

KEYWORDS: modeling, rolling process, field lines

1. Introduction

In a previous paper [1] was presented a method for modeling of the rolling process based at the deformable continuous medium mechanics, the theory of field lines. Using the calculus algorithm described above we developed a computation program. The results of the calculus program are presented in this paper. We consider the rolled body as a deformable continuous medium. The volume occupied by the continuous medium, at the really moment, is divided in three domains (figure 1):
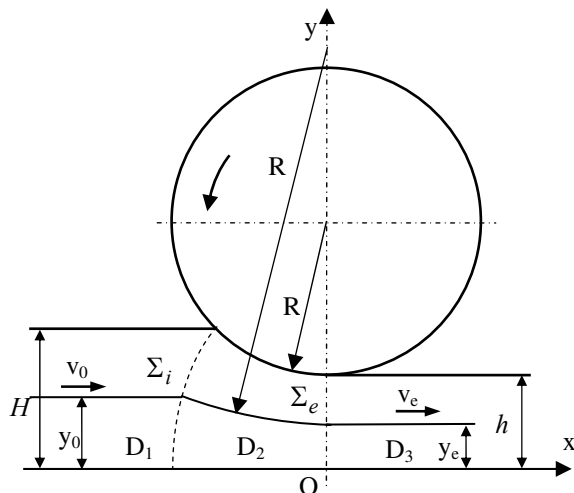
Fig.1. *The deformation domain and field line.*

- the domain D_1 before the entrance of medium between the rolls (rigid plastic medium),
- domain D_2, deformation domain, the medium is between the rolls. In this domain is developed the deformation process,
- domain D_3 at the exit of material between the rolls (rigid plastic, too).

For the numerical calculus we use the following normalized coordinates:

$$\eta = \frac{x}{x_o} \quad \text{respective ly,} \quad \varphi = \frac{y_o}{H} \qquad (1)$$

The data used by the computation program are the following:

R=500 mm
H=25 mm
h=20 mm
v_0=4 m/s

2. The speed field

In the conditions of a stationary regime of the continuous medium flow the field lines coincide to the movement trajectories of the material particles. In the Figure 2 we represent the field line of the material particles that are situated to y_0 of the axe Ox, the symmetry axe of the body. The continuity condition is defined by the constant material flux in the long of the field line. The components of the speed field are presented in figure 2.
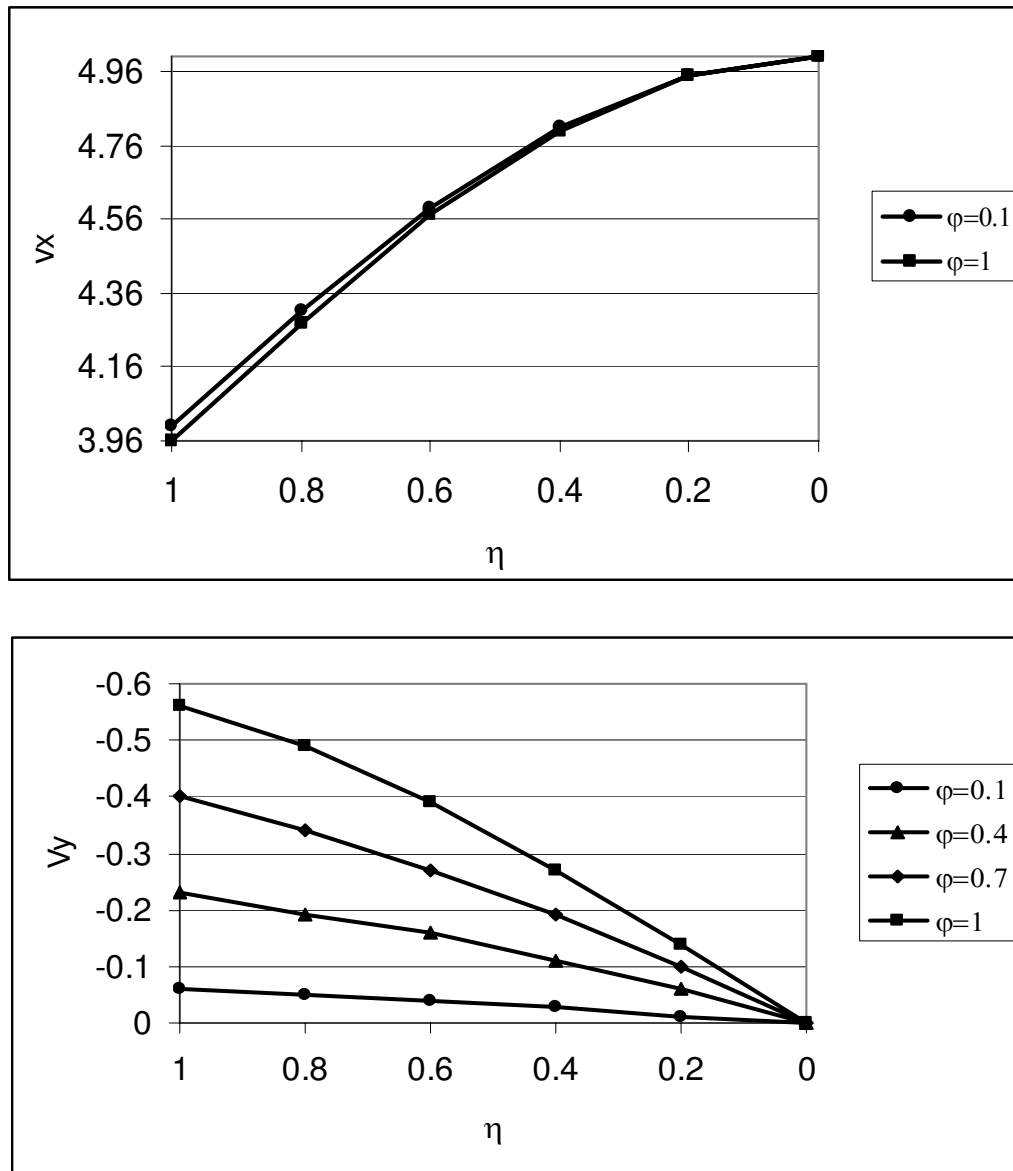
Fig.2. *The components of the speed field.*

3. The strain rate field

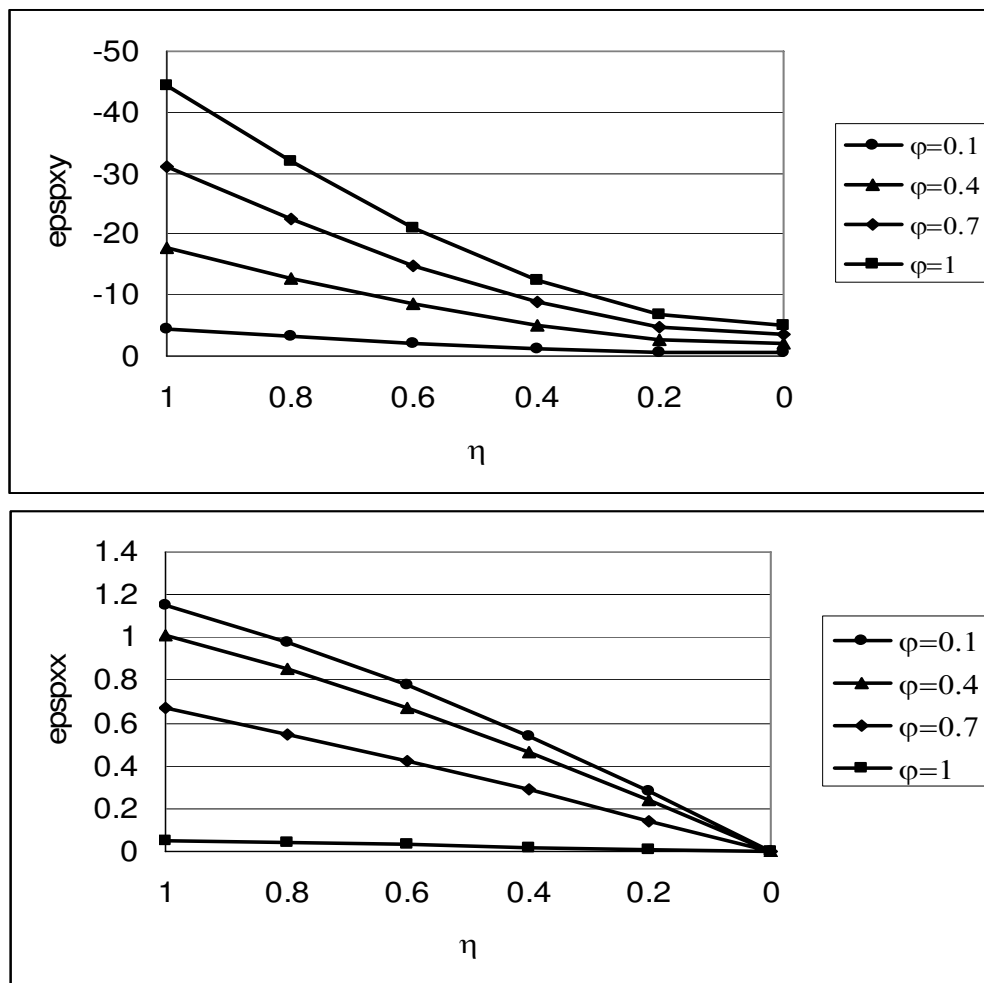The components of the strain rate tensor are defined by equations:

$$\dot{\varepsilon}_{xx} = \frac{\partial v_x}{\partial x}; \quad \dot{\varepsilon}_{yy} = \frac{\partial v_y}{\partial y}; \quad \dot{\varepsilon}_{xy} = \frac{1}{2}\left(\frac{\partial v_x}{\partial y} + \frac{\partial v_y}{\partial x}\right)$$
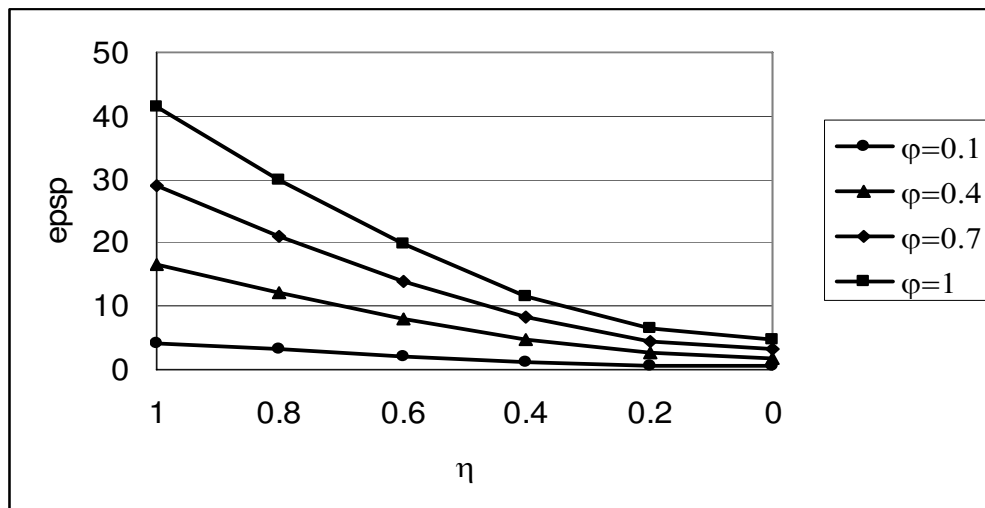
The strain rate intensity is defined by the relation:

$$\bar{\dot{\varepsilon}} = \frac{2}{3}\sqrt{\dot{\varepsilon}_{xx}^2 + \dot{\varepsilon}_{yy}^2 + 2\dot{\varepsilon}_{xy}^2} \qquad (2)$$

The components of the strain rate tensor are presented in Figure 3.
The strain rate intensity is presented in figure 4.

Fig. 3. *The components of the strain rate tensor.*

Fig. 4. *The strain rate intensity.*

4. The field of strain intensity

The field of strain intensity is defined by the expression:

$$\bar{\varepsilon} = \int_0^t \bar{\dot{\varepsilon}} \cdot dt \qquad (3)$$

For the numerical solve we will use the following principle (fig.5):

We defined the time differential as:

$$dt = \frac{dx}{v_x}$$

The numerical expression of the equation (3) is:

$$\bar{\varepsilon}_k = \bar{\varepsilon}_{k-1} + \left(\bar{\dot{\varepsilon}}_{k-1} + \bar{\dot{\varepsilon}}_k\right) \cdot \frac{x_k - x_{k-1}}{v_{x_k} + v_{x_{k-1}}} \qquad (4)$$

In this expression the index k is defined in function of the index i as $k=n-i$, where i is the division operator in the long of the field line $(i=1,2,...,n)$.

For initialization of the values of $\bar{\varepsilon}$ we consider what at the $k=0$, respectively, $i=n$, that is in the point of surface Σ_i the deformation is defined by the rotation of speed vector of angle θ_o.

Thus the initial strain is:

$$\bar{\varepsilon}_0 = \mathrm{tg}\,\theta_0 \qquad (5)$$

The field of strain intensity is presented in figure 6.

Fig. 5. The calculus scheme of the strain intensity.
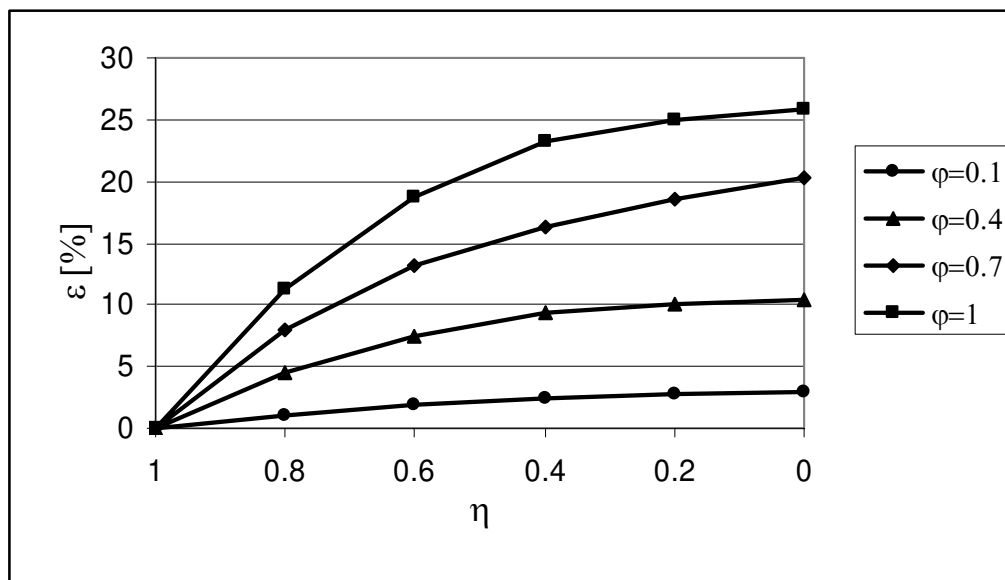
Fig. 6. The field of strain intensity.

5. Conclusions

The solving of the deformation process is possible using various methods. The field (or flow) line is one of these.

First we must defined clearly the domain that, at the real moment, is occupied of the body and the initial and limit conditions. The body is considered as deformable continuous medium. Then, we must define the equation of the flow line.

Using the equations of the mechanics of the deformable continuous medium, applying the initial conditions and the conditions at the limits we obtained, in the analytical form, the expressions of the components of the speed, and, derived by these, the components of the strain rate tensor.

If the components of strain rate tensor are defined, that is the field of strain rate tensor is defined, we can calculate the strain rate intensity, and finally, the strain intensity. Thus, the analyze of cinematic process is solved.

The data presented in this paper will be used for the calculation of the process parameters of the profiles rolling.

References

[1] Cananau N., Petrea I, Corobete G., *Modelling of the flow and deformation fields at the profiles rolling by field lines method* , The Annals of "Dunarea de Jos" University of Galati, Fascicle IX, Nov. 2005

[2] Moussy F., Franciosi P. *Physique et mecanique de la mise en forme des meteaux*. Presses du CNRS, Paris, 1990, ISBN 2-87682-023-4

[3] Dumitrescu A.T. *Contributii la modelarea laminarii in calibre. T*eza de doctorat, Institutul Politehnic Bucuresti, 1986.

[4] Adrian M., Badea S. *Bazele teoretice ale proceselor de deformare plastica.* Editura tehnica, Bucuresti, 1983.

[5] Cananau N. *Teoria deformarii plastice.* Universitatea Dunarea de Jos din Galati, vol.2, 1995.

THE LABORATORY EXPERIMENTS REGARDING THE INTERCRITICAL HEAT TREATMENTS APPLIED ON THE LOW - ALLOYED STEEL

Elisabeta VASILESCU, Marian NEACŞU
"Dunarea de Jos" University of Galati
e-mail: **vasilescu.elisabeta**

ABSTRACT

The paper presents the research results regarding the influence of the intercritical thermal treatments carried out on some hypoeutectoid steel castings.

The purpose of this research at the laboratory scale is to measure the effect of the thermal treatment which precedes the intercritical thermal treatment as well as to establish the optimum experimental variant in order to replace the classical thermal treatments.

KEYWORDS: intercritical thermal treatments, steel castings, hypoeutectoid steel

1. Introduction

Thermal treatments carried out on steels provide, according to the classical technologies, the complete austenitizing (for hypoeutectoid steels) or incomplete austenitizing (for hypereutectoid steels) and subsequently, the austenite transformation by various treatments: annealing, quenching (hardening). [1]

The latest research showed that the convenient mechanical characteristics could be obtained by intercritical thermal treatment carried out on some hypoeutectoid steels as well as on low alloyed steels.

Heating a hypoeutectoid steel, in balance condition between Ai - A3 interval, its microstructure ferrite - perlite, initially will become ferrite - austenite one.

The structural modifications, produced in the Ai - A3 interval by heating, are very complex and are depending on the chemical composition of the steel by its initial structural condition and isothermal maintaining length, by the cooling way and - specific to such treatments - the way in which the given temperature is reached: "down to up " (by heating from environment temperature) or " up to down" (by preliminary complete austenitizing and cooling in the critical interval).

Afterwards, these heating - cooling possibilities are combined with various thermal treatments, for example: quenching + tempering, normalization, annealing or, after the preliminary treatment carried out on the respective parts. [2]

A favorable influence of the intercritical treatments on the final characteristics came out.

2. Laboratory Experiments and their Results

The intercritical treatments of Cr, Ni, Mn, Mo, low alloyed and half-hard steels lead to satisfactory results only if the quenching temperature is AC3 - 50°C but final characteristics are depending on the initial condition of the steel, heating speed of the intercritical quenching and final tempering (annealing) temperature. The toughness - strength tests made on both: positive - negative temperature values resulted in sensitive higher values than for classic hardening and tempering treatment.

As a result, some research was made following the use of the intercritical treatment ranges on 34MoCrNil6 steel castings from which various items are made for industrial equipment. Steel characteristics are shown in table no.l.

In the industrial condition, the final thermal treatment for such items consists in quenching and high tempering (annealing) to get core characteristics (290 - 300 HB) and a thermal-chemical treatment (ionic nitriding) for surface (700 - 900 HV) according to fig. 1.

Table 1. *34 Mo Cr Ni 16 Steel characteristics*

Chemical composition[%]						Rm	Rpo,2	KCU
C	Mn	Si	Cr	Ni	Mo	N/mm^2	N/mm^2	J/cm^2
0,3... 0,38	0,4...0,7	0,17... 0,37	1,4...1,7	1,4...1,7	0,15... 0,3	1180... 1370	980	min. 39

In the industrial condition, the final thermal treatment for such items consists in quenching and high tempering (annealing) to get core characteristics (290 - 300 HB) and a thermal-chemical treatment (ionic nitriding) for surface (700 - 900 HV) according to fig. 1.
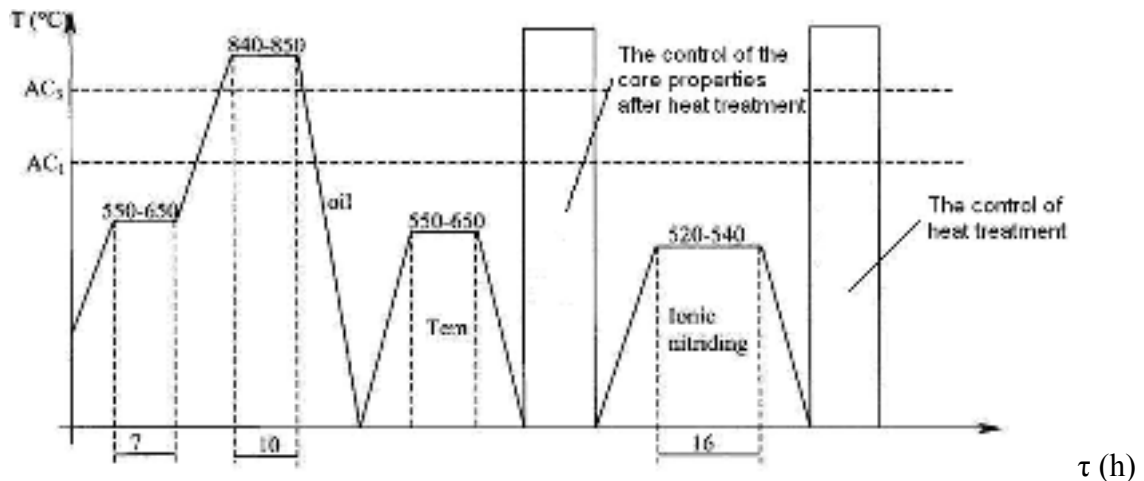
Fig. 1. *Thermal and final thermal-chemical treatments of 34 Mo Cr Ni 16 steel castings.*

The industrial treatment technology is complex, covering: the long time operation, expensive installation with high power and fuel consumption. As a result, the possibility of using the intercritical thermal treatment on such items and their influence on the structure and final mechanical characteristics were studied in the laboratory conditions.

The intercritical treatment conditions were used on castings after the following preliminary operation (table).

1 - initial condition: classical quenching + tempering after casting

2 - casted condition

3 - annealing after casting

4 - normalizing after casting

The intercritical treatment was made to the following diagram (fig. 2, table 2).
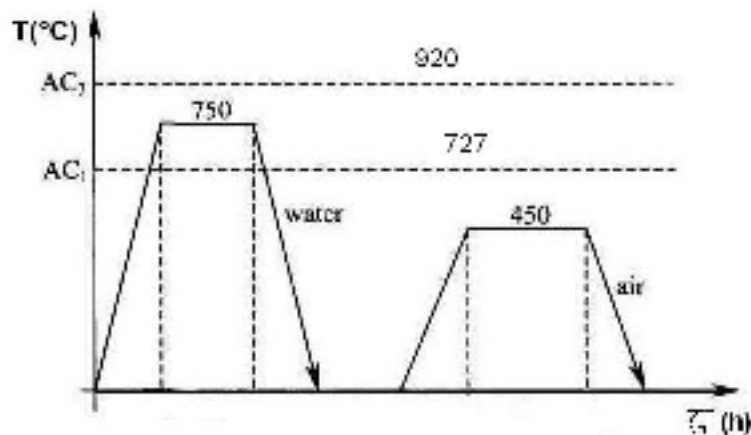
Fig.2. *Treatment regime.*

For 34 MoCrNi 16 the critical temperature values Aci and AC3 were calculated by Grange relations, recommended for such steel grades: [3]

$Ac_1 = 723 - 14 (0,56Mn + 1,47Ni) + 22 (0,4Si + 1,5Cr) = 727°C$

$Ac_3 = 854 - 180 . 0,33C - 14 . 0,56Mn - 18 . 1,47Ni + 45 . 0,4Si + 1,7 . 1.5Cr = 920°C.$

Table 2. The experimental conditions of the intercritical treatment

Experimental variants	Preliminary operations	Intercritical quenching		Tempering	
		Temperature	Time(hours)	Temperature	Time
Q_1	Quenching + tempering	750°C	1	450°C	2,5min/mm
Q_2	Quenching + tempering	750°C	5	450°C	2,5min/mm
C	Casted condition	750°C	5	450°C	2,5min/mm
A_1	Annealing	750°C	1	450°C	2,5min/mm
A_2	Annealing	750°C	5	450°C	2,5min/mm
N_1	Normalizing	750°C	1	450°C	2,5min/mm
N_2	Normalizing	750°C	3	450°C	2,5min/mm

As it was previously shown, the austenitization temperature is established at A_{C3} - 50°C for intercritical treatment and thermal retardation is chosen so that the distribution by diffusion of the alloying elements and their segregation to be avoided.

For experiments two holding times were chosen for quenching: 1h and 5h. The results were compared to those of the conventional treatments used in various working conditions of casting and considered as initial state for items - table 2 (table 3).

Table 3. Conventional treatments

Experimental variants	Treatment	Temperature(°C)	Time(min/mm)	Cooling agent
Q_3	Quenching + Tempering	830 450	2 2,5	Water, Air
A_3	Annealing	830	2	Furnace
N_3	Normalizing	830	2	Air
N_4	Normalizing + subcritical annealing	830 680	2 2	Air Air

According to [4] the intercritical treatments are used for casting parts after their preliminary treatments: quenching + classical tempering or hardening so that a fine and oriented structure to be assured. In the research framework, the quenching + tempering, annealing,

normalizing (according to table 3) were used as preliminary treatments. After treatments, the test specimens were taken and toughness-strength tests and microstructural analyses were made. Results are

shown in fig. 3(a-c). Temperature of the toughness -   strength tests: 20°C; 0°C; -50°C.
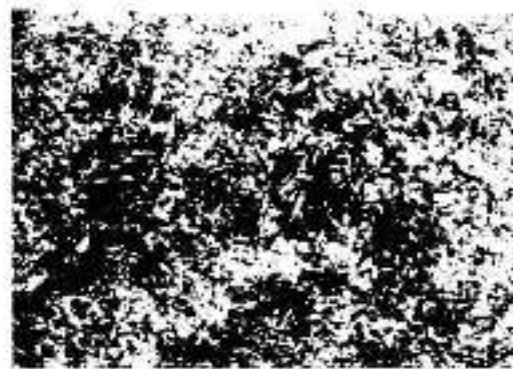

a

b

c
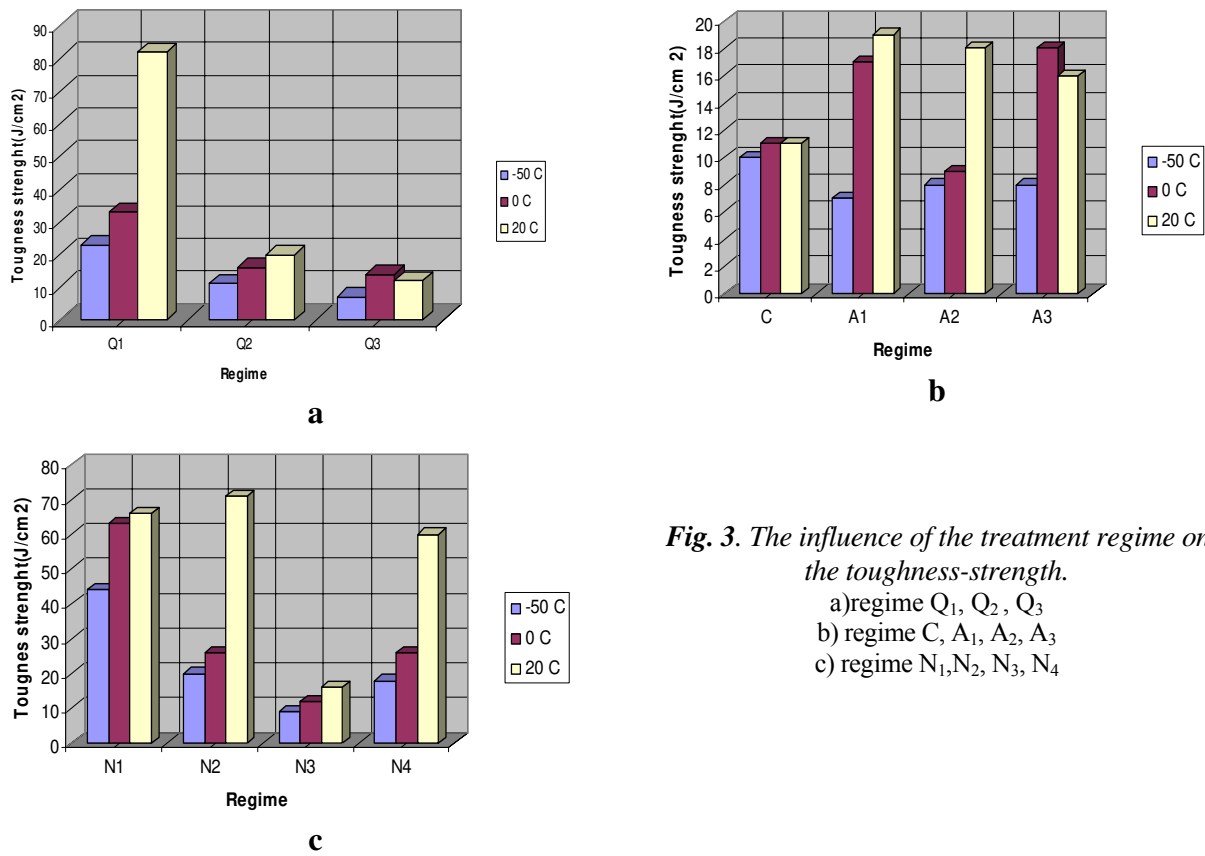
Fig. 3. *The influence of the treatment regime on the toughness-strength.*
a)regime Q_1, Q_2, Q_3
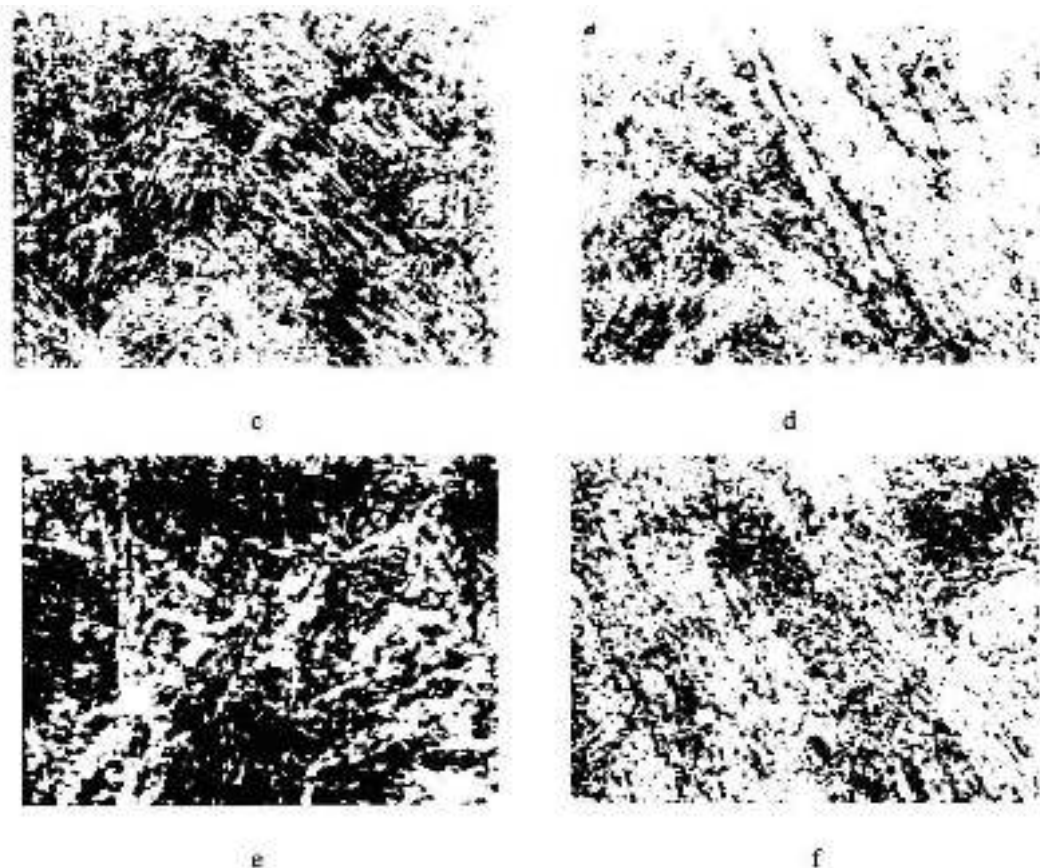b) regime C, A_1, A_2, A_3
c) regime N_1, N_2, N_3, N_4

The microstructures are shown in fig 4 (a-f).
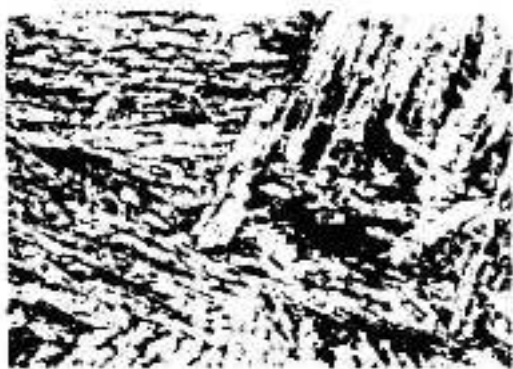
a

b

Fig.4 *Microstructure aspects after intercritical treatments.(x500 magnification) etching: nital 2%.*
a*-steel cast;* ***b*** *- quenching + tempering (Q + T) of cast;* ***c****-Q + T(lh) of Q + T*
d *- Q + T (5h) of Q + T; **e** - normalizing; **f**-Q + T(lh) of normalizing; g - Q + T (3h) of normalizing.*

3. Conclusions and discussions

From the result analysis the following are established:

- the highest values of the toughness-strength are obtained by an intercritical quenching treatment + tempering from normalizing initial condition, lh at 750°C and tempering at 450°C, 2,5 min/mm - toughness-strength = 62 J/cm at 0°C (according to STAS 8185-80, - toughness-strength = min. 39J/cm^2).

- quite high values of the toughness-strength are obtained after quenching + tempering from initial condition of the quenching + tempering and also, after a quenching + tempering from normalizing initial condition (3h holding).

- It comes out that the increase of the heating holding time for quenching in the intercritical domain doesn't improve the toughness-strength values.

The structure appearance (fig. 4) to a certain extent can explain the toughness-strength values. Thus, in the cast condition the structure is a rough acicular one (fig4a). After the intercritical thermal treatment a fine structure is obtained but with very low characteristics of tenacity yet (regime C). In the other cases, the preliminary treatments Q + T or N determine a fine and oriented structure, which, after the intercritical treatment, emphasizes the structural fineness. This characteristic was noted in the fracture surface (impact-bending test) too, which appears dull and silky (fibrously) unlike fracture surface of Q + T classic treatment where the appearance is crystalline, the fracture being on the former austenitic grains borders.

In acicular or globular austenite (initial structure) determines the martensite morphology when martensite is made, after the preliminary quenching treatment, that will result in the formation of acicular austenite at (the final treatment) the heating in the intercritic field.

As the heating is achieved in the intercritical field, besides austenite, there is also a quantity of ferrite. The increase of the holding time, at the quenching temperature, will determine a movement of the ferrite grains due to the austenite phase that is rising. Therefore the toughness might get lower to the increase of the quenching holding time (lh to 5h). Thus, for a quenching holding time t_c = lh a toughness value of 33 J/cm^2 was obtained (at 0°C) while t_c = 5h, a toughness value of 16J/cm^2 has resulted.

The tempering process brings back the toughness to higher values close to those of the initial structure.

Thus, the existence of the supersaturated ferrite with substitution and interstitial atoms, the internal tension resulted from the local transformation of the austenite into martensite, the high density of dislocation in the residual austenite grains and separation of some carbides determine the toughness values, after tempering treatment.

With the increase of the tempering temperature, the separation process of the interfaces between M plates of the lamellar carbides is emphasized, the latter becoming more and more coarsen and with a tendency to spheroidize.

Therefore it was established that the temperature of 400 - 450°C is the best for tempering, when the main phenomena are: density growth of the fine grains (d < 5mm) and the apparition of fine cementite at the border of the ferrite grains and sub-grains. These explanations given by the literature of specialty are confirmed in the experiments made on 34 Mo Cr Ni 16 steel.

Intercritical quenching and tempering at 450°C might be used on the castings but only after a preliminary treatment that is Q + T. The experiments proved that preliminary normalizing + intercritical quenching and tempering at 450°C can give better toughness values than preliminary quenching + tempering.

Intercritical treatment might replace some of the actual treatment of long time and high fuel consumption.

References

[1]. **Gadea S. s.a,** *Metalurgie fizica si studiul metalelor* vol.Ill, EDP - Bucuresti 1983

[2]. **Popescu N. s.a**., *Tratamente termice neconventionale* - Ed. Tehnica, Bucuresti 1990

[3]. **Popescu N. s.a**., *Tratamente termice si prelucrari la cald*, EDP - Bucuresti 1983

[4]. * * * *Cercetari privind aplicarea tratamentelor termice in domeniul intercritic la oteluri* - Contract de cercetare / 2000 S.C. Engineering Uzinsider S.A. Galati.

ASPECTS OF NITRATED LAYER STRUCTURE FOR SOME TYPES OF AUSTENITE STAINLESS STEEL

Ovidiu DIMA, Sanda LEVCOVICI,
Constantin GHEORGHIES
"Dunarea de Jos" University Galati
e-mail: dima.ovidiu@ugal.ro

ABSTRACT

The analysis of nitrated layer diffractograms and the structure marked out the presence of complex nitrides combinations layer for all types of steel except for code 6 steel type 2CuMoNiCr200 which because of the very high index of austenite stability, 29.9, presented a layer made of nitrogen solid connate solution in austenite. In the case of stainless austenite steel types nitrogen diffusion and, consequently nitrated layer formation depends on the concentration of alloying elements in steel, on austenite stability indices. Code 2 and code 3 steel types that have the smallest stability indices have the thickest layer and are followed by code 3 and code 4 steel types. On the fifth place is code 1 steel type which has a thinner layer, approx. 21 jam and on the last place there is code 6 steel type that, as it was shown, does not form a nitrides layer.

KEYWORDS: austenite, stainless steel, nitrated, structure

1. Introduction

In order to point out the nitration behavior of stainless steel, a number of six characteristic steel types CrNi, CrNiMo with low and higher carbon content, titanium stabilized or not, was chosen. The steel types have been subjected to fluidized bed thermo chemical nitration treatment for 1, 2, 3 hours, at a temperature of 550 ^{o}C so as to marl-out the process dynamics. The treatment has been applied in order to increase surface hardness and implicitly materials resistance to abrasion.

2. Materials studied

The materials that have been studied were plates made from stainless austenite steel Cr-Ni and Cr-Ni-Mo with low carbon content %C<0.03, with higher carbon content %C=max. 0.12 but also steel types with higher carbon content and stabilized with Ti or Nb. The chemical composition of these steel types is presented in table 1.

Table 1

Steel code	Related mark	%C	%S	%P	% Mn	% Si	%Cu	%Cr	%Ni	% Mo	% Ti	% V
1	12NiCrl80	0.12	0.028	0.055	1.24	1.64	0.06	23.2	9.8	0.11	0.01	0.02
2	10TiNiCrl80	0.06	0.008	0.036	1.55	0.65	0.08	17.1	9.3	0.05	0.60	
3	2NiCrl85	0.03	0.005	0.028	1.27	0.42	0.19	18.9	8.95	0.15	0.01	0.02
4	2MoNiCrl75	0.02	0.005	0.039	2.06	0.78	0.27	20.0	8.8	2.7	0.03	0.03
5	10TiMoNiCrl75	0.045	0.012	0.031	0.96	0.54	0.16	18.1	11.6	2.04	0.32	
6	2CuMoNiCr200	0.02	0.008	0.027	1.12	0.41	0.70	20.1	18.1	6.1		0.2

In order to point out process dynamics samples of 60x20x3 have been made from plates and then subjected to fluidizing bed thermo-chemical nitration treatment for 1, 2, 3 hours, at a temperature of 550°C. The treatment has been made in order to increase surface hardness and implicitly the resistance of materials to abrasion.

Metallographic samples which have been subjected to grinding, polishing and electrochemical attack so as to show the structure by optical microscopy were cut off from nitrated samples by means of the abrasive wheel and with abundant cooling.

2. Results

Structure analysis points out a nitrides surface which has a distinct aspect and is separated from the base austenite structure by a buffer zone, more or less thick, made of a mechanical mixture of austenite and complex nitrides. Electrolytic attack in nitric acid - 50% is more emphasized on the layer and on the buffer line and more reduced upon the matrix. The layer presents a poly-phase structure. Nitrogen diffusion determines the separation between complex nitrides and iron and all other steel alloying elements. This justifies the increase in hardness. After one hour of treatment the layer is thin and even discontinuous if we speak about steel type code 3. For steel types code 1 and 6 a metallographic distinct metallographic aspect layer is not pointed out. The discontinuous aspect is explained by the fact that on the samples surface are shown areas with different degrees of absorption and diffusion.

The more active areas alternate with less active ones. The fact that for steel types code 1 and 6 there is no nitrides layer after the first hour of treatment is explained by the high stability of austenite.

For these steel types nitrogen diffuses in austenite structure, nitrogen concentration increases and this is completely diluted.

The metallographic analysis can point out only nitrides, the combinations layer resulted after nitration treatment but not the diffusion and dilution layer. After two hours of treatment the combinations layer is leveled and becomes more continuous and more uniform for the major part of the steel types except steel type code 1 for which the combinations layer is thin and discontinuous and code 6 which has no combinations layer.

After three hours of treatment the combinations layer is pointed out for all steel types, with great and uniform thickness exception is the steel type code 6 which presents small combinations areas of micro-metrical dimensions. Granulation of austenite grains within the combinations layer area as a result of nitrides chains that have been formed is expected to lead to some reduction of the resistance to corrosion.

In Figures 1 a, b, c, d, e, f we present the aspects of surface layer microstructures for all 6 steel types that have been analyzed in 3 nitration conditions of 1, 2 respectively 3 hours. The microstructures have been made at an increase of x400.
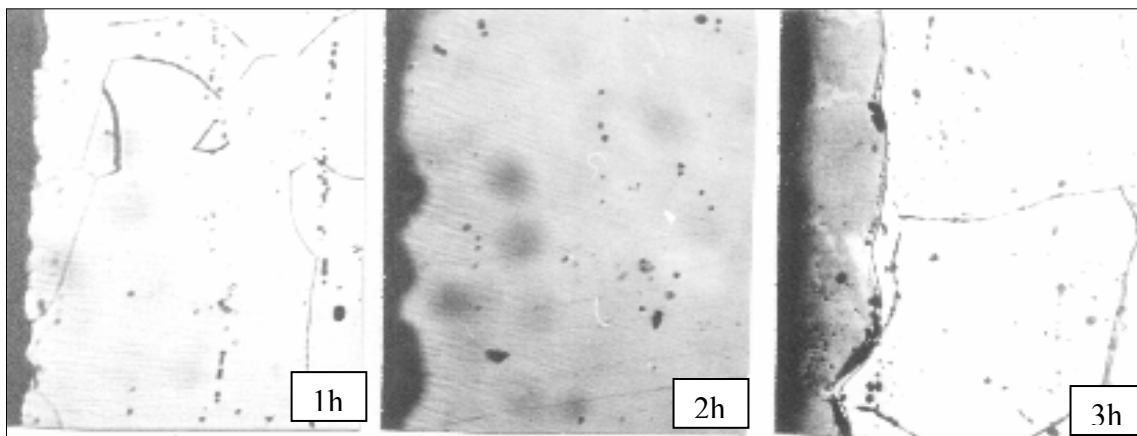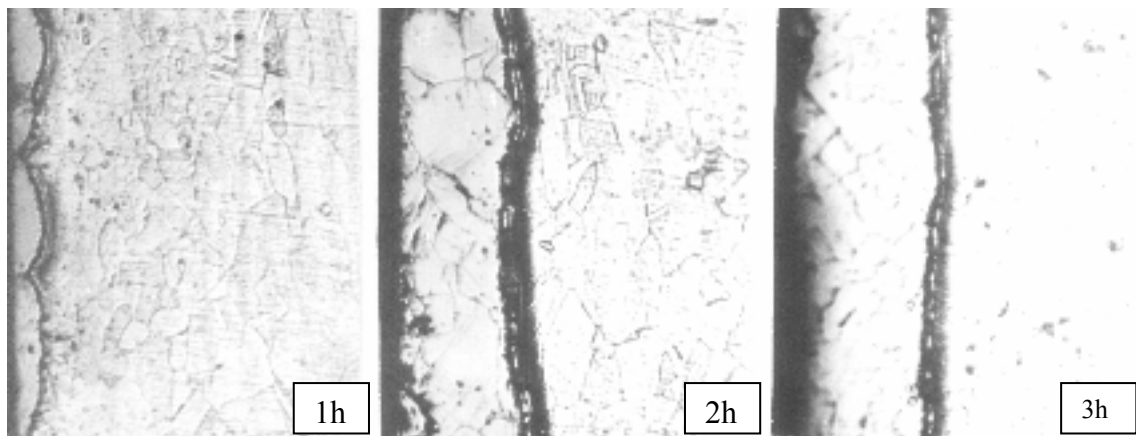

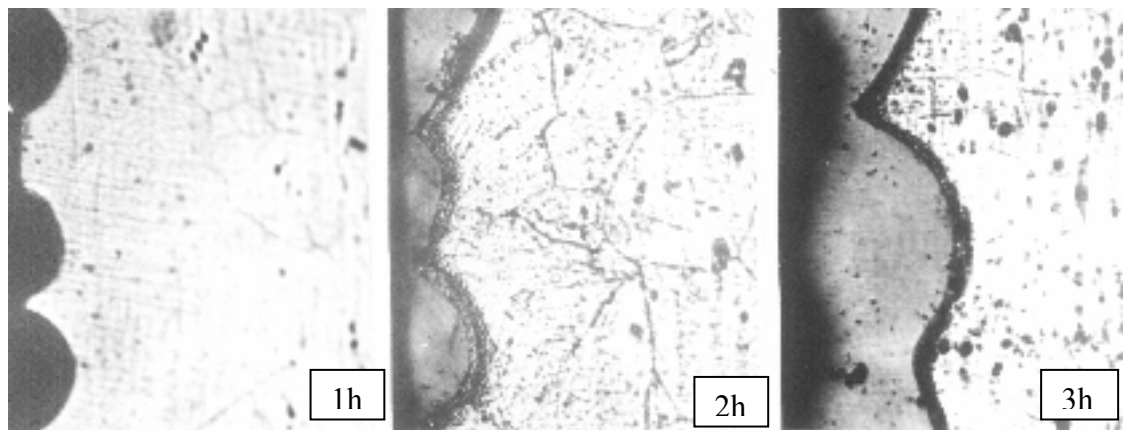*Fig.1a* *Microstructures of nitrated samples code 1 steel type -12NiCr180*

The aspect of diffractograms for steel type code 6 is very likely to that of the initial samples of stainless austenite steel types. Its analysis points out some bits that correspond to diffraction angles which are determined by the presence of gamma phase Fe$_\gamma$ inside nitrated layer's structure. For nitrated stainless austenite steel types gamma phase is solid connate nitrogen in the austenite structure highly alloyed with chrome, nickel, and molybdenum.

As it was told above, steel type code 6 has a content of more than 50% alloying elements, a high index of austenite stability S-29.8 and, when nitrated, nitrogen is diluted in austenite without causing nitrides separations. But austenite enrichment with nitrogen determines a smaller increase in hardness. Hardness maximum value is 508 HV$_{005}$
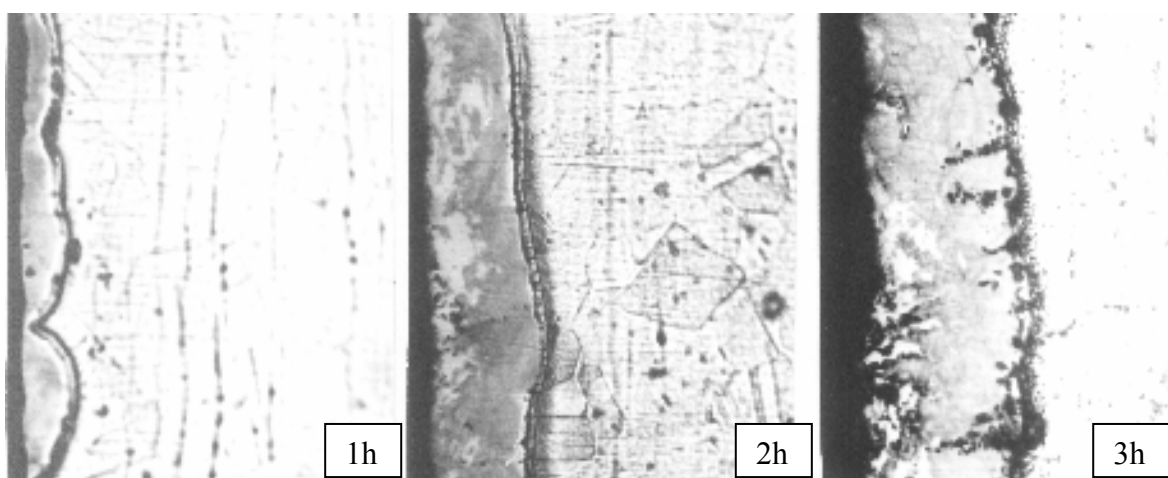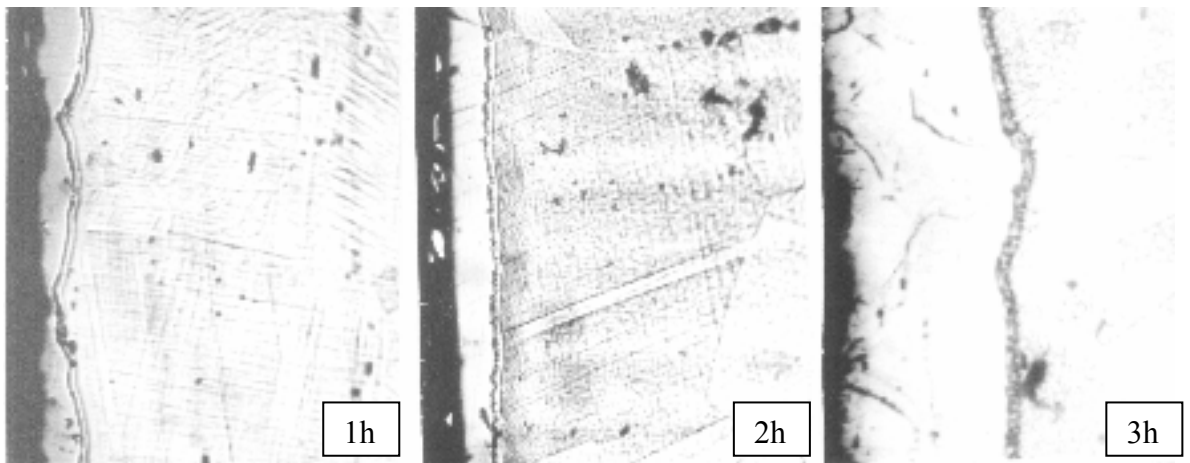
Fig.1b. *Microstructures of nitrated samples code 2 steel type –10TiNiCr180.*
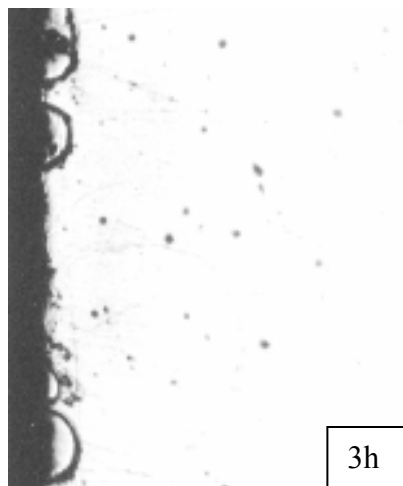

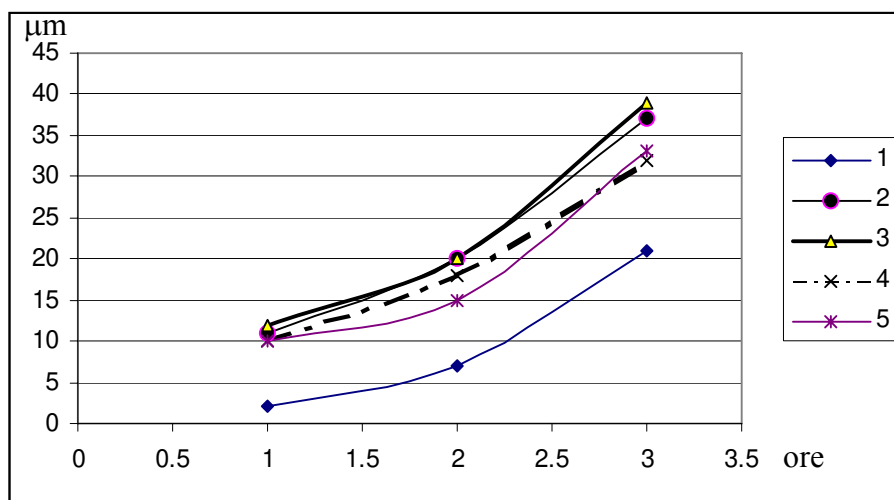**Fig.1c.** *Microstructures of nitrated samples code 3 steel type -2NiCr185.*

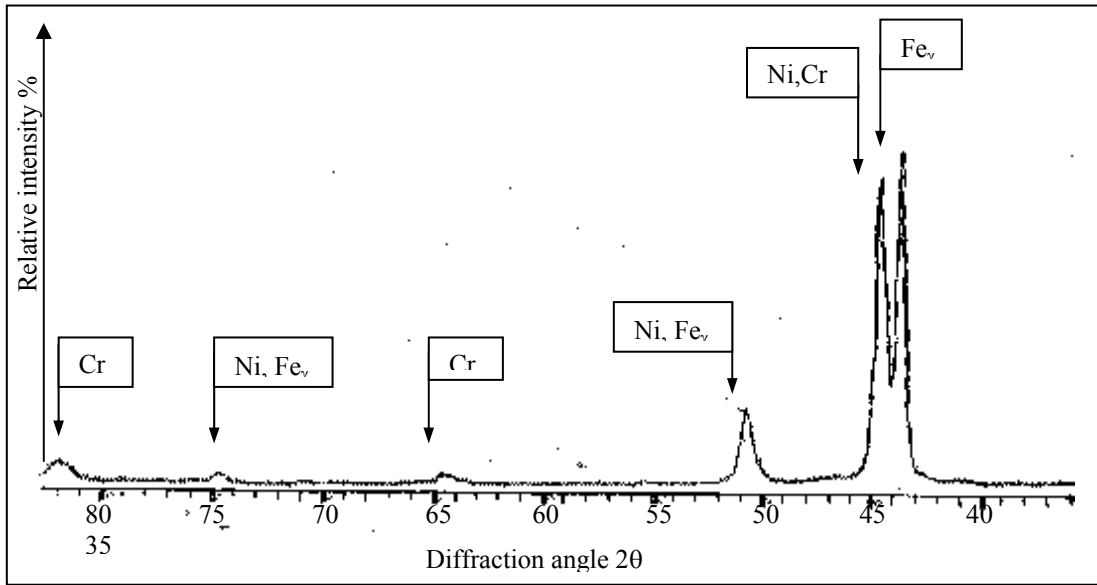**Fig.1d.** *Microstructures of nitrated samples code 4 steel type –2MoNiCr175.*

Fig.1e. Microstructures of nitrated samples code 5 steel type –10TiMoNiCr175.
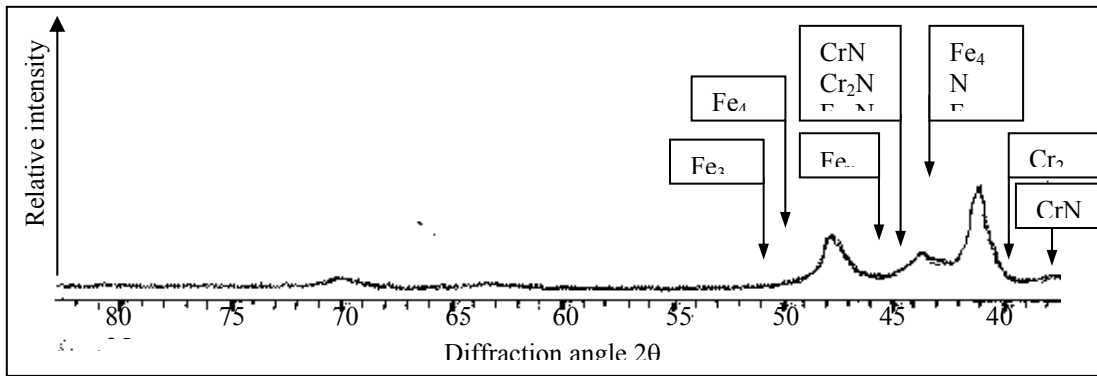

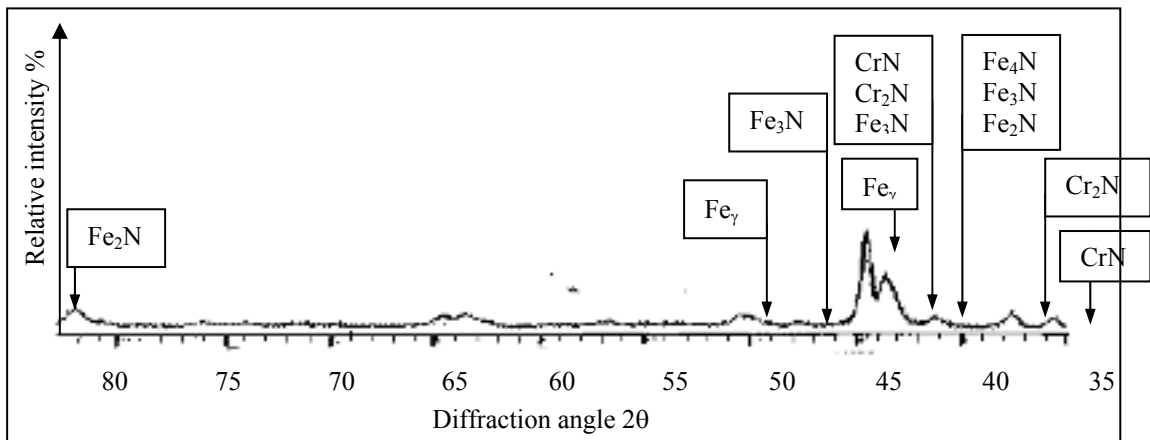*Fig.1f.* Microstructures of nitrated samples code 6 steel type –2CuMoNiCr200.

Fig.2. Variation in thickness of nitrated layer and the duration of nitration process.

Fig.3. *Diffractograms for sample 6 stel type –2CuMoNiCr200.*

Fig.4 *Diffractograms for sample 2 stel type –10TiNiCr180*

Fig.5 *Diffractograms for sample 4 stel type –2MoNiCr175*

Diffractograms analysis for steel type code 2 10TiNiCrl80 indicate the presence of bits that correspond to iron nitrides Fe_2N, Fe_3N, Fe_4N, presence of chrome nitrides CrN, Cr_2N and less for gamma phase Fe_γ. The presence of nitrides and solid solutions in austenite determines a strong increase of hardness for values that can be more than 1000 HV_{005}

Diffractograms aspect is almost the same for the first 5 steel types but with the remark that bits intensity corresponding to gamma phase has a bigger or smaller value, depending on its stability degree.

Fig. 5 presents the diffractograms for steel type code 4 2MoNiCrl75, the austenite stability index being bigger if compared to steel type code 2.

It is also noticed that relative intensity of gamma phase bits is greater.

3. Conclusions

Nitrogen diffusion and, in consequence, nitrated layer forming for stainless austenite steel depends on the concentration of steel alloying elements, of austenite stability indices.

Steel types code 2 and code 3 have the smallest stability indices and the thicker layer, being followed by steel types code 3 and code 4.

On the 5th place there is steel type code 1 having a very thin layer, approx. 21um and on the last place is steel type code 6 that as we showed above does not form nitrides layers.

References

[1]. **Truşculescu M. Ieremia A.** *Oţeluri inoxidabile şi refractare* Ed.Facla Timişoara 1983

[2]. **Cheşa I. s a** *Alegerea şi utilizarea oţelurilor* Ed. Tehnică Buc. 1984

[3]. **Dumitrescu T.** *Tratamente termochimice* Ed. Universităţii din Galaţi 1980

[4]. **Dobrovici S.** *Cercetări privind tehnologia carbonitrurării în strat fluidizat aplicată oţelurilor*. Teză de doctorat Galaţi 1999.

[5]. **Truşculescu M.** *Oţeluri inoxidabile şi refractare*. Ed. FACLA Timişoara 1983.

[6]. **Berns H.** *Case hardening of stainless steel using nitrogen.* Ruhr University, Bochum, Germany 2002.

[7]. **Berns H.** *Solution nitriding of stainless steel for process engineering,* Mat.-wisws. u. Werkstofftech. 31/2000.

[8]. **Mocanu D. R.** *Încercarea materialelor*. Ed.Tehnică Buc. 1982.

[9]. **Vellier M.** *Solution apportees aux problemes de la corosion-abrasion par certaines aciers inoxydables austenitiques et austenito-feritiques.* Conference internationale des arts chimiques Paris 1976.

[10]. **Dima O. Mitoşeriu O. Levcovici S.** *Studiu asupra aspectelor de coroziune evidenţiate pe table şi îmbinări sudate din instalaţiile de fabricaţie a celulozei chimice prin procedeul sulfit din cadrul combinatelor CCH Zărneşti, CCH Letea Bacău, CCH Brăila.* Tehnologii Calitate Maşini şi Utilaje 36 Ed. Tehnică Buc.1999. Lucrările simpozionului Ecologie. Acoperiri metalice. Braşov 1999.

[11]. **Dima O.** *Surface hardening by nitration for some stainless austenite stainless steel type*. Galati 2006

MANUSCRISELE, CĂRŢILE ŞI REVISTELE PENTRU SCHIMB, PRECUM ŞI ORICE CORESPONDENŢE SE VOR TRIMITE PE ADRESA:

MANUSCRIPTS, REVIEWS AND BOOKS FOR EXCHANGE COOPERATION, AS WELL AS ANY CORRESPONDANCE WILL BE MAILED TO:

LES MANUSCRIPTS, LES REVUES ET LES LIVRES POUR L'ECHANGE, TOUT AUSSI QUE LA CORRESPONDANCE SERONT ENVOYES A L'ADRESSE:

MANUSCKRIPTEN, ZIETSCHRITFTEN UND BUCHER FUR AUSTAUCH SOWIE DIE KORRESPONDENZ SID AN FOLGENDE ANSCHRIFT ZU SEDEN:

UNIVERSITATEA "DUNĂREA DE JOS" DIN GALAŢI
REDACŢIA ANALELOR
Str. Domnească nr. 47 – 800036 Galaţi, ROMÂNIA
E-mail: marian.bordei@ugal.ro